Print edition ISSN 2615-5109
Electronic edition ISSN 2621-0541

Publisher:
Center of Technology, Fakultas Teknik, Universitas Hasanuddin

Address:
Engineering Faculty Campus, Hasanuddin University
Jl. Poros Malino km. 6, Bontomarannu
Kabupaten Gowa, Sulawesi Selatan, Indonesia, 92171
Email : epi-ije@unhas.ac.id
Website : cot.unhas.ac.id/journals/index.php/epiije
Telp/Fax : +62-(0)411-58601

EPI International Journal of Engineering
Editorial Board

Foreword

We are pleased to present Volume 6, Number 2, of the EPI International Journal of Engineering (EPI-IJE), published in August 2023. This edition continues to highlight diverse and innovative research contributions from esteemed academics and professionals across various fields of engineering. Each manuscript has been carefully reviewed to ensure the highest standards of academic rigor and practical relevance.

This issue features seven (7) manuscripts that explore a wide range of topics. The first manuscript investigates "Real-Time Data Acquisition and Monitoring of Three-Phase Load Balance in Electricity Distribution," offering valuable insights into improving power distribution systems. The second manuscript, contributed by researchers from Muroran Institute of Technology, Japan, delves into "Rectangular Plate Rebound Vibration Suppression using Double Collision Phenomena," presenting novel approaches to vibration control.

The third manuscript examines the "Analysis of Ability to Pay and Willingness to Pay in Trans Sulawesi Train Makassar - Parepare Route," shedding light on the economic feasibility of transportation projects. In the fourth paper, an assessment of stone ash with additives as a lightweight concrete material highlights innovative construction techniques.

Yoshihiro Narita from Hokkaido University contributes the fifth manuscript, focusing on the "Free Vibration of Annular Plates Constrained by Translational and/or Rotational Springs," advancing theoretical studies in structural dynamics.

The sixth paper evaluates the "Post-Occupancy Evaluation of Hasanuddin University Urban Park," providing critical insights into urban space utilization and user satisfaction. Finally, the seventh manuscript identifies "Thermal Comfort of Open Space in Soppeng Regency," addressing important aspects of environmental design and public comfort.

We extend our deepest gratitude to the authors for their exceptional contributions and to the reviewers for their invaluable efforts in maintaining the quality of this publication. We also thank our readers for their continued interest in and support of the EPI-IJE.

We hope that this edition will inspire further research and contribute to the advancement of science and technology in the engineering field.

Sincerely,

Dr. Faisal Mahmuddin
Editor-in-Chief of EPI-IJE

TABLE OF CONTENTS

EPI International Journal of Engineering
Volume 6, Number 2, August 2023, pp. 56-61
DOI: 10.25042/epi-ije.082023.01

*p*ISSN 2615-5109
*e*ISSN 2621-0541

Real-Time Data Acquisition and Monitoring of Three Phase Load Balance in Electricity Distribution

Dharma Aryani[a,*], Muhammad Yusril[b], Ahmad Rosyid Idris[c], Nur Aminah[d], Rusdi Wartapane[e], Muhammad Fajri Raharjo[f], Christian Lumembang[g]

[a]Department Of Electrical Engineering, State Polytechnic of Ujung Pandang. Email:dharma.aryani@poliupg.ac.id
[b]Department Of Electrical Engineering, State Polytechnic of Ujung Pandang. Email:yusmuh16@gmail.com
[c]Department Of Electrical Engineering, State Polytechnic of Ujung Pandang. Email:ahmadrosyid@poliupg.ac.id
[d]Department Of Electrical Engineering, State Polytechnic of Ujung Pandang. Email:nuraminah_elka@poliupg.ac.id
[e]Department Of Electrical Engineering, State Polytechnic of Ujung Pandang. Email:rusdiwartapane@poliupg.ac.id
[f]Department Of Electrical Engineering, State Polytechnic of Ujung Pandang. Email: fajri_raharjo@poliupg.ac.id
[g]Department Of Electrical Engineering, State Polytechnic of Ujung Pandang. Email:christian@gmail.com

Abstract

A real-time monitoring mechanism for three-phase electrical power distribution panels is essentially needed to ensure that the power is evenly distributed across all phases, so that the efficiency of energy usage could be maintained. This paper presents monitoring and data acquisition system for three-phase balance distribution. The system ensures balanced distribution of electrical power in order to enhance the efficiency and reliability of power systems. It leverages advanced technologies to collect, analyze, and report data, providing valuable insights into the performance of the power distribution network. Data acquisition is established by using sensor PZEM004T to measure the electricity parameters which is integrated with Arduino microcontroller. In addition, real-time monitoring system is visualized through dashboard data management for more informative data acquisition and analytic purposes. The performance is evaluated by testing the instrument and application at a distribution panel within a span of five days to monitor electrical parameters.. The results show that real-time monitoring system for three phase balance works perfectly to provide actual data and phase balance condition. The phase imbalance values are higher during the peak working hours where the loads are dynamics and extensively used.The highest value of imbalance obtained from monitoring results was 105.68% at 07.00 AM – 10.00 AM.56 while the lowest imbalance value obtained from monitoring results was 57.18% at 14.10 PM – 04.00 PM.

Keywords: 3-Phase Power Balance; IoT System; load balance dashboards;PZEM-004T

1. Introduction

Power distribution system is directly related to users of electrical energy, especially users of medium voltage and low voltage electricity. Usually there is often an unbalanced load on the phases or an overload occurs due to the use of electrical equipment from electrical energy consumers. Load balance between phases is required for equal distribution of loads so as to minimize changes caused by full load. This is also important because it is useful in optimization techniques to produce a reliable and efficient system [1], [2]. In low voltage electricity distribution networks, one of the main equipment used is the 3 phase distribution transformer. This transformer functions to lower the voltage so that the voltage can be used safely by consumers on low voltage networks such as households, street lights, schools, and so on.

In electric power distribution, a load imbalance occurs due to the asynchronous timing of the load ignition. Load imbalance between each phase (R phase, S phase, and T phase) causes current to flow in the transformer neutral. So that the unbalanced factor leads to the occurrence of neutral current could increase the power losses and reduce the efficiency of the transformer [3]. Therefore, in the distribution of electric power, load imbalances must be minimized in order to achieve optimal distribution efficiency. The distribution system needs to be properly planned to guarantee that it operates within the set parameters [4]. In every building construction, there must be an electrical installation plan according to the needs required by the building itself. However, it is often found that field conditions change after the building is put into operation and the load is added. This condition will cause load contention [5].

The 3-phase balance data monitoring and acquisition system are an early detection of imbalances and faults in the system, allowing for preventive maintenance, optimization of energy consumption and load distribution across phases, and enhanced system reliability and reduced downtime. As well as to gain better understanding

*Corresponding author. Tel.: +62-888-4888-000
Jalan Perintis Kemerdekaan km. 10, Tamalanrea Makassar, Indonesia, 90245

of the power usage patterns, helping with energy management strategies. An earlier study designed a smart monitoring system for Three Phase inverters using an Android Application which saves time and simplifies the process of monitoring the condition of a 3-phase electrical system [6]. Another study has developed an electrical energy controller by employing IoT technology, utilizing Arduino, PZEM-004T Module, Wemos, and a real-time clock as a microcontroller. The tool offers several advantages, including the ability to remotely switch on/off household electrical systems, automatic overload or short circuit protection, and the ability to monitor current, voltage, power, and energy/cost consumption [7]. An electrical current balancing monitoring device using current sensor and an Arduino microcontroller has been designed [8], [9]. Microcontroller and relay switching has been used in lowering three phase line unbalance as well as lowering current in the system's neutral wire to keep the three phase voltage stable and regulated [10]. Today, real-time monitoring using microcontrollers has been expanded for robotic controllers and tracking system [11].

Voltage unbalance factors (VUF) [12], [13], and the percent voltage unbalance (PVU) [14] are the key performance measurements for the three-phase imbalance detection. To improve distribution system performance and reduce losses, it is crucial to reorganize the network by rescheduling the loads [15]. This can only be conducted if the load imbalance is predicted using historical data or implementing machine learning algorithm [16].

Previous studies that have been conducted to monitor the balance of electricity provide real time information of voltage, current, and frequency variables. However, the monitoring system do not have data acquisition system which offers reporting feature of all the measurement results. Therefore, a more comprehensive monitoring system is developed by expanding the monitoring range so that the system can carry out real-time monitoring and the system becomes more effective and efficient in terms of accessing the monitoring system, as well as adding data acquisition to obtain data to determine the imbalance presentation.

The structure of the paper is outlined as follows, the material and method used in this work is described in Section 2. Section 3 covers results and discussion and the conclusion is provided in Section 4.

2. Materials and Methods

The 3-phase balance monitoring system is established using the Arduino Pro Mini microcontroller, Wemos and the PZEM-004T sensor as the main component and other components such as the Nextion LCD to display measurement values of voltage, current, power factor, average current, and percentage of imbalance.

2.1. Hardware system

The block diagram created is intended as a reference for making hardware in order to simplify the assembly process.

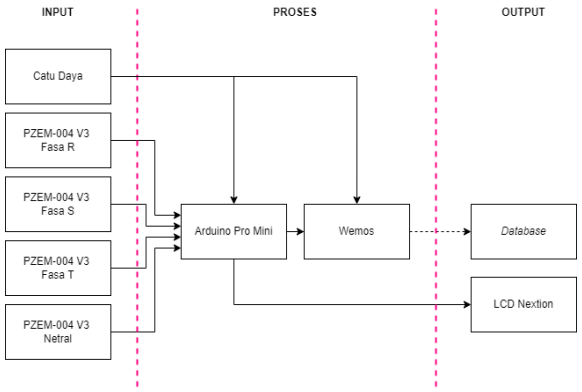

Figure 1. Hardware block diagram

Figure 1 shows the diagram of the hardware design frm input to output part. The power supply from the HLK 10M02 which will be connected to all components including the sensor. The PZEM-004T sensor will send data in the form of serial software to the Arduino pro mini so that the value of the voltage and current on each phase that has been installed will be processed by Arduino. Arduino will calculate these values and display the data on the Nextion LCD and will also send the data to Wemos for further processing as database. Furthermore, the dashboard monitoring application will automatically update the values on the graph about the condition of the distribution panel being measured. Figure 2 shows the wiring diagram of the instrument.

The schematic diagram of electronics design is presented in Fig. 3. This figure shows the connection and configuration of electronic elements.

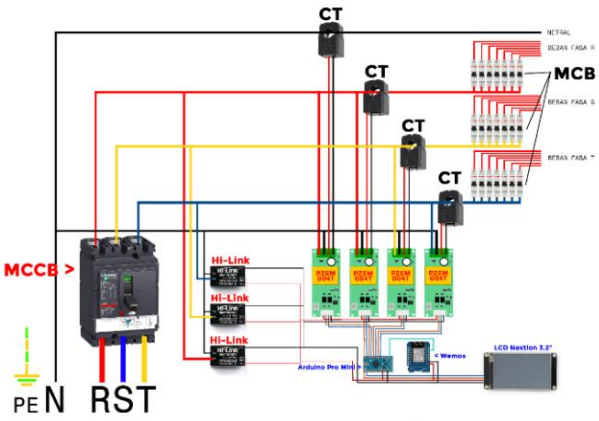

Figure 2. Design wiring diagram

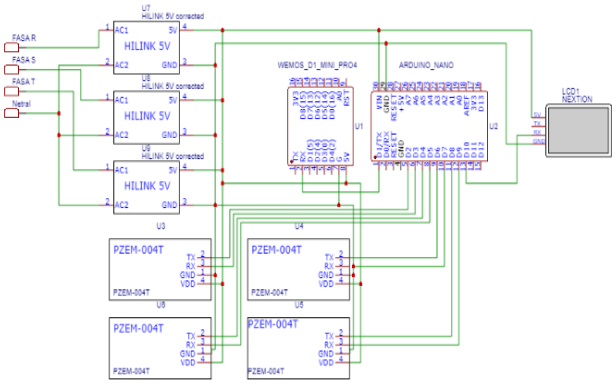

Figure 3. Schematic diagram

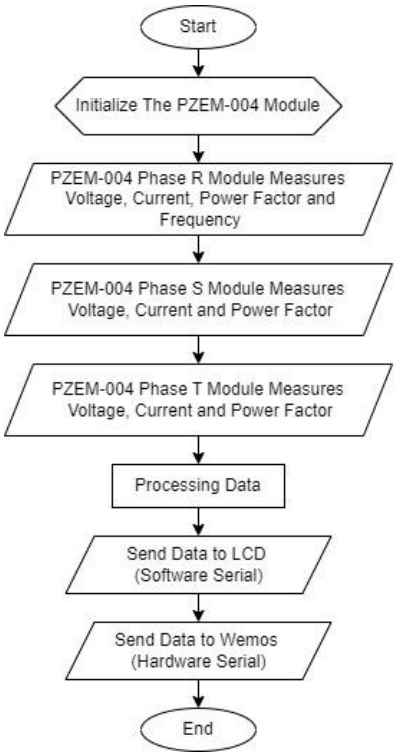

Figure 4. Arduino flow chart

2.2. Software system

The monitoring application and data acquisition are built through several stages. Firstly, data reading system on the Arduino which functions to manage measured data and send the data to the LCD and also Wemos. Secondly, designing the system displays on the Nextion LCD received from Arduino, and the latter is data acquisition and dashboard monitoring system.

2.2.1. System design on Arduino

This system includes data retrieval from the PZEM-004T sensor which will manage data in the form of voltage, current, power factor, frequency and also unbalance values. This is programmed in the Arduino IDE software. Figure 4 shows the flow chart of system where PZEM-004 sensor measures the electrical variables in each phase than send it to LCD for real time display and also to Wemos for data acquisition and monitoring system.

2.2.2. Monitoring design on LCD

For direct media monitoring, the Nextion LCD is used, which must be programmed and designed in the Nextion Editor software before it can be used to get a Human Machine Interface (HMI). Figure 5 shows the results of HMI design to visualize the electricity parameters which are measured. It displays variables are voltage, current, power factor, frequency, and the imbalance value.

2.2.3. *Data acquisiton and dashboard monitoring*

Electricity power parameters will be sent to the database via a wi-fi network connected to Wemos. This system is programmed on the Arduino IDE software. The following is a flow chart of this system.

Figure 5. Human Machine Interface (HMI) design on the Nextion LCD

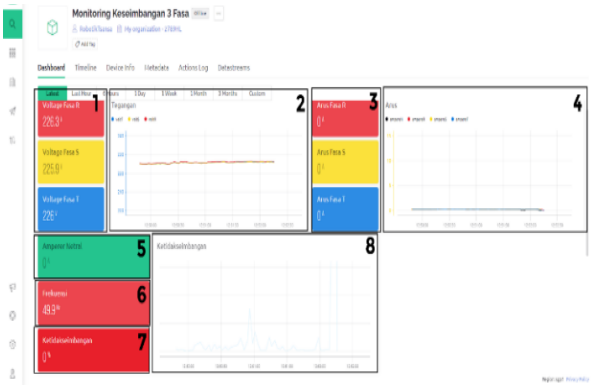

Figure 6. Dashboard design result

A dashboard monitoring designed on the *blynk* website using label components and also a chart where each value is sourced from the blynk database. The values on the labels and charts will change according to the updated data sent from Wemos. The dashboard preview can be seen in Fig. 6.

From the image of the results of the dashboard design, there is a description of each component as follows:

1. Voltage Label (Red for R phase, yellow for S phase, and blue for T phase).
2. Voltage graph (red line for R phase, yellow for S phase, and blue for T phase).
3. Current Label (Red for R phase, yellow for S phase, blue for T phase)
4. Current Graph (red line for R phase, yellow for S phase, blue for T phase, and black for neutral current).
5. Neutral Flow Labels
6. Frequency Labels
7. Imbalance label
8. Imbalance Chart

3. Results and Discussion

The real time measurements start from a 3-phase sources, each phase and grounded neutral will have an Open CT from the PZEM-004T sensor as a reading for each phase. Then the measurement value will be displayed on the LCD screen and parsed to Wemos to be recorded in the database. Furthermore, remote monitoring can be accessed from the dashboard and presented in the form of numbers and graphs.

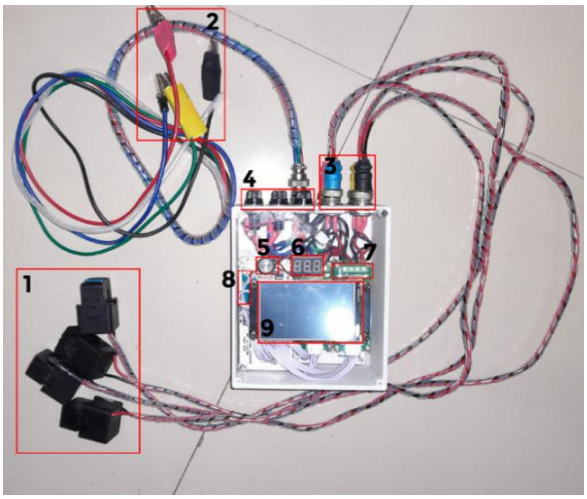

Figure 7. The instrument

3.1. Hardware

The results of the mechanical and electrical design are shown in Fig. 7. The instrument consists of :

1. Current transformer (red for R phase, yellow for S phase, blue for T phase, and black for neutral wire)
2. Crocodile Clips (Red for R phase, yellow for S phase, blue for T phase, and black for neutral wire)
3. CB Connectors for Current Transformers and Alligator Clips
4. Fuse Holders
5. Switches
6. DC Voltage Indicator
7. PZEM-004T
8. Wemos & Arduino
9. LCD Nextion

Furthermore, the results of the Human Machine Interface of monitoring system which consists of display on LCD Nextion and web-based dashboard monitoring are shown in Figure 8. The LCD provides data presentation on decimal values while web dashboard uses combination of decimal values and graphical visualization of each variable.

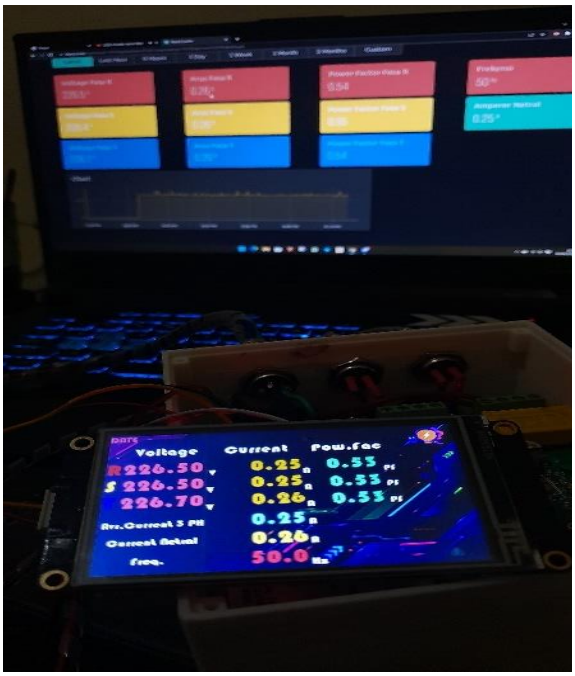

Figure 8. Human Machine Interface of monitoring system

3.2. Testing results

Testing is conducted to evaluate the system's performance of measurement instrument and the real-time monitoring application. The instruments is placed at the Electrical Mechanical Workshop, Department of Electrical Engineering, PNUP.

Data collection for system testing was carried out by installing a 3-phase Balance Monitoring System tool on the electrical panel of the electrical workshop, Campus Electrical Engineering building 1. Data collection is taken five days in a row. Table 4, Table 5, and Table 6 presented the measurement results by PZEM-004T sensor and multimeter of voltage, phase current, and frequency variables respectively. Error percentage is calculated from the difference of measured value using Multimeter over the measured value using sensor PZEM-004T.

3.2.1. Voltage

Table 7 shows that the highest voltage conditions occurred on Day 5 at 10.05.39 AM with a voltage of 259.9 V. The lowest voltage occurred on Day 1 at 2.38.37 PM with a voltage of 217.3 V. The voltage value has exceeded the tolerance limit for the voltage value set by PT.PLN (Persero) where the reasonable voltage limit is 231V (220V + 5%). The cause of this is the occurrence of sudden changes in load resulting in over voltage.

3.2.2. Frequency

Table 8 presents the lowest and highest frequency measurement. It can be seen that the highest frequency conditions occurred on Day 5 at 09.29.42 PM with frequency 50.4Hz. The lowest frequency is on Day 1 at 08.20.37 AM at 49.6 Hz.

Tabel 4. Comparison of voltage measurement results of PZEM, dashboard, and multimeter

Voltage	PZEM-004T (V)	*Dashboard*	Multimeter (V)	Error (%)
VR	232.1	232.1	231.5	0.259
VS	224.9	224.9	225.2	0.133
VT	228.1	228.1	227.2	0.395
Average				0.262

Tabel 5. Comparison of current measurement results of PZEM, Dashboard, and Multimeter

Phase Current	PZEM-004T (A)	*Dashboard*	Multimeter (A)	Error (%)
IR	4.48	4.48	4.58	2.183
IS	0.58	0.58	0.593	2.192
IT	0.56	0.56	0.573	2.269
IN	0.21	0.21	0.214	1.869
Average				2.128

Tabel 6. Comparison of frequency measurement results of PZEM, Dashboard, and Multimeter

Measurement	PZEM-004T (Hz)	*Dashboard* (Hz)	Multimeter (Hz)	Error (%)
1	49.9	49.9	49.5	0.81
2	50.2	50.2	50.0	0.40
3	49.9	49.9	49.4	1.01
Average				0.74

Table 7. Lowest and highest voltage measurement data

Day	line	Lowest Voltage		Highest Voltage	
		Value (V)	Hour	Value (V)	Hour
Day 1	RN	217.3	2:38:37PM	236.2	3:29:50PM
	SN	217.1	10:04:42AM	232.1	6:54:22 AM
	TN	217.4	2:42:09PM	230.5	7:48:14 AM
Day 2	RN	219.1	7:44:59AM	235.3	7:06:39AM
	SN	218.7	2:35:52PM	232.1	7:04:32AM
	TN	218.4	1:30:57PM	230.4	7:00:09AM
Day 3	RN	218.4	9:58:07AM	234.9	7:03:15AM
	SN	218.2	10:01:29 AM	231.2	9:58:07AM
	TN	219.6	1:42:09PM	229.9	10:01:29 AM
Day 4	RN	220	10:39:52 AM	234.3	9:21:11AM
	SN	222	6:55:46 AM	232.2	5:23:12PM
	TN	223.1	6:55:47 AM	232.5	11:09:34 AM
Day 5	RN	220.8	6:58:57AM	234	10:04:09 AM
	SN	219.3	6:58:57AM	232.8	7:16:49 AM
	TN	219.6	9:46:25AM	259.9	10:05:39 AM

Based on the standards set by PT.PLN (Persero), the nominal frequency on the network is 50.00 (fifty point zero zero) Hz, the system frequency can go up to 52.00 (fifty two point zero zero) Hz and down to with 47.00 (forty seven point zero zero) Hz in extraordinary circumstances. From these standards the frequency that occurred during the testing is still classified as the standard set by PT. PLN (Persero).

Table 8. Lowest and highest frequency measurement data

Day	Hour	Frequency (Hz)	Information
Day 1	08:20:52 AM	49.6	Lowest
	10:59:18AM	50.3	Highest
Day 2	07:36:33 AM	49.7	Lowest
	10:27:10AM	50.3	Highest
Day 3	04:32:20 PM	49.6	Lowest
	03:14:50PM	50.2	Highest
Day 4	02:30:48PM	49.5	Lowest
	08:54:10 AM	50.3	Highest
Day 5	04:32:20 PM	49.6	Lowest
	09:29:42 AM	50.4	Highest

Figure 9 shows the frequency value on Day 5 from 06.58.57 AM to 16:45:45 PM. The highest frequency shown is 50.4 Hz and the lowest is 49.6 Hz.

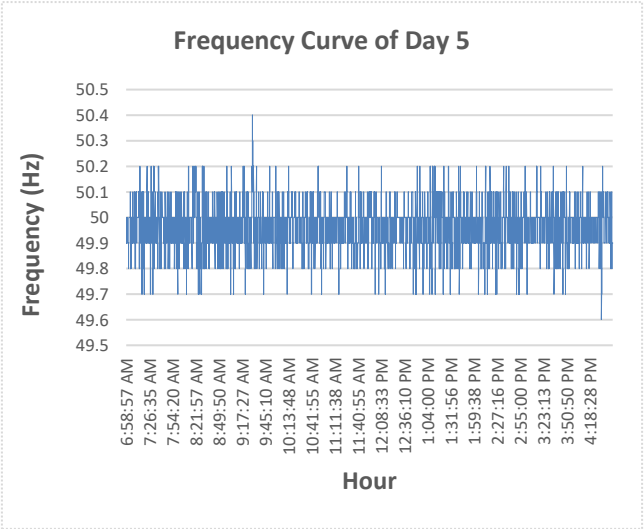

Figure 9. Frequency chart on Day 5

3.2.3. *Current/Load*

As a natural law, the current measurement current is inversely proportional to voltage. It can be evaluated that the lowest current conditions occurred on Day 5 at 10.04.54 PM with a current of 0.12 A (Phase T). Meanwhile, the highest current is on Day 1 at 12.42.45 PM was 10.51 A (Phase R).

Table 9. Lowest and highest current measurement data

Day	line	Lowest Current		Highest Flow	
		Value (A)	Hour	Value (A)	Hour
Day 1	R	0.29	6:54:14 AM	10.51	12:42:45PM
	S	0.49	7:32:46AM	6,46	1:28:57PM
	T	0.2	10:49:38AM	1.52	2:07:50PM
	N	0.03	7:03:55 AM	0.96	1:58:40PM
Day 2	R	0.28	5:08:40 PM	9.93	8:25:42 AM
	S	0.48	4:15:05PM	2.05	11:19:53 AM
	T	0.31	1:38:12PM	3.69	9:17:10AM
	N	0.03	5:49:52PM	0.6	11:08:36AM
Day 3	R	0.27	4:09:27PM	9.88	12:45:25PM
	S	0.49	7:45:42AM	2.81	8:06:50AM
	T	0.31	10:29:12 AM	1.74	12:45:25PM
	N	0.03	7:05:15 AM	0.91	10:29:43 AM
Day 4	R	0.26	4:12:17PM	9,41	10:55:32AM
	S	0.48	4:06:02PM	2,23	3:05:28PM
	T	0.31	4:12:00PM	1.81	12:37:17 PM
	N	0.03	7:20:46AM	0.8	9:42:21AM
Day 5	R	0.27	6:59:02AM	9.88	12:45:25PM
	S	0.49	7:27:37AM	2.62	8:10:49AM
	T	0.12	10:04:54 AM	1.74	12:45:25PM
	N	0.03	7:14:19AM	2.63	9:50:52 AM

3.2.4. *Phase imbalance*

The 3-phase imbalance is analyzed by calculating the imbalance coefficient which consists of the coefficients a, b and c which are calculated from the load imbalance percentage equation. For example, on the reading of Day 1 at 07.00 AM – 10.00 AM the values for the coefficients a, b and c are calculated as follows, so that an imbalance of 76.31% is obtained.

$$a = \frac{IR}{\frac{IR+IS+IT}{3}} = \frac{7,42}{3,4583} = 2,1447 \quad (1)$$

$$b = \frac{IS}{\frac{IR+IS+IT}{3}} = \frac{2,52}{3,483} = 0,7298 \quad (2)$$

$$c = \frac{IT}{\frac{IR+IS+IT}{3}} = \frac{0,43}{3,483} = 0,1255 \quad (3)$$

$$\%\ \text{Load Imbalance} = \frac{\{|a-1| + |b-1| + |c-1|\}}{3} \times 100\% \quad (4)$$

$$= \frac{\{|2,1447-1| + |0,7298-1| + |0,1255-1|\}}{3} \times 100\%$$

$$= \frac{1,1447 + 0,2702 + 0,8745}{3} \times 100\%$$

$$= \frac{2,2894}{3} \times 100\% = 0,764 \times 100\% = 76,31\%$$

Table 10 provides the results of imbalance coefficients during the testing in five days.

Data from load current measurements can be seen the percent imbalance from the lowest of 57.18% to the highest of 105.68%. From this value it is far from the standard load imbalance regulated in IEEE std 446 – 1980, which is 5% - 20%. This happens bec ause the current in phase R serves a very large load than phases S and T. One of the consequences of an imbalance is that there is a current in the Neutral wire. The tendency for the highest imbalance to occur occurs at 10.01 AM to 14.00 PM because at that time the peak load occurs.

Table 10. Calculation of imbalance

Day	Hour	Average Line Flow				Imbalance (%)
		R	S	T	N	
Day 1	07.00 AM - 10.00 AM	7.42	2.52	0.43	0.26	76.31
	10.01AM - 14.00 PM	7.13	3.98	0.54	0.25	57.35
	14.10 PM - 04.00 PM	7.75	5.47	0.66	0.23	57.18
Day 2	07.00 AM - 10.00 AM	8.03	0.89	0.40	0.32	105.68
	10.01 AM - 14.00 PM	6.34	0.86	0.77	0.24	92.38
	14.10 PM - 04.30 PM	6.40	0.93	0.33	0.25	100.41
Day 3	07.00 AM - 10.00 AM	5.09	0.86	0.33	0.25	95.65
	10.01 AM - 14.00 PM	5.92	0.89	0.33	0.27	99.26
	14.10 PM - 04.00 PM	4.08	0.86	0.33	0.18	88.25
Day 4	07.00 AM - 10.00 AM	3.98	0.83	0.66	0.19	78.92
	10.01 AM - 14.00 PM	5.38	0.74	0.72	0.25	90.61
	14.10 PM - 04.00 PM	4.89	0.77	0.81	0.23	84.50
Day 5	07.00 AM - 10.00 AM	5.55	0.76	0.33	0.27	100.67
	10.01AM - 14.00 PM	5.88	0.89	0.33	0.26	99.13
	14.10 PM - 04.00 PM	4.08	0.86	0.33	0.18	88.25

3. Conclusion

The 3-phase balance monitoring system has been successfully designed using Arduino as a microcontroller, PZEM-004T sensor as a measure of electrical parameters, Nextion LCD as a direct interface and Wemos as communication to the dashboard application. Therefore, the 3-phase balance condition can also be remotely monitored in real-time and recorded data can be accessed anytime. The voltage, frequency and current monitoring system are functioning properly and can monitor dynamic conditions during five days of testing. On the period of testing, it is revealed that the lowest measured voltage is 217.3 V and the highest is 259.9 V from the measured value there is an over voltage due to the tolerance set by PT. PLN (Persero) with a maximum over voltage of 231V. This over voltage incident occurred due to a sudden change in load, it can be seen in the load curve at that time which jumped from 4.84 A to 7.88 A. The phase imbalance value obtained higher during the peak working hours which is relevant with the load characters on the workshop testing location.

References

[1] W. Kong, K. Ma, and Q. Wu, "Three-Phase Power Imbalance Decomposition Into Systematic Imbalance and Random Imbalance," *IEEE Trans. Power Syst.*, vol. 33, no. 3, pp. 3001–3012, 2018.

[2] A. B. Turumi, "Analisis Ketidakseimbangan Beban Sistim Kelistrikan Kampus Politeknik Negeri Manado," Politeknik Negeri Manado, 2015.

[3] Y. A. Pradita, "Analisis Ketidakseimbangan Beban Terhadap Arus Kawat Netral Gedung E11 Dan Gedung Dekanat Fakultas Teknik Universitas Negeri Semarang," Universitas Negeri Semarang, 2019.

[4] L. Alhmoud and W. Marji, "Optimization of Three-Phase Feeder Load Balancing Using Smart Meters," *IEEE Can. J. Electr. Comput. Eng.*, vol. 45, no. 1, pp. 9–17, 2022.

[5] Hasbulah, "Analisa Pengaruh Beban Tidak Seimbang terhadap Rugi Daya Listrik pada Jaringan Distribusi Sekunder," *J. Tek. Elektro, Progr. Stud. Tek. List. Politek. Negeri Sriwij.*, pp. 1–6, 2016.

[6] M. J. Mnati, A. Van den Bossche, and R. F. Chisab, "A Smart Voltage and Current Monitoring System for Three Phase Inverters Using an Android Smartphone Application," *Sensors*, vol. 4, p. 872, 2017.

[7] S. U. Haq, B. Arif, A. Khan, and J. Ahmed, "Automatic Three Phase Load Balancing System by Using Fast Switching Relay in Three Phase Distribution System," in *2018 1st International Conference on Power, Energy and Smart Grid (ICPESG)*, 2018.

[8] N. Aminah, R. Wartapane, D. Aryani, and H. Yani, "Desain Alat Pengontrol Energi Listrik Digital Berbasis Internet of Things," in *Prosiding 5th Seminar Nasional Penelitian & Pengabdian Kepada Masyarakat*, 2021, pp. 81–86.

[9] A. Rohmanu and Riswandi, "Pemodelan Alat Monitoring Keseimbangan Arus Listrik Tiga Phasa Menggunakan Arduino dan SMS Gateway Dengan Berbasis Web," *J. Inform. SIMANTIK*, vol. 1, pp. 26–31, 2016.

[10] C. G. I. Partha, "Design and Balancing Load Current in 3-Phase System Using Microcontroller ATMEGA 2560," *Int. J. Eng. Emerg. Technol.*, vol. 2, pp. 76–83, 2017.

[11] D. Aryani, K. Dewi, F. Ta'by, and E. P. Sanggaria, "Real-time Ball Detection and Tracking using Raspberry PI," *INTEK J. Penelit.*, vol. 10, pp. 48–54, 2023.

[12] A. von Jouanne and B. Banerjee, "Assessment of Voltage Unbalance," *IEEE Trans. Power Deliv.*, vol. 16, no. 4, pp. 782–290, 2001.

[13] P. Pillay and M. Manyage, "Definitions of Voltage Unbalance," *IEEE Power Eng. Rev.*, vol. 21, no. 5, pp. 49–51, 2001.

[14] T. Routtenberg and L. Tong, "Joint Frequency and Phasor Estimation in Unbalanced Three-Phase Power Systems," in *2014 IEEE International Conference on Acoustics, Speech and Signal Processing (ICASSP)*, 2014.

[15] J. Wang, N. Zeng, and H. Hao, "Three-phase imbalance prediction: A hazard-based method," in *2016 IEEE International Conference on Power and Renewable Energy (ICPRE)*, 2016.

[16] P. N. Thanh, M.-Y. Cho, C.-L. Chang, and M.-J. Chen, "Short-Term Three-Phase Load Prediction With Advanced Metering Infrastructure Data in Smart Solar Microgrid Based Convolution Neural Network Bidirectional Gated Recurrent Unit," *IEEE Access*, vol. 10, pp. 68686–68699, 2022.

EPI International Journal of Engineering
Volume 6, Number 2, August 2023, pp. 62-71
DOI: 10.25042/epi-ije.082023.02

*p*ISSN 2615-5109
*e*ISSN 2621-0541

Rectangular Plate Rebound Vibration Suppression using Double Collision Phenomena

Hiroki Matsumoto[a,*], Kazuhiro Kawakita[b]

[a]Department of Engineering, Mechanical Engineering Research Unit, Muroran Institute of Technology, Hokkaido, Japan.
Email:h_matsu@mmm.muroran-it.ac.jp
[b]Department of Engineering, Mechanical Engineering Research Unit, Muroran Institute of Technology, Hokkaido, Japan.

Abstract

The rectangular plate is a model of the internal mirror of a single lens reflex (SLR) camera. The internal mirror model was a rectangular metal plate rotated along its axis around one side of the rectangle. Rebound vibrations occur when the mirror hits the stopper. A double-collision method was introduced to reduce rebound vibration. The timing of the double collision varies with the amount of rebound vibration. 3-Conpornents Particle Image Velocimetry (3-C PIV) and 3-D motion analysis were used to investigate rebound phenomena. The 3-C PIV measured the rebound vibration velocity of the mirror model surface at the moment of the collision. 3-D motion analysis was used to measure the rebound vibration displacement at the moment of collision. When the rebound vibration was small, the low-velocity region on the surface of the mirror model moved in the longitudinal direction. This indicates that the mirror model underwent wave deformation at the moment of collision. When the timing of the second collision was optimized, the deformation of the mirror model at the moment of collision increased and the rebound amount was suppressed.

Keywords: Vibration;Collision;Rebound;PIV;Flat plate;SLR camera

1. Introduction

Single-lens reflex (SLR) cameras have a moving mirror system. When the shutter release button is pressed, the mirror swings up to the upper side of the camera, and the light passing through the lens moves straight to the shutter curtain. After the image sensor is exposed, the mirror swung down and hit the stopper. At this moment, an impact force is applied to the mirror, and rebound vibration occurs. A mirror-rebound vibration-suppressing mechanism is required to continuously capture the picture.

The collision behavior of objects has been studied for a long time. Examples include an elastic sphere and an elastic half-space [1], an elastic sphere and a large thin elastic plate [2]–[5], a tennis racket and a ball or a bat and a ball [6]–[10], and a circular ring [11], [12].

We studied the phenomenon of mirror rebound. To consider a structure that can suppress rebound vibrations, a collision experiment was performed between a mirror model and stopper model. The rebound vibration is indicated by the rebound angle of the mirror model. Previous studies on the collision behavior of mirror models with a single stopper have considered the rebound angle to vary with stopper position. In the case of the single-stopper model, the rebound angle depends on the stopper position. The stopper position, where the rebound angle is the minimum value, was determined in a previous study [13]. This suppression method is based on the vibration mode of the mirror models [14]. Another suppression method is the two-plate bonded mirror model, which changes the bonding points [15].

In this study, a suppression method for the rebound amount of a mirror model, which is a double-collision model, is proposed. This model has two stoppers located on both sides of the mirror model. The amount of suppression was greater than that in previous methods. In this method, double collision phenomena occur and the rebound angle is reduced. The stopper position was important for reducing the rebound angle.

An examination of the effect of pre-impact vibration on the response to low-velocity impact on a rectangular plate showed that impact damage mitigation can be considered [16]. The effect of pre-elastic waves on the amount of rod bounce has been analytically demonstrated [17]. This suggests that in the case of a large bounce, the relationship between the pre-elastic wave and the elastic wave caused by the collision is important. This suggests that the phenomenon may be explained by a concept similar to that of the double-collision condition in the present study. Therefore, to investigate the mechanism of the change in the amount of bounce due to the double impact on a flat plate, we visualized the behavior of the flat plate during the impact and discussed the effect of the timing of the second impact on the elastic deformation caused by the first impact.

*Corresponding author. Tel.: +81-143-46-5334
Mizumoto-cho 27-1
Muroran-shi, Hokkaido, Japan, 050-8585

The purpose of this study was to determine the optimal stopper position to reduce the rebound angle. We explain the suppression mechanisms through visualization using the 3-Components Particle Image Velocimetry (3-C PIV) method for the double collision phenomena of the mirror model.

2. Experimental Method

2.1. Mirror model

The actual internal mirror has parts in the mirror system, such as a sub-mirror or support frame. To measure the vibration behavior of the mirror model with high precision, a simple scaled-up mirror model was used. The mirror model was made of an aluminum plate with 1 mm thick 60x80mm rectangular plates. The characteristics of the rebound phenomenon were almost the same between the actual-size and scaled-up models [8]. The mirror model shown in Fig. 1 is a scaled-up version. Figure 1 and 2 show the mirror model and the stoppers, respectively. As shown in Fig. 1, M3 bolts were used in the fixture to attach the mirror models to the rotating shaft. The mirror model was rotated by using jigs and shafts. The stainless-steel shaft was 4mm in diameter and was mounted on the main body with ball bearings. In the experiment, a mirror model, supported horizontally by a release, was allowed to fall freely. Two stoppers are placed on either side of the mirror. The right stopper was positioned 45 degrees downward and its position was the origin of the stopper position. The stopper was an aluminum column with a diameter of 5 mm and length of 1 mm in contact with the mirror model. The natural frequency of the stopper structure was very large compared with that of the mirror model. Thus, the stopper structure did not affect the rebound phenomenon in this study. The right stopper position was determined by the distance Y_R and Z_R was fixed at 0 mm. As shown in Figure 2, the origin of the right stopper is the right-side edge of the mirror model. The origin of the left stopper was opposite to that of the mirror model and was at the same height as that of the right stopper. The stopper position was determined by the distances Y_R, Y_L, and Z_L from the model edge, as shown, and Y_R could vary from 0 mm to 40 mm in 2 mm increments. Z_L varied in the negative range. Therefore, the mirror model first collided with the right stopper.

2.2. Experiment setup

The rebound vibration of the mirror model was measured using a laser-displacement meter. Figure 2 shows the measurement position of the laser displacement meter (KEYENCE LK-G80). Figure 3 shows a general view of the experimental setup. Figure 4 shows a right view of the experimental setup and schematic of the mirror model angle. The rebound angle was measured at each stopper position. The measured displacement was converted into a mirror model angle θ. As shown in Fig. 4 b, the mirror model was set at an angle θ = 45 degrees by the release bar. When the release bar moved upward, the mirror model fell freely and hit stoppers. To adjust the start angle of the mirror, a release bar was included, and the release stand at the top of the unit could be adjusted from 0 to 13 mm vertically and horizontally. The stopper adjustment stand (Y-Z stage) at the bottom of the unit could be adjusted from 0 to 40 mm in the Y-axis direction and from -10 to 3 mm in the Z-axis direction from the bottom of the stoppers.

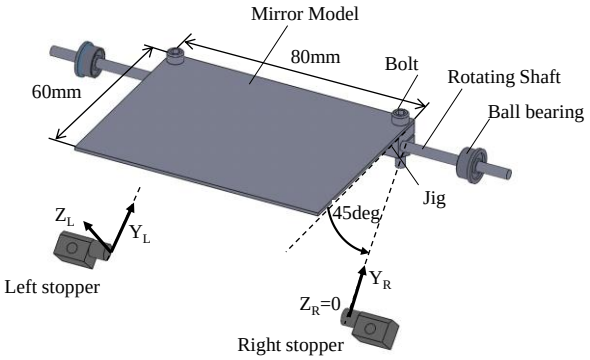

Figure 1. Mirror model and stoppers

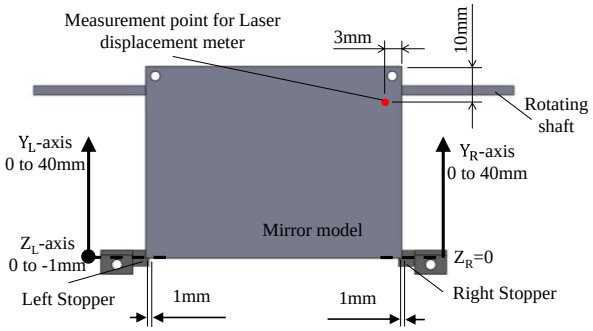

Figure 2. Measurement points and stopper positions

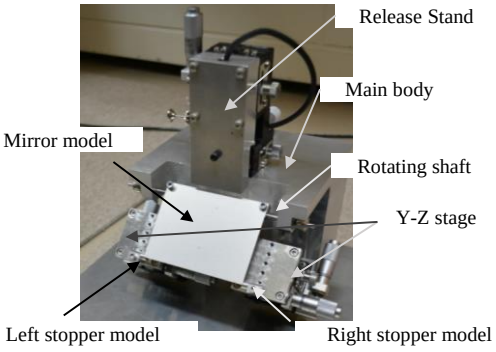

Figure 3. Experimental setup

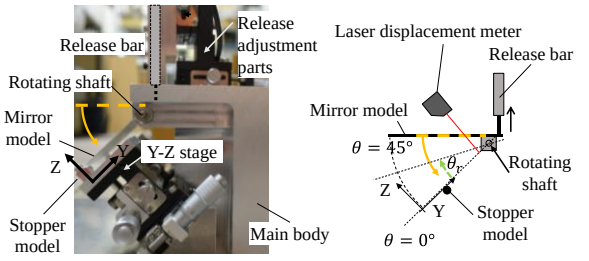

a. Right side view of experiment setup

b. Schematic of the mirror model and the stopper model

Figure 4. Right view of the experimental setup

Figure 5 shows a schematic of the experimental setup of the 3-Components PIV system. A typical stereo particle image velocimetry (PIV) system was used to measure the flow field. Stereo PIV systems use two high-speed cameras to capture images of the particles distributed in a flow field. The spatial motion of the particles was measured by calculating the image correlation of the particle distribution, which was changed for each recorded image. This study used the reflection of the flat plate and mosaic pattern instead of a laser light sheet. This was the originality of the proposed method. Because the plate surface is illuminated, a laser light sheet is not required, and a mosaic pattern instead of particles can be used to measure the behavior of the surface.

The software used for the calculation was Flownizer2D3C from DITECT. This method was used to visualize the transient motion of the mirror model. As shown in Fig. 5, a mosaic pattern was printed on the surface of the mirror model instead of on the particles in the flow. When the mirror hits the stopper, it deforms in the out-of-plane direction, thereby changing the mosaic pattern on the surface of the mirror model captured by the high-speed camera. The change in the mosaic pattern with the deformation of the mirror model was captured using two high-speed cameras, and the moving speed of the mosaic pattern in the 3D space was obtained using the image correlation method. Figure 6 shows the calibration plate used in this method. The displacement of the plate surface was determined by using a dot pattern on the calibration plate. Before the experiment, a calibration plate was placed instead of a mirror model, and the calibration plate dot pattern was captured using two cameras. Two types of images were used to obtain projection functions for each camera. One is the initial position image and the other is the offset image in the Z-direction. Consequently, four projection functions were obtained from the calibration images. The three components of plate displacement require four projection functions. In the software, we set the actual size of the dot, interval of the dot, and offset length. The displacement in the Z-direction is obtained from the mosaic pattern motion of the inspection area. We obtained a mosaic pattern motion in the captured image using the image correlation method in the mirror model measurement.

Figure 7 shows the displacement measurement system for the mirror model. The displacement of the mirror model during collision was measured using a 3D motion analysis method with two high-speed cameras. Using the obtained images, seven markers on the mirror model were tracked using motion analysis software DIPP-MotionV/3D from DITECT.

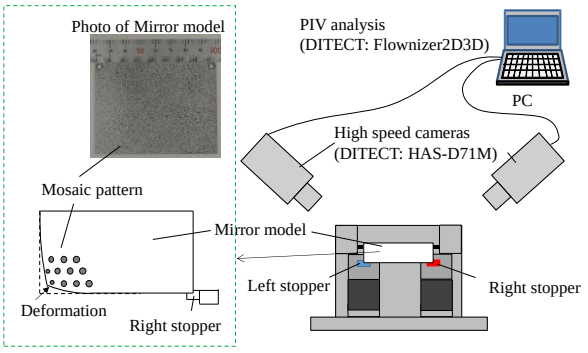

Figure 5. Stereo PIV system

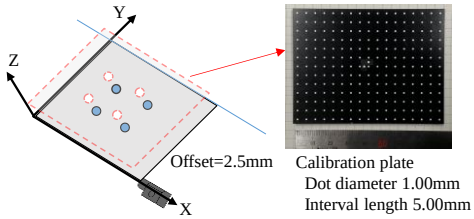

Figure 6. The calibration plate for the stereo camera displacement measurement system

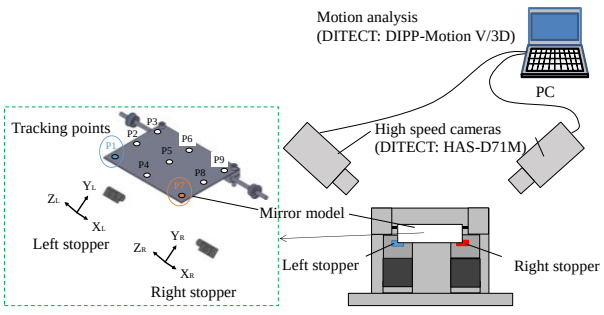

Figure 7. Stereo camera displacement measurement system

3. Experimental Results

3.1. Rebound angle

Figure 8 shows an example of the measured rebound vibration of the mirror model. The vertical displacement of the mirror model was measured using a laser-displacement meter. The vertical displacement was converted into the angle of the mirror model based on the geometric relations. The mirror model falling 45 degrees above the stopper collided with the stopper and rebounded. The maximum rebound angle is defined as the value obtained from the maximum angle recorded at the first impact.

3.2. Rebound angle the mirror model with a single stopper

First, the bounce characteristics of a single stopper were presented. Figure 9 shows the measured maximum rebound angle with a single stopper.

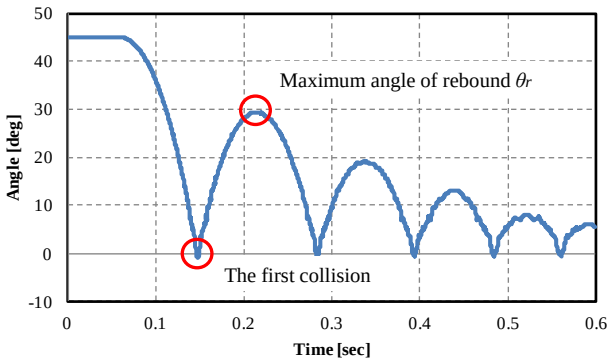

Figure 8. Example of the rebound vibration of the mirror model

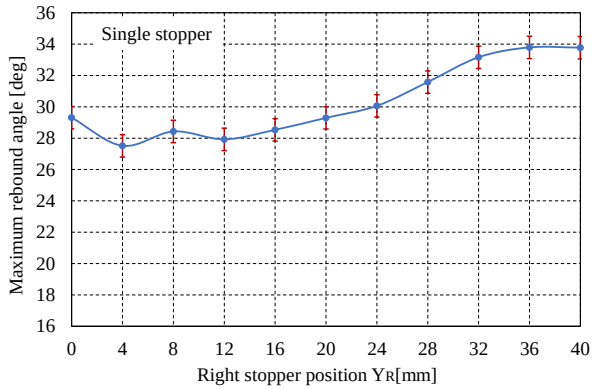

Figure 9. Maximum rebound angle of the mirror model with single-stopper

The graph shows the mean of three experiments, and the error bars represent standard deviations. The position of the stopper on the right side was kept constant at $Z_R = 0$ mm and varied in 4 mm increments from the tip of the mirror model to 40 mm. The maximum rebound angle was measured at each stopper position and plotted. Figure 9 shows that the maximum rebound angle was influenced by the position of the right stopper position. The minimum rebound angle was approximately 27 degrees at $Y_R = 4$ mm.

3.3. Rebound angle of the mirror model with double stoppers

Subsequently, the results for the double-stopper are presented. The right stopper was located at the tip of the mirror model and was fixed at $Y_R = 0$ mm and $Z_R = 0$ mm. The left stopper is located in the Z-direction at $Z_L = 0$ mm, -0.5 mm, and -1 mm. $Z_L = 0$ mm indicates that the left and right stoppers and the mirror model collide simultaneously. A negative Z_L indicates that the mirror model first collides with the right stopper and then with the left stopper.

Figure 10 shows the change in the maximum rebound angle as the position of the left stopper varies during the double collision. When Z_L = -1 mm, the maximum rebound angle was slightly smaller at $Y_L = 0$ mm but was constant with respect to the change in Y_L. The reason for this change is believed to be that the torsional elastic deformation of the mirror model that affects the right stopper produces an elastic deformation of approximately

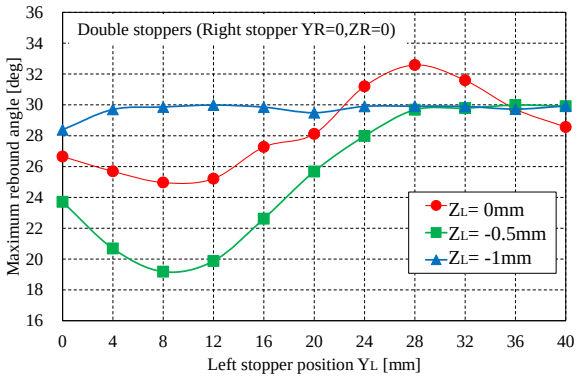

Figure 10. Maximum rebound angle of the mirror model with double stoppers

1 mm at the left tip of the mirror model. When the left stopper is located at the tip of the mirror model, a double collision occurs for $Z_L = 1$ mm, as Y_L increases, the left stopper moves toward the rotation axis of the mirror model, and the elastic deformation of the left end of the mirror model becomes smaller; thus, the left stopper does not collide with the left stopper. Therefore, for $Z_L = -1$ mm and $Y_L = 4$ mm or more, the situation is the same as in the single-stopper case.

The graph for $Z_L = 0$ mm, that is, when both sides collide simultaneously, shows that the maximum rebound angle was smaller than that of the single stopper case for Y_L from 0 to 20 mm, but was larger for Y_L greater than 24 mm. When the two sides of the mirror model collided, a bending deformation occurred. The deformation state is expected to differ depending on the distance between the rotation axis of the mirror model and stopper. When the distance between the rotation axis and the stopper is small, the rebound angle is expected to be larger owing to convex deformation, and when the distance is large, the rebound angle is expected to be smaller owing to concave deformation.

For $Z_L = -0.5$ mm, the rebound angle was smaller than in the single-stopper case over a wide range from $Y_L = 0$ to 24 mm. For $Z_L = -0.5$ mm, the rebound angle was smaller than in the single-stopper case because as Y_L changed, the timing of the collision between the mirror model and the left stopper changed. It can be seen that in the double collision case when the second collision occurs at the appropriate time, the rebound angle is very small. The minimum rebound angle was approximately 19 degrees for $Y_L = 8$ mm and $Z_L = -0.5$ mm, a 40% decrease compared to the single-stopper case.

3.4. Transient response of the mirror model surface velocity

Figures 11 and 12 show the results of the 3-C PIV measurements of the surface velocity of the mirror model colliding with the single-stopper.

Figure 11 shows the results of a single-stopper collision. The stopper positions were $Y_R = 0$ and $Z_R = 0$. The rebound angle is 29.6 degrees. The blue color represents the velocity in the negative direction of the Z-axis, red color represents the velocity in the positive direction, and positive direction of the Z-axis corresponds to the rebound direction. In the case of a single stopper, the collision occurred only once and its duration was set to 0 msec. At the moment of impact, the velocity on the right-side surface of the stopper position is zero, indicating that it is in contact with the stopper. Subsequently, the lower left edge of the mirror model had a negative velocity, which caused elastic deformation of the mirror model with the stopper and rotation as the fulcrum. The deformation continued until 0.875 msec. Subsequently, the lower-left end of the mirror model was found to have a positive velocity. Therefore, the model reached its maximum deformation state at 0.875 msec, after which the lower-left end moved in the positive direction and returned to its original shape. The deformation was restored while maintaining the velocity, and at 2.625 msec, the velocity

of the mirror model near the right stopper became positive, indicating that the stopper and mirror models had separated.

Figure 12 shows the results of a single-stopper collision with a rebound angle of 32.8 degrees. The stopper positions were Y_R = 40 and Z_R = 0. This is the stopper position where the largest rebound angle is measured for all single-stopper conditions. The time from the initial impact to separation from the stopper was 4.125 msec. This indicates that the stopper was in contact with the surface for a longer period than that shown in Fig. 11, where the amount of rebound was smaller. However, the change in the surface velocity distribution of the mirror model was almost the same as that shown in Fig. 11. This indicates that the deformation state of the mirror model was restored after the edge opposite to the stopper was shifted in the negative direction of the Z_R axis. However, in Fig. 12, the position of the stopper is close to the rotation axis of the mirror model. Therefore, after 2.87 msec the region with a positive velocity on the Z_R axis continues to expand along the entire longitudinal direction at the lower edge of the mirror model. This indicates that the range of elastic deformation of the mirror model in the out-of-plane direction is larger than that shown in Fig. 11, and the rebound angle is considered to have increased because of the restoring force of the mirror model.

Figure 13 shows the measurement results of a double stopper, in where the two stoppers collide simultaneously. The coordinates of the left stopper are Y_L = 0 and Z_L = 0, and the coordinates of the right stopper are Y_R = 0 and Z_L = 0. In this case, the left and right stoppers are in the same position relative to the rotation axis; therefore, the mirror model and stopper collided almost simultaneously. In this case, the maximum rebound angle was 25.0 degrees, which was slightly smaller than that in the single-stopper case. The surface velocity distribution of the mirror model after the collision showed that the velocity at the center of the lower edge of the mirror model had a negative component after 0.125 msec, whereas the velocity at both ends in contact with the stopper was zero. This result indicates that the center of the bottom edge of the mirror was elastically deformed in a concave manner. Subsequently, the velocity became almost zero at 0.625 msec, which is expected to indicate that the maximum deformation has occurred. As time passed, the velocity of the center section became positive, and it was found to

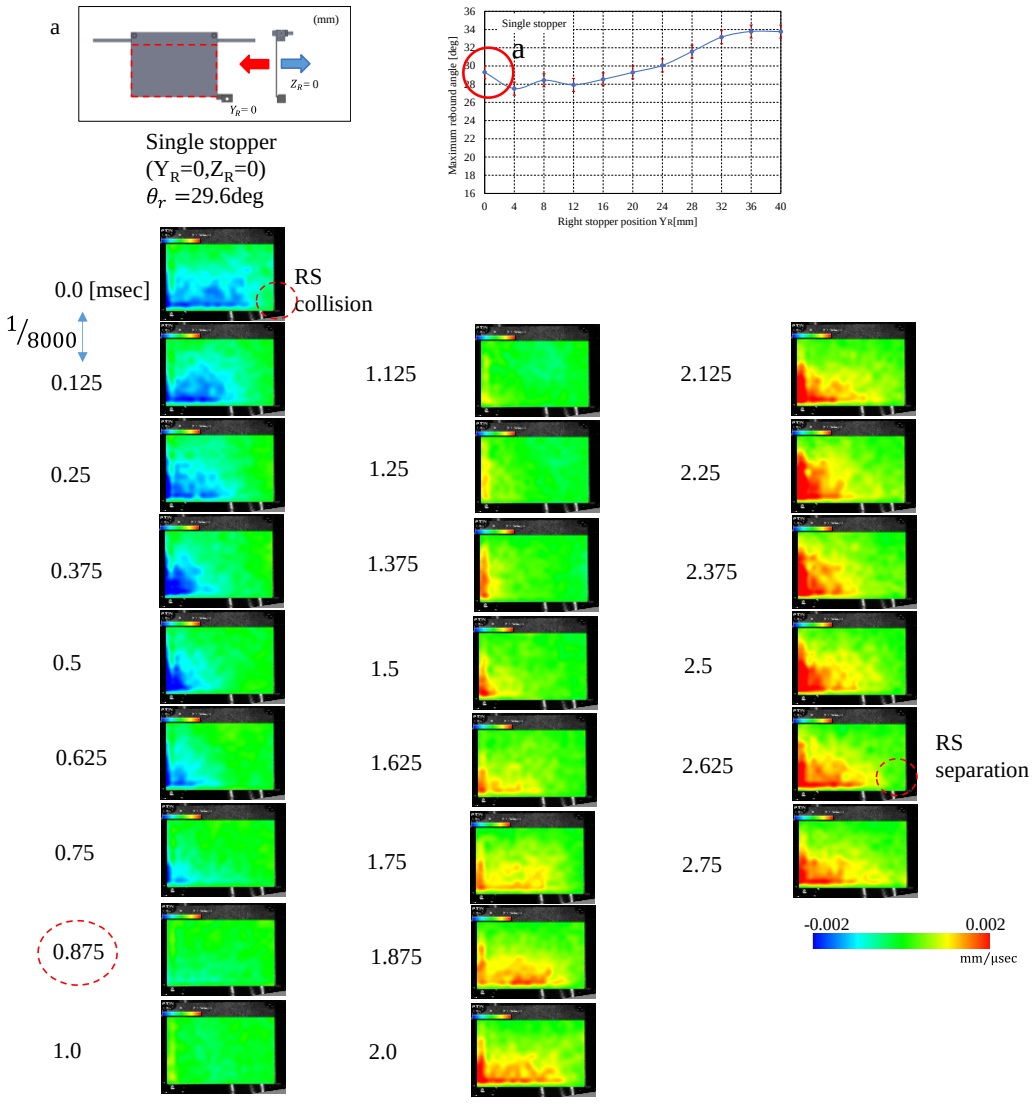

Figure 11. Transient response of mirror model surface velocity measured by PIV. Single stopper (Y_R=0, Z_R=0)

bounce back with the stoppers at both ends as a support. It was found that the model bounced off the stoppers 1.5 msec after the initial collision. After leaving the stoppers, the velocities on both sides of the bottom edge of the mirror model became positive, which was expected to produce an oscillation with a vibration belly at the center. The time from the impact to rebound was shorter than that for a single stopper. This was because the stopper supported the mirror model at two points, resulting in less deformation of the mirror model.

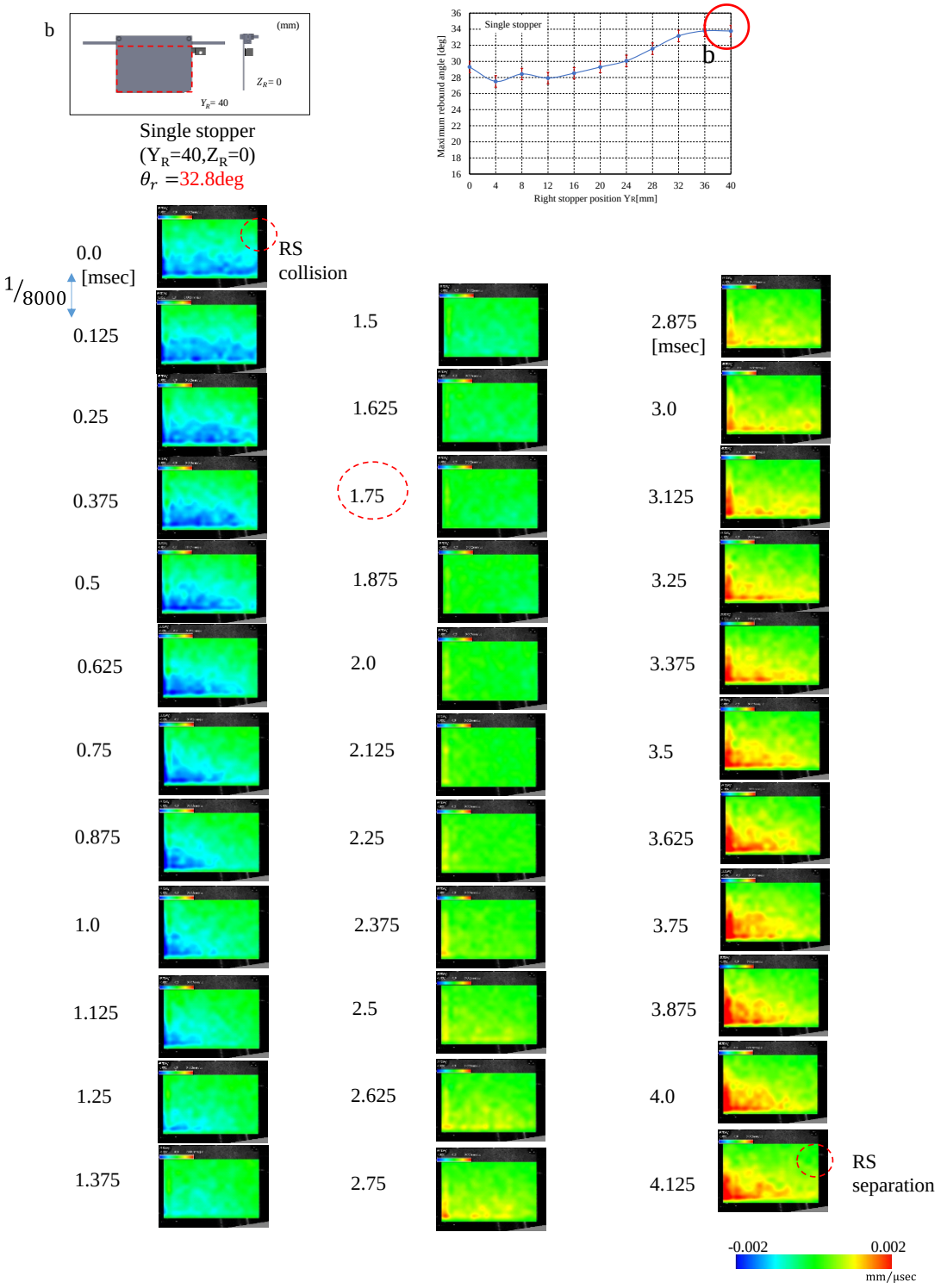

Figure 12. Transient response of mirror model surface velocity measured by PIV. Single stopper (Y_R=40, Z_R=0)

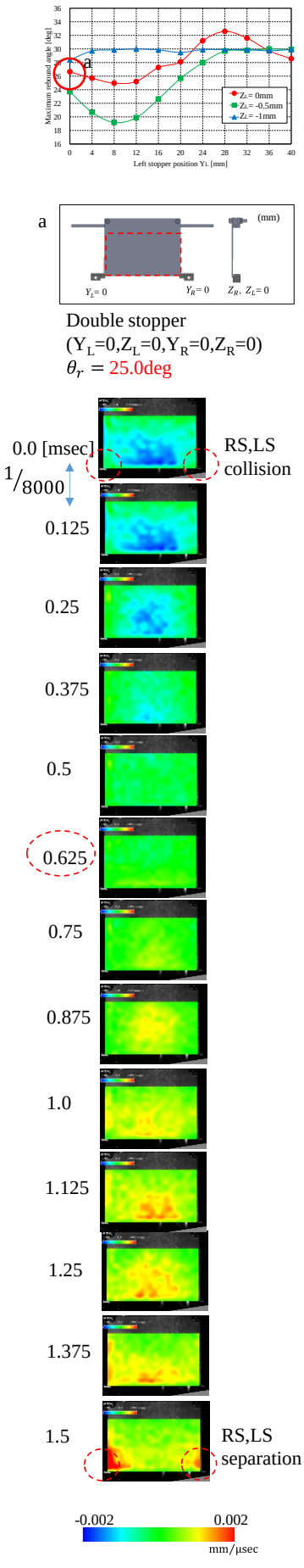

Figure 13. Transient response of the mirror model surface velocity measured by PIV. (a) Double stopper (Y_L=0, Z_L=0, Y_R=0, Z_R=0)

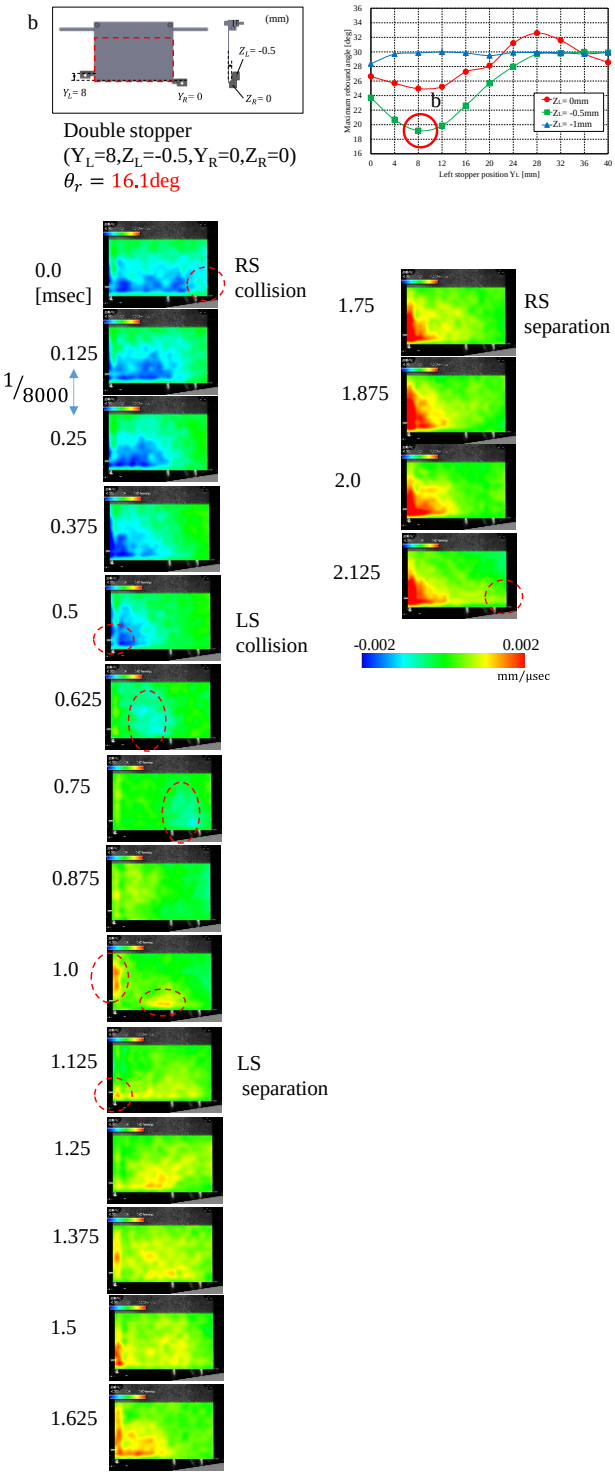

Figure 14. Transient response of the mirror model surface velocity measured by PIV. (b) Double stopper (Y_L=8, Z_L=-0.5, Y_R=0, Z_R=0)

Figure 14 shows the measurement results of the mirror model when the amount of bounce was minimized. The coordinates of the left stopper are Y_L = 0 and Z_L = -0.5, and the coordinates of the right stopper are Y_R = 0 and Z_L = 0. The right stopper was the same as that in Fig. 13, but the position of the left stopper was changed and the time of the second collision with the mirror model was different. The mirror model first collided with the right stopper, and the time was set to 0 msec. After collision with the right stopper, the lower left edge of the mirror model has a negative velocity, indicating that it has been deformed in

the same manner as the single stopper. Subsequently, the mirror model collided with the left stopper. After the second collision at 0.5 msec, the left end of the mirror model had zero velocity, but there was a light blue region near the center of the model, indicating that a negative velocity region was generated. This region moves slightly to the right at 0.625 to 0.75 msec, indicating that the mirror model is deformed in a wave-like manner. In Fig. 13, there is no such shift in the velocity distribution, and the deformation of the mirror model is assumed to be the same as that of the vibration mode at the boundary condition where the model is in contact with the stopper. However, in Fig. 14, the position where the maximum velocity is generated transiently changes from 1 msec to 1.5 msec, producing a more complex deformation and vibration state. This suggests that the second collision occurred before the elastic deformation caused by the first collision was complete, resulting in a more complex deformation and energy consumption. This mechanism resulted in a smaller maximum rebound angle.

Figure 15 shows the maximum rebound measured in the case of double collision. The stopper positions are Y_L = 28 and Z_L = 0 on the left side and Y_R = 0 and Z_R = 0 on the right side. Because the Z-axis heights of the left and right stoppers are the same, we can see that they initially hit the mirror model simultaneously. The tip of the mirror model then elastically deformed in the negative direction of the Z-axis, and at 0.625 msec, the surface velocity reached zero, indicating the maximum deformation state. The elastic deformation of the mirror model then began to recover, with the left side of the mirror model having a greater velocity than the right side. Therefore, the left stopper was the first to be separated from the mirror model at 1.0 msec. Subsequently, the positive velocity distribution at the tip of the mirror model extended along the entire length of the tip of the mirror model, showing the same behavior of increasing the amount of rebound, as shown in Fig. 12. This indicates that a large rebound occurred during the double collision.

3.5. Transient response of the mirror model displacement

Figures 16 - 18 show the transient behavior of the mirror model tip displacement, as measured by 3-D motion analysis.

Figure 16 shows the transient behavior during collision with a single stopper. The model collided with the stopper approximately 2 msec after the start of analysis. The measured velocity of the surface of the mirror model by 3-C PIV corresponds to the 0.0 msec figure in Fig. 11.

Tracking point P1 on the left side of the mirror model showed a negative displacement after the collision, indicating that it had a negative velocity. It is also clear that tracking point P7 on the right side of the mirror model was not displaced and had a velocity of almost zero, which is consistent with the slope of the displacement measurement results from the 3D motion analysis and the measurement results from the 3-C PIV. This confirms the validity of the 3-C PIV measurement for a solid surface. When the mirror model collided with a single stopper, the opposite side of the mirror model was elastically deformed

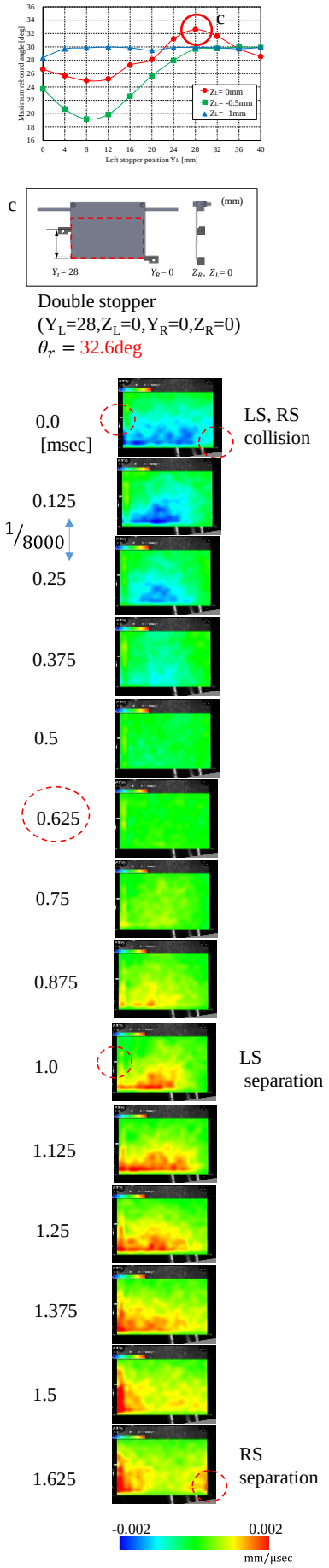

Figure 15. Transient response of the mirror model surface velocity measured by PIV. (c) Double stopper (Y_L=28, Z_L=0, Y_R=0, Z_R=0)

in the negative direction and rebounded because of its restoration. The measurement results in Fig. 16 show that the mirror model after detachment from the stopper vibrated with its tip in the opposite phase after detachment from the right stopper. The left tip had a higher velocity and the right tip had a lower velocity when it detached from the stopper, indicating that torsional vibrations occurred after the model detached from the stopper.

Figure 17 shows the transient behavior of the mirror model tip displacement when the rebound angle was minimized using a double stopper. In this case, the mirror model collided with the right stopper and then with the left stopper at approximately 0.5 msec later. Therefore, the displacement of P1 after 2.5 msec in the graph is limited to 0.5 mm. As shown in the previous section, in contact with the stopper, the mirror model oscillates in a complex manner, and vibrational motion appears in the displacement waveform immediately before the stopper disengages. At the time of disengagement, the positive velocity on the left side was extremely high, and the velocity difference with the right side caused torsional oscillations. In addition, high-frequency oscillations, which are expected to have higher vibration energy, are superimposed. Therefore, positional energy was consumed by the vibration of the mirror model, resulting in a smaller rebound angle.

Figure 18 shows the transient behavior of the mirror model tip displacement when the maximum rebound angle was reached using the double stopper. In this case, the mirror model and stopper collided almost simultaneously because the height of the stoppers were the same. As in the case of collision with a single stopper, the left tip of the mirror model was slightly displaced in the negative direction.

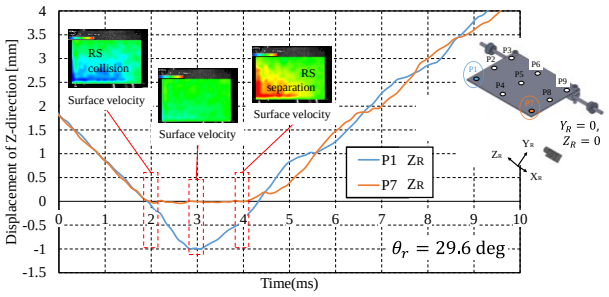

Figure 16. Transient response of the mirror model displacement with the single-stopper (Y_R=0, Z_R=0)

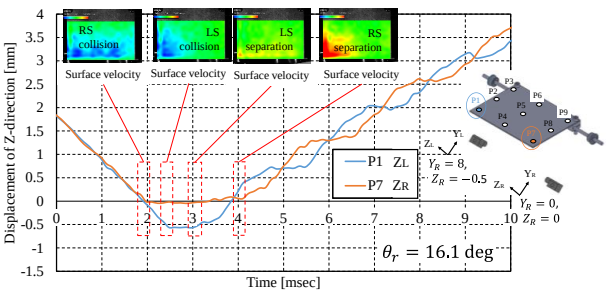

Figure 17. Transient response of the mirror model displacement with the double stoppers (Y_L=8, Z_L=-0.5 and Y_R=0, Z_R=0)

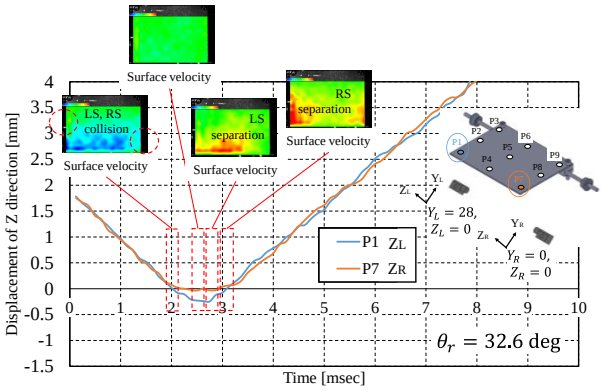

Figure 18. Transient response of the mirror model displacement with the double stoppers (Y_L=28, Z_L=0 and Y_R=0, Z_R=0)

This indicated that the mirror model was elastically deformed. However, in contrast to the single stopper, both sides of the tip of the mirror model rebound at almost the same velocity and without oscillation. Therefore, it can be assumed that the potential energy of the mirror model is not consumed by the vibration of the mirror model and that the amount of rebound is greater.

4. Conclusion

In this study, we investigated a method for suppressing the collision rebound angle of a mirror model by using the double collision phenomenon. The following conclusions were drawn:

(1) The rebound angle of the mirror model varies according to the stopper position and the number of stoppers. The double-stopper case was able to reduce the rebound angle compared to the single-stopper case. The minimum rebound angle was approximately 19 degrees for Y_L = 8 mm and Z_L = -0.5 mm, a 40% decrease compared to the single-stopper case.

(2) From the results of the 3-Component PIV measurement, the transient deformation of the mirror model can be observed from the velocity distribution. After the second collision, the left end of the mirror model had zero velocity, but a negative velocity region was generated in the center region. This region moved slightly to the right, indicating that the mirror model was deformed in a wave-like manner. The second collision causes a more complex deformation than the other stopper positions.

(3) When a double collision occurs during the elastic deformation after the collision, the vibration of the mirror model after the bounce increases, and the vibration of higher frequency components is also generated, resulting in a smaller bounce angle of the mirror model.

References

[1] S. C. Hunter, “Energy Absorbed by Elastic Waves During Impact,” *J. Mech. Phys. Solids*, vol. 5, no. 3, pp. 162–171, 1957.

[2] C. Zener, “The Intrinsic Inelasticity of Large Plates,” *Phys. Rev. Journals*, vol. 59, pp. 669–673, 1941.

[3] P. Mueller, R. Boettcher, A. Russell, M. Truee, and J. Tomas, “A

Novel Approach to Evaluate the Elastic Impact of Spheres on Thin Plates," *Chem. Eng. Sci.*, vol. 138, pp. 689–697, 2015.

[4] P.-K. Tsai, C.-H. Li, C.-C. Lai, K.-J. Huang, and C.-W. Cheng, "Approximation Solution for the Zener Impact Theory," *Mathematics*, vol. 9, p. 2222, 2021.

[5] J. Tengfei *et al.*, "Numerical–Analytical Model for Transient Dynamics of Elastic-Plastic Plate Under Eccentric Low-Velocity Impact," *Appl. Math. Model.*, vol. 70, pp. 490–511, 2019.

[6] Y. Kawazoe, "CAE of Tennis Rackets with Impact Phenomena. Prediction of Racket Response and a View of Restitution in Racket-Ball Impact (in Japanese)," *Trans. Japan Soc. Mech. Eng. Ser. C*, vol. 58, pp. 143–150, 1992.

[7] Y. Kawazoe, "Effect of Racket Frame In-Plane Hoop Vibrations on the Coefficient of Restitution and Energy Losses in Tennis Rackets (in Japanese)," in *The Proceedings of Joint Symposium Symposium on Sports Engineering Symposium on Human Dynamics*, 2006, pp. 130–135.

[8] H. Hata, H. Utsuno, and H. Matsuhisa, "Modal analysis of a metal baseball bat considering the restitution of ball (in Japanese)," in *The Proceedings of Joint Symposium Symposium on Sports Engineering Symposium on Human Dynamics*, 2004, pp. 89–94.

[9] T. Reilly, M. Hughes, and A. Lees, *Science and Racket Sports I*. Taylor & Francis, 2013.

[10] T. Allen, S. Choppin, and D. Knudson, "A Review of Tennis Racket Performance Parameters," *Sport. Eng.*, vol. 19, pp. 1–11, 2016.

[11] R. H. Bao and T. X. Yu, "Impact and Rebound of an Elastic–Plastic Ring on a Rigid Target," *Int. J. Mech. Sci.*, vol. 91, pp. 55–63, 2015.

[12] Y. Wang, Y. L. Yang, S. Wang, Z. Huang, and T. Yu, "Dynamic Behavior of Circular Ring Impinging on Ideal Elastic Wall: Analytical Model and Experimental Validation," *Int. J. Impact Eng.*, vol. 122, pp. 148–160, 2018.

[13] H. Matsumoto and M. Hirashima, "Vibration Behavior and Rebound Angle on the Collision of Mirror Models inside a SLR Camera," *J. Syst. Des. Dyn.*, vol. 7, pp. 393–404, 2013.

[14] H. Matsumoto and M. Hirashima, "Suppression Method for Rebound Amount of the Internal Mirror Model of an SLR Camera," *Mech. Eng. J.*, vol. 2, 2015.

[15] H. Matsumoto, M. Kumagai, and A. Kikuchi, "Rebound Vibration of Two -Plates Bonded Model for an Internal Mirror of SLR Camera," *J. Phys. Conf. Ser.*, vol. 744, 2016.

[16] E. O. Ekpruke, C. V. Ossia, and A. Big-Alabo, "Effect of Pre-Impact Vibrations on the Low-Velocity Impact Response of a Rectangular Plate," *Uniport J. Eng. Sci. Res.*, vol. 5, pp. 18–27, 2020.

[17] B. Lundberg, T. Rastemo, and J. Huo, "Effect of Pre-Impact Waves in an Elastic Rod on Coefficient of Restitution".

EPI International Journal of Engineering
Volume 6, Number 2, Aug 2023, pp. 72-77
DOI: 10.25042/epi-ije.082023.03

*p*ISSN 2615-5109
*e*ISSN 2621-0541

Analysis of Ability to Pay and Willingness to Pay in Trans Sulawesi Train Makassar - Parepare Route

Rizki Amaliah[a,*], Hera Widyastuti[b]

[a]Department of Civil Engineering, Faculty of Civil Planning and Geo Engineering, Institut Teknologi Sepuluh Nopember, Surabaya, Indonesia. Email : rizkyamaliaw97@gmail.com
[b]Department of Civil Engineering, Faculty of Civil Planning and Geo Engineering, Institut Teknologi Sepuluh Nopember, Surabaya, Indonesia. Email : hera@ce.its.ac.id

Abstract

The Trans Sulawesi train on the Makassar – Parepare route will traverse four significant stations with a planned length of ± 144 km and start operating in October 2022. Currently, it is not known the amount of travel fare applied to the Makassar - Parepare route. An analysis study of the ability to pay and willingness to pay for the Trans Sulawesi train for the Makassar - Parepare route aims to determine the value of the ability and willingness to pay for prospective service users to determine the Trans Sulawesi train rate. The data was collected by using interview surveys and distributing questionnaires through revealed preference and stated preference approaches. The ability to pay value was analyzed using the household budget method, and the willingness to pay value was analyzed based on the respondent's perception approach. Based on the results of the study obtained, the value of the ability to pay (ATP) of Rp144.279,00 and the value of willingness to pay (WTP) of Rp61.426,00.

Keywords: ATP; SDG number 9, 11; stated preference; Trans Sulawesi train; WTP

1. Introduction

Makassar City is the fourth largest city in Indonesia and the largest in eastern Indonesia, which continues to develop yearly. As a service center in Eastern Indonesia (KTI), the city of Makassar acts as a trade and service center, a center for industrial activities, a center for government activities, a node for goods and passenger transportation services on both land, sea, and air and a center for education and health services making the development of the city of Makassar Very fast [1]. There has been an increase in the population of the city of Makassar in the last five years. In 2015, the population of the city of Makassar reached 1,449,401 people, while in 2019 there were 1,545,373 people, and there was a population increase of 95,972 people during the last five years [2], [3].

In the Regional Spatial Plan for the Mamminasata Metropolitan National Strategic Area, Makassar City is designated as an urban planning zone and has become the center of growth and movement destination. (PEP RES RI No. 59 of 2011 concerning RTRW KSN Mamminata). With this stipulation, Makassar city has officially become the center of growth and the center of the agglomeration of economic activities of the Mamminasata KSN. The agglomeration area is an area that has many facilities (socio-economic facilities) so that it becomes the center of attraction for population activities [4].

In 2015 the Trans Sulawesi railway network began to be built to connect major cities in Sulawesi. This project is one of the national strategic projects of inter-city railways, and railway line work begins with the Makassar – Parepare route [5]. Before the existence of the Trans Sulawesi train, there were three choices of transportation modes to travel from Makassar to Parepare or vice versa, namely passenger cars with fares ranging from Rp60.000,00 – Rp70.000,00, with a travel time of ± 4 hours, motorbikes with a travel time of ± 3-4 hours and a private car with a travel time of ± 4 hours, the cost of traveling for a motorbike and a private car is enough to pay for fuel.

The Trans Sulawesi railway line Makassar – Parepare is planned with a total length of ± 144 km, crossing 4 major stations namely Maros, Pangkajene, Tanete Rilau, Barru and 8 smaller stations namely Mandai, Rammang-Rammang, Labakkang, Ma'rang, Mandalle, Takalasi, Mangkoso and Palanro [6]. The Trans Sulawesi train is planning to start operating on October 2022. Hoping that motorbike, private car, and passenger car service users will be able to use a new mode of transportation, the Trans Sulawesi train. Since now, there has been no rate for the Makassar-Parepare route. In determining the value of

*Corresponding author. Tel.: +62-851-5657-7273
St. Garuda Hallway Sriwijaya B 18 South Palu.
Palu, Indonesia, 94231

travel fares, the ability to pay and the willingness to pay off potential service users will need [7].

This study aims to determine the value of the ability to pay (ability to pay) and willingness to pay (willingness to pay) prospective users of the Trans Sulawesi train service, where this value can later be used to determine the fare for the Trans Sulawesi train route Makassar - Parepare.

2. Research Methods

The study was conducted by interviewing and distributing questionnaires using a revealed preference and stated preference approach to Makassar – Parepare travellers, because the research was conducted during the COVID-19 pandemic, the distribution of questionnaires was carried out online and offline.

2.1. Number of samples

In order to achieve best research results, especially in preference surveys, the number of samples must be between 75-100 samples for each category [8]. So, in this study, a sample of 200 respondents was taken consisting of users of motorbikes, private cars, passenger cars and Damri buses in the Trans Sulawesi train service route that is Makassar city, Marros regency, Pangkajene and Islands regency, Barru regency, and Parepare city.

2.2. Research settings

The location in this study is the Makassar-Parepare route, which means that the district-city areas that are in the route are part of the research location so that the travel agents who are the sample in this study are travellers.

2.3. Data collection

This research collected data based on facts in the field or what is commonly called primary data. The primary data in this study were obtained from interviews to determine the habits of travellers and surveys (questionnaire distribution) to service users of motorbikes, private cars, passenger cars and damri buses to achieve the research objectives, knowing the characteristics, the value of ability to pay, the value of willingness to pay and probability of switching modes, while secondary data, supporting data that supports primary data in achieving research objectives, are obtained from related agencies [9].

2.4. Questionnaire preparation

To obtain primary data in this study, a survey was conducted using a questionnaire which was divided into 4 parts, the characteristics of the respondents, the probability of switching modes, ability to pay and willingness to pay.

2.5. Data analysis

The data from the research survey that has been collected is processed and analyzed to achieve the research objectives, while the data analysis in this study is as follows:

- Characteristic Analysis

Analysis of passenger characteristics will be carried out using descriptive statistical methods, statistical techniques used to analyze data by describing or describing the data that has been collected so that a picture of the data will be obtained in the form of a percentage value of each characteristic [10].

- Ability to pay analysis

Ability to pay (ATP) is a person's ability to pay for transportation services he receives based on income that is considered ideal. The approach used in the ATP analysis is based on the allocation of costs for transportation and the intensity of the user's journey [11]. The factors that affect ATP is shown in Fig. 1.

ATP analysis is carried out using the household budget method, with the following formula 1 [11]:

$$ATP_{umum} = \frac{It.Pp.Pt}{Tt} \quad (1)$$

Description:

It : Total family income a month

Pp : % Income for transportation a month from total family income.

Pt : % Cost of using transportation from family transportation income a month

Tt : Total length of family trips a month a trip.

- Willingness to pay analysis

Willingness to pay (WTP) is the willingness of users to pay for the services they get. The approach used in the WTP analysis is based on the user's perception of the tariff for services. WTP is influenced by several factors as shown in Fig. 2.

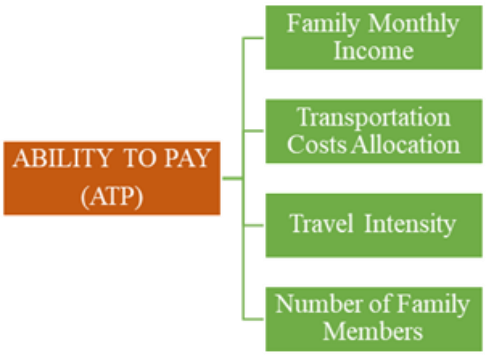

Figure 1. Factors of ability to pay [12]

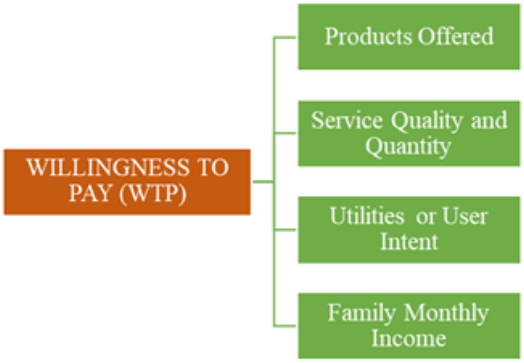

Figure 2. Factors of willingness to pay [12]

Willingness to pay value obtained from each respondent and processed to get the average value (mean) of the WTP value, with the formula 2 [7]:

$$MWTP = \frac{1}{N}\sum_{i=1}^{n} WTPi \quad (2)$$

Description:
MWTP : average
n : sample size
WTP i : the maximum WTP value of the i-th respondent

3. Results and Discussion

The samples obtained in this study were 211 respondents consisting of motorcycle users, private cars, and passenger cars. Before the distribution of the survey form, the questionnaire was tested online on the initial ten respondents, who were also part of the 211 respondents.

3.1. Characteristic analysis

Based on the research survey results, the frequency distribution per variable will then be analyzed descriptively to determine the characteristics of prospective users of the Trans Sulawesi railway service. The following is a recapitulation of the frequency distribution of respondents' characteristics that show in Table 1.

Table 1. Frequency distribution recapitulation

Variable	Category	Percentage
Gender	Male	37.0%
	Female	63.3%
Age	≤ 17 Years	0.5 %
	18 - 25 Years	69.2 %
	26 - 35 Years	18.0 %
	36 - 50 Years	10.4 %
	≥ 50 Years	1.9 %
Job	Not Working	12.8%
	Students	30.8 %
	Civil Servant/Army/Police	12.3 %
	Private/Contracted/SOE Employees	19.9 %
	Entrepreneur/Freelancer	19.0 %
	Housewife	4.7 %
	Retired	0.5 %
Income	≤ Rp. 1,000,000	49.3 %
	Rp1.000.0001 - Rp3.000.000	19.9 %
	Rp3.000.001 - Rp5.000.000	19.4 %
	Rp5.000.001 - Rp7.000.000	5.7 %
	Rp7.000.001 - Rp9.000.000	2.8 %
	≥ Rp9.000.000	2.8 %
The Number of Dependents	No dependents	55.9 %
	1 dependents	18.0 %
	2 dependents	9.5 %
	3 dependents	8.5 %
	4 dependents	5.2 %
	5 dependents	2.4 %
	6 dependents	0.5 %
Desire to Switch	Want to Switch	92.4 %
	Don't want to switch	7.6 %
Origin of Travel	Makassar City	50.7 %
	Maros Regency	7.6 %
	Pangkep Regency	13.7 %
	Barru Regency	10.9 %
	Parepare City	17.1 %
Travel Destination	Makassar City	43.1 %
	Maros Regency	11.8 %
	Pangkep Regency	10.4 %
	Barru Regency	10.0 %
	Parepare City	24.6 %
Travel Purpose	Working	18.5 %
	School/university	20.9 %
	Get treatment	0.9 %
	Holiday	38.4 %
	Homecoming	19.0 %
	Others	2.4 %
Travel Frequency	1 times	40.8 %
	2 times	18.5 %
	3 times	14.7 %
	4 times	8.5 %
	5 times	4.7 %
	6 times	3.3 %
	8 times	1.4 %
	10 times	2.4 %
	12 times	0.9 %
	15 times	0.9 %
	20 times	0.9 %
	25 times	0.9 %
	30 times	1.4 %
	40 times	0.5 %
Travel Cost	Rp10.000	0.5 %
	Rp20.000	4.3 %
	Rp30.000	2.8 %
	Rp35.000	0.5 %
	Rp40.000	2.4 %
	Rp45.000	0.5 %
	Rp50.000	9.0 %
	Rp60.000	1.9 %
	Rp70.000	2.4 %
	Rp80.000	0.5 %
	Rp100.000	26.1 %

Variable	Category	Percentage
	Rp120.000	2.8 %
	Rp140.000	1.4 %
	Rp150.000	9.0 %
	Rp160.000	0.5 %
	Rp165.000	0.5 %
	Rp180.000	0.5 %
	Rp200.000	20.4 %
	Rp240.000	0.9 %
	Rp250.000	2.4 %
	Rp300.000	4.7 %
	Rp350.000	1.4 %
	Rp400.000	0.9 %
	Rp500.000	3.8 %
Travel Time	90 Minutes	2.4 %
	120 Minutes	9.5 %
	150 Minutes	4.7 %
	180 Minutes	4.3 %
	210 Minutes	5.2 %
	240 Minutes	23.7 %
	270 Minutes	2.8 %
	300 Minutes	6.6 %
	330 Minutes	1.9 %
	360 Minutes	3.3 %
	390 Minutes	2.4 %
	420 Minutes	14.2 %
	450 Minutes	3.3 %
	480 Minutes	14.2 %
	510 Minutes	1.4 %
Main Mode of Transportation	Private Car	38.9 %
	Passenger Car	27.5 %
	Motorcycle	33.6 %
Alternative Mode of Transportation	Private Car	19.4 %
	Passenger Car	38.4 %
	Motorcycle	22.3 %
	Damri Bus	18.0 %
	Online Motorcycle Taxi	0.9 %
	Public Transportation	0.9 %

The frequency distribution is used to analyze the characteristics of the respondents so that later the characteristics of respondents who want to switch to using the Trans Sulawesi train will be known, as well as to see the distribution of the sampling frequency in this study [13].

3.2. Ability to pay analisis analysis

The value of the ability to pay respondents in this study was processed using the household budget method, namely based on family income, allocation of funds for transportation, and frequency of travel [14]. The results of the ability to pay calculation can be seen in Table 2.

Table 2. Ability to pay value of respondents

Sample	Income (Rp)	Transport. Fund allocation 1 month (Rp)	% transport. Fund allocation 1 month	Travel fund allocation 1 month (Rp)	% travel fund allocation 1 month	Travel frequency 1 month	ATP (Rp)
	A	B	C = B / A	D	E = D / B	F	G = D / F
1	7.000.000	600.000	8.57%	500.000	83.33%	3	166.667
2	1.000.000	500.000	50.00%	200.000	40.00%	2	100.000
3	3.000.000	500.000	16.67%	200.000	40.00%	4	50.000
4	1.000.000	300.000	30.00%	100.000	33.33%	1	100.000
5	3.000.000	100.000	3.33%	100.000	100.00%	1	100.000
6	3.000.000	200.000	6.67%	200.000	100.00%	3	66.667
7	1.000.000	100.000	10.00%	200.000	200.00%	3	66.667
8	9.000.000	100.000	1.11%	50.000	50.00%	1	50.000
9	1.000.000	100.000	10.00%	100.000	100.00%	5	20.000
10	1.000.000	100.000	10.00%	100.000	100.00%	4	25.000
….	…….	……	……	……	……	……	……
….	…….	…….	…….	…….	…….	…….	…….
195	3.000.000	100.000	3.33%	200.000	200.00%	1	200.000
ATP average (Rp)							144.279
ATP price (Rp)							144.279

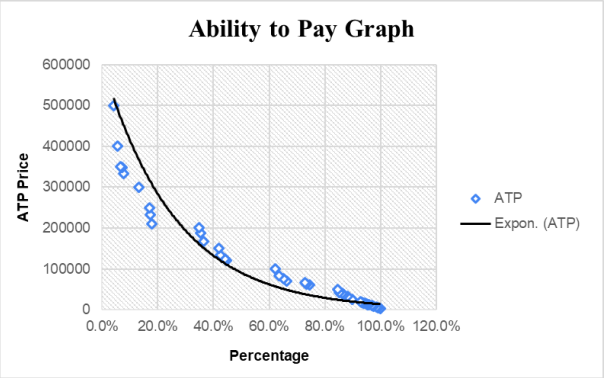

Figure 3. Graph of respondent's ability to pay value

Table 2 shows that the value of the ability to pay for respondents who want to switch to using the Trans Sulawesi train is Rp144.279,00 with a minimum value of Rp2.500,00 and a maximum value of Rp500.000,00. The results of the calculation of the respondents' ATP values are shown in Fig. 3.

Figure 3 shows that respondents have different values of ability to pay, influenced by family income, transportation funds allocation, and trip frequency.

3.3. Willingness to pay analisis analysis

The analysis based on the respondent's perception approach is needed to determine the value of the respondent's Willingness to pay, where the respondent determines the ideal fare that is willing to be issued for one trip. The following is the result of calculating the value of respondents' Willingness to pay, that show in Table 3.

Table 3. Willingness to pay value of respondents

Sample	Trans sulawesi rail ideal price (Rp)	WTP (Rp)
1	40.000	40.000
2	150.000	150.000
3	50.000	50.000
4	25.000	25.000
5	100.000	100.000
6	30.000	30.000
7	35.000	35.000
8	50.000	50.000
9	100.000	100.000
10	50.000	50.000
…….	…….	…….
…….	…….	…….
195	50.000	50.000
Average WTP (Rp)		61.426
WTP price (Rp)		61.426

Table 3 shows that the Willingness to pay the value of respondents who want to switch to using the Trans Sulawesi train is Rp61.426,00 with a minimum value of Rp3.000,00 and a maximum value of Rp150.000,00. The value of respondents' Willingness to pay is poured into a graph as shown in Fig. 4.

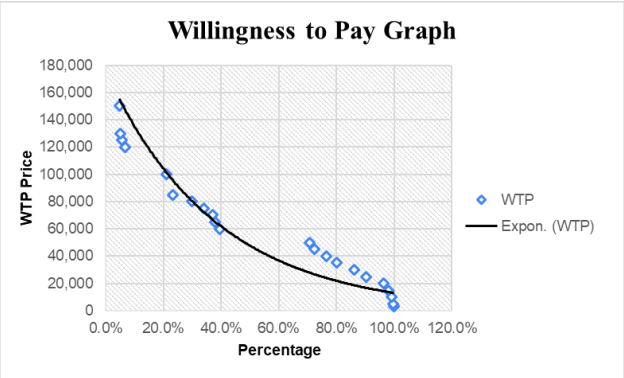

Figure 4. Graph of respondents willingness to pay value

Figure 4 shows that the ideal tariff value varies based on respondents' perceptions. This respondent's Willingness to pay was obtained from the average value of the respondent's WTP.

3.4. ATP – WTP relationship

Based on the calculation of ATP and WTP, the ability to pay value is Rp144.279,00 and Willingness to pay Rp61.426,00, which means that the respondent's ability to pay is greater than the respondent's Willingness to pay, so the respondent or prospective user of the Trans Sulawesi KA services in this study is a chosen rider, namely respondents who can have their vehicle or can choose the mode to be used [15]. The relationship between the value of ATP – WTP is shown in Fig. 5.

Based on Fig. 5, relationship between the value of ATP - WTP, the determination of the tariff as far as possible is not above the threshold of the ATP value of Rp. 144,279, but if it exceeds the ATP value, the government should provide support in the form of a subsidy for the difference between the tariff price and the respondent's ATP value so that the tariff applied is the same as the respondent's ATP value. The WTP value of respondents below the ATP

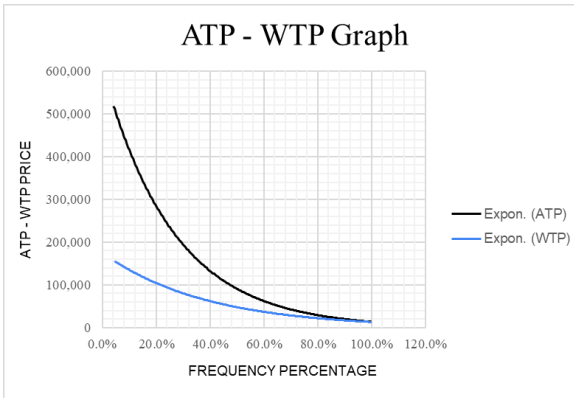

Figure 5. Ability to pay and willingness to pay value relationship

value can still increase rate by increasing service quality or improving service performance.

4. Conclusion

Based on the results of calculations and analysis, it can be concluded that:

1. From 211 respondents spread across Makassar city, Maros regency, Pangkajene and Islands regency, Barru regency, and the City of Parepare, it is known that the majority of the respondents are 63.0% are female, 69.2% aged between 18-25 years, 30.8% work as a student/student, 55.9% have no dependents, 49.3% earning Rp1.000.000,00, 50.7% are from Makassar, 43.1% have a trip destination to Makassar, 38.4% intend to go on vacation, 40.8% travel once a month, 26.1% spent a trip cost of Rp100.000,00, 23.7% spent 240 minutes of travel time, 38.9% use passenger cars as the main transportation, 38.4% use passenger cars as alternative transportation, 92.4% of respondents want to switch to using the Trans Sulawesi Railway
2. The value of the ability to pay respondents who want to switch to using the Trans Sulawesi train is Rp144.279,00, and the value of willingness to pay of respondents who want to switch to using the Trans Sulawesi train is Rp61.426,00, this shows that the ATP value is greater than the WTP value.

Acknowledgements

We want to thank the Transportation Department of Parepare City and all respondents willing to fill out the research questionnaire and become the sample in this study.

References

[1] M. Arsyal, “Strategi Pengendalian Fungsi Ruang Perumahan Bumi Tamalanrea Permai (BTP),” *J. Plano Madani*, vol. 4, pp. 101–108, 2015.
[2] “Kecamatan Makassar dalam Angka 2015,” Makassar, 2015.
[3] “Kecamatan Makassar dalam Angka 2020,” Makassar, 2020.
[4] R. F. Bakri, M. Ali, and V. V. Natalia, “Disparitas Pembangunan antar Wilayah Makassar, Maros, Gowa, dan Takalar,” in *Conference: Temu Ilmiah Ikatan Peneliti Lingkungan Binaan Indonesia (IPLBI) Malang*, 2016, pp. 1–6.
[5] I. N. Jelita, “Ini Tujuan Dibangunnya Jalur Kereta Api Trans-Sulawesi,” *Media Indonesia*, 2020. https://mediaindonesia.com/ekonomi/353996/ini-tujuan-dibangunnya-jalur-kereta-api-trans-sulawesi
[6] “Jalur kereta api Makassar–Parepare,” *Wikipedia*, 2021. https://id.wikipedia.org/wiki/Jalur_kereta_api_Makassar–Parepare
[7] W. Kriswardhana, “Probabilitas dan Willingness to Pay Pengguna Bus untuk Beralih ke Kereta Api dalam Rencana Re-Aktivasi Rute Kereta Api Jember-Panarukan,” Institut Teknologi Sepuluh Nopember, 2015.
[8] R. S. Irsadi and H. Widyastuti, “Probability Modal Transfer to the Forwarder at Terminal Lamong Bay Surabaya,” *ITS J. Civ. Eng.*, vol. 32, pp. 32–37, 2017.
[9] I. Basuki and S. Chuadinata, “Analisis Ability to Pay and Willingness to Pay Jasa Kereta Api Yogyakarta International Airport,” *J. Spektran*, vol. 7, pp. 140–146, 2019.
[10] A. Pramudita and H. Widyastuti, “Studi Pemilihan Moda Kereta Api Eksekutif dan Kereta Api Semi Cepat Rute Jakarta-Surabaya Menggunakan Teknik Stated Preference,” *J. Apl. Tek. Sipil*, vol. 18, pp. 165–170, 2020.
[11] E. Zohra, R. S. Suyono, and S. N. Kadarini, “Analisis Abillity To Pay (ATP) dan Willingness To Pay (WTP) untuk Penetuan Tarif Pada Perencana Angkutan Umum BRT di Kota Pontianak,” *J.*

Mhs. Tek. Sipil Univ. Tanjungpura, vol. 5, pp. 1–8, 2018.
[12] M. R. Permata, "Analisa Ability to Pay dan Willingness to Pay pengguna jasa Kereta Api Bandara Soekarno Hatta-Manggarai," Universitas Indonesia, 2012.
[13] R. Hariwahyudi, D. F. Suprapto, and S. Malkhamah, "Pelayanan dan Tarif Kereta Api Perkotaan di Yogyakarta," *J. Transp.*, vol. 16, pp. 173–182, 2016.
[14] A. Anggunani, "Analisis Ability to Pay dan Willingness to Pay Pengguna Layanan Kereta Api Kaligung dan Kereta Api Kamandaka (Studi Kasus: Kereta Api Kaligung dan Kereta Api Kamandaka Lintas Layanan Semarang-Tegal)," Universitas Gadjah Mada, 2016.
[15] Zulfikar, "Analisis Ability To Pay dan Willingness To Pay Penumpang Angkutan Umum Minibus L 300. Studi Kasus :Rute Meulaboh di Banda Aceh," Universitas Teuku Umar, 2015.

EPI International Journal of Engineering
Volume 6, Number 2, Aug 2023, pp. 78-82
DOI: 10.25042/epi-ije.082023.04

*p*ISSN 2615-5109
*e*ISSN 2621-0541

Assessment of Stone Ash as a Lightweight Concrete Constituent Material with the Addition of Bestmittel Additives

Budiman[a], James Williams Tiranda Patanduk[b]

[a]Department of Civil Engineering, Polytechnic State of Fakfak. E-mail: budiman@polinef.id
[b]Department of Civil Engineering, Polytechnic State of Fakfak.

Abstract

Technological advances in the field of building construction have developed very rapidly, so we need a construction technology that can reduce exploitation of nature. Utilization of stone ash is one of the new material alternatives in concrete mixtures with the addition of the bestmittel additive to accelerate drying in concrete. The purpose of this study is to determine the aggregate characteristics, specific gravity and compressive strength of concrete. The method used is laboratory experimental research with variations in stone ash samples of 5%, 10% and 15% to the weight of sand with the addition of 0.6% bestmittell additive to the weight of cement. The results showed that stone ash and bestmittell additives affect the characteristics of the concrete. The value of specific gravity increases with increasing percentage of stone ash, namely 1898.77 kg/m^3 in normal concrete, 1911.35 kg/m^3 of 5% stone ash concrete, 1922.34 kg/m^3 of 10% stone ash concrete and 1927.06 kg/m^3 on 10% stone ash concrete. The compressive strength value of characteristic for the compositions AB 5%, AB 10% and AB 15% are 10.08 Mpa, 10.35 Mpa and 10.88 Mpa respectively, an increase compared to normal AB 0% concrete, namely 9.03 Mpa at 28 days.

Keywords: Compressive strength; bestmittel additive; stone ash; *volume weight*

1. Introduction

The development of the concrete industry in Indonesia is very advanced and developing. As development increases in a country, the use of construction materials increases. Concrete is a mixture consisting of cement, fine aggregate, coarse aggregate and air. The Principles of Infrastructure Asset Management say that infrastructure must be managed well so that it can always function well economically throughout its life [1].

Split stone industrial companies are needed a lot in construction, from the production of split stone with various size variants it will produce waste called stone ash waste. Stone ash is very abundant and less desirable as a material. Based on this problem, stone ash waste was raised in this research to provide innovation as an additive to good construction materials, in the form of using stone ash waste material in lightweight concrete mixtures with the addition of bestmittel. Therefore, concrete technological innovation is always required to answer the challenges of needs, including being environmentally friendly and having a low specific gravity (lightweight concrete). Lightweight concrete generally has a specific gravity of less than 1850 kg/m^3 [2].

Lightweight concrete is concrete whose specific gravity is smaller than normal concrete. According to [3], lightweight concrete is concrete that contains light aggregate and has a specific gravity of no more than 1900 kg/m^3, whereas according to [4] lightweight concrete has a specific gravity of between 1000-2000 kg/m^3. Lightweight concrete can be made using additional materials, namely lightweight aggregate, concrete without fine aggregate (non-sand) and foam concrete

Lightweight concrete can be defined as a type of concrete which includes an expanding agent in that it increases the volume of the mixture while giving additional qualities such as nailibility and lessened the dead weight [5]. It is lighter than the conventional concrete with a dry density of 300kg/m up to 1840 kg/m 87 to 23% lighter. It was first introduced by the Romans in the second century where 'The Pantheon' has been constructed using pumice ,the most common type of aggregate used in that particular year [6]. From there on, the use of lightweight concrete has been widely spread across other countries such as USA, UK and Sweden.

In recent years, more attention has been paid to the development of lightweight aggregate concrete [7]. The specific gravity of concrete can be lowered either by using porous, therefore lightweight aggregates instead of ordinary ones, or introducing air into the mortar, or removing the fine fractions of aggregate and compacting concrete only partially. In all cases, the main goal is to introduce voids into the aggregate and the mortar or between mortar and aggregate. A combination of these methods can also be made in order to reduce further the weight of concrete. The use of lightweight aggregates

*Corresponding author. Tel.: +62-812-7706-1052
Jalan TPA Imam Bonjol Atas Air Merah, Kelurahan Wagom Fakfak, Papua Barat, Indonesia 98611

is by far the simplest and most commonly used method of making a lightweight concrete [6].

Several previous studies with added materials, both natural and artificial fibers, such as: [8] examined the opportunity for nutmeg shells as a replacement material for gravel in lightweight concrete, [9] examined the effect of a mixture of banana fiber on concrete. [10] researched the effect of coconut shell (endocarp) substitution in concrete mixtures as a sound dampening fiber material. [11] examined lightweight concrete from a mixture of styrofoam and sawdust. [12] researched the manufacture of lightweight concrete from artificial aggregates with the addition of plastic. [13] researched the effect of candlenut shells as a substitute for coarse aggregate on the mechanical properties of concrete. The research will be carried out using stone ash and the additive Bestmittel in lightweight concrete.

Additives are materials other than the main elements of concrete (water, cement and aggregate) that are added to the concrete mix. The aim is to change one or more properties of concrete while it is still fresh or after hardening, for example accelerating hardening, increasing ductility (reducing brittle properties), reducing hardening cracks, and so on [4].

This research uses stone ash as a building block for lightweight concrete by adding the additive besmittel. The research was carried out in the Fakfak State Polytechnic Civil Engineering materials testing laboratory. The aim of this research is to determine the characteristics, specific gravity and compressive strength values of lightweight concrete. rock ash composition of 5%, 10% and 15% with 0.6% besmittel. This research is a development of previous research. Previous research results have shown that stone ash can contribute as a replacement material for sand.

2. Literature Review

2.1. Light concrete

Lightweight concrete has a density of not more than 1900 kg/m^3 [14] and has a compressive strength value of 0.35-6.90 Mpa while [15] provides a limitation for lightweight concrete, namely concrete with a weight below 1800 kg/m^3. A according to [16] lightweight concrete has a density between 1000-2000 kg/m^3.

Table 1. Types of lightweight concrete by [14]

Weight concretes (kg/m^3)	Compressive strength (MPa)	Types lightweight concretes
240-800	0.35-6.9	Low-Density concretes
800-1440	6.9-17.3	Moderate Strength lightweight concretes
1440-1900	>17.3	Structural lightweight concretes

Table 2. Types of lightweight concrete by [15]

Weight concretes (kg/m^3)	Compressive strength (MPa)	Types lightweight concretes
1400-1800	>17	Structural lightweight concretes
500-800	7-14	Masonry concretes
<800	0.7-7	Insulating concretes

Types of lightweight concrete based on concrete weight and compressive strength [14], [15] as shown in Tables 1 and 2.

Normal concrete is obtained by mixing Portland cement, water and aggregate, while for lightweight concrete the constituent materials are very dependent on the type of lightweight concrete. According to [17] there are 3 types of lightweight concrete, namely lightweight aggregate concrete, foam concrete and concrete without fine aggregate. The same thing was also conveyed by [4], several methods that can be used to reduce the weight of concrete include the following:

1) Making gas / air bubbles in the cement mix.
2) Using light aggregate, for example fired clay, pumice stone or artificial aggregate.
3) Making concrete without using fine aggregate grains (non-sand concrete).

Several parameters that affect the fine aggregate (sand) in determining the quality of the concrete are sludge content, moisture content, volume weight, absorption, specific gravity, fineness modulus and organic content [16].

The level of sludge is the percentage of size that passes filter No.200 according to ASTM and British Standards or 80 DIN (Germany) or standard filter hole size = 0.075 mm. Laboratory testing is generally carried out by the washing method according to ASTM C-117 (2000 Sieve in Mineral Aggregate by Washing) Standard Test Method for Materials. Tolerance for testing the fine aggregate sludge content is 0.2%-6%.

The water content in the aggregate is greatly influenced by the amount of water contained in the aggregate. The bigger the difference between the original aggregate weight and the aggregate weight after oven drying, the more water is contained by the aggregate and vice versa. Tolerance of testing moisture content in fine aggregate is 3%-5%.

The volume weight is the ratio between the dry aggregate weight and its volume. The aim is to determine the weight of the fine aggregate. The test tolerance for fine aggregate is 1.4 kg/ltr-1.9 kg/ltr.

The absorption is the percentage by weight of water that can be absorbed by the material to the weight of dry aggregate. Tolerance of testing fine aggregate 0.2%-2% and coarse aggregate 0.2%-4%.

The specific gravity is the ratio between the weight of dry aggregate and the weight of distilled water whose content is the same as the aggregate content in a saturated state at a certain temperature. The test tolerance for fine aggregate is 1.6%-3.3%.

The organic Ingredients, are materials contained in aggregates that can cause damage to concrete. The organic substances contained in fine aggregates generally come from destroyed plants, especially in the form of humus and organic sludge. Harmful organic substances include sugar, oil and fat. Sugar can inhibit cement binding and the development of concrete strength, while oil and grease can reduce cement binding capacity. The test tolerance for fine aggregates is less than a value of 3.

2.2. Stone ash

Stone ash is a fine aggregate that passes through a 4.75 mm diameter sieve and is retained on a 0.075 mm sieve, so stone ash is a waste that is useful as a mixture of construction building materials because stone ash can function as a fine aggregate to replace sand in concrete and asphalt mixtures.

2.3. Bestmittel

Bestmittel is a special formula that is very economical in the casting process so it makes concrete harden faster at a young age and reduces water usage during casting thereby increasing the quality/strength of the concrete and is very helpful for casting with a very tight time schedule because the concrete hardens quickly at an early age (7 – 10 days) and increases the quality/strength of concrete by 5% - 10% with a content used of 0.2% - 0.6% of the cement weight.

2.4. Compressive strength

Compressive strength [18] provides an understanding of the compressive strength of concrete, which is the amount of load per unit area, which causes the concrete specimen to crumble when loaded with a certain compressive force, which is generated by a compression machine.

3. Research Methodology

3.1. Research stages

The stages of research, prepare tools and materials. The main materials consist of gravel, sand, cement, stone ash and bestmittel. Testing the characteristics of coarse and fine aggregate and calculating the combination of fine aggregate and stone ash with a bestmittel percentage of 0.6% to obtain the appropriate composition. Designing a concrete mix (mix design) with an f'c of 10 MPa. Preparation of concrete mix composition with AB variations of 5%, 10% and 15% of the weight of sand. Concrete maintenance for 3, 7 and 28 days. The compressive strength values of the concrete were analyzed and concluded.

3.2. Characteristic testing

Aggregate characteristic testing uses study literature as shown [15] in Table 3.

3.3 Compressive strength testing

Concrete compressive strength test results using compression machine test were analyzed by using compressive strength equation [18] :

$$fc = \frac{P}{A} \qquad (1)$$

where,

fc = compressive strength (kg/cm^2)

P = load (kg)

A= the weighted cross-sectional area (cm^2)

Table 3. Aggregate testing and method

No	Types of testing	Method
1	Filter Analysis	SNI 03-1968-1990
2	Specific Weight and Fine Aggregate Absorption	SNI 03-1970-1990
3	Specific Weight and Absorption of Coarse Aggregates	SNI 03-1969-1990
4	Water Content	SNI 03-1971-1990
5	Volume Weight	SNI 03-4804-1998

4. Results and Discussion

The results of testing the characteristics test of coarse (gravel) and fine (sand) aggregates are as in Tables 4 and 5.

Testing the characteristics of fine aggregate obtained a mud content value of 3.6% which meets the requirements and is suitable for use in concrete mixtures. According to [4], fine aggregate must not contain more than 5% mud and not contain organics that can damage concrete. Its use is to fill the space between coarse aggregates and provide workability. The sand fineness modulus value of 3.66 meets the requirements for zone 1 and is included in the coarse sand category. Likewise, testing the sludge content of coarse aggregate obtained a value of 0.27% which meets the requirements and is feasible. According to [19] coarse aggregate should not contain more than 1% silt. The coarse aggregate modulus is in the 4.75 - 40 mm zone. [20] A normal weight washed sand with a (4.75mm) maximum size is used as fine aggregates its use is to fill the space between coarse aggregates and provide discomfort.

To know the strength and quality of concrete using a stone ash (AB) composition of 0%, 5%, 10% and 15% with

Table 4. The result of coarse aggregate testing

No	Aggregate characteristics	Interval	Testing result	Description
1.	Mud leves	Maks. 1%	0.27 %	Meets
2.	Water content	0.5 - 5%	0.50 %	Meets
3.	Volume weight	1.6 - 1.9 kg/liter	1.61 kg/liter	Meets
4.	Absorption	Maks. 4%	4 %	Meets
5.	Specific weight			
	Dry-based S.W	1.6 - 3.3	2.45	Meets
	Dry-surfaced S.W	1.6 - 3.3	2.57	Meets
6.	Roughness modulus	5.5 – 8.5	6.74	Meets

Table 5. The result of fine aggregate testing

No	Aggregate characteristics	Interval	Testing result	Description
1.	Mud leves	Maks. 5%	3.60 %	Meets
2.	Water content	0.5 - 5%	2.24 %	Meets
3.	Volume weight	1.4 - 1.9 kg/liter	1.51 kg/liter	Meets
4.	Absorption	0.2 – 2%	1.08 %	Meets
5.	Specific weight			
	Real S.W	1.6 - 3.3	2.33	Meets
	Dry-based S.W	1.6	2.28	Meets
	Dry-surfaced S.W	1.6	2.30	Meets
6.	Roughness modulus	1.5 – 3.8	3.66	Meets

a bestmittel percentage of 0.6% with a planning cement water factor (W/C) = 0.45 as shown in Tables 6-9.

The calculating the planning results above, it is obtained that the percentage of natural sand aggregate required with an AB percentage of 5% can save the use of natural sand by 4.99%, for AB 10% it can save the use of natural sand. natural sand of 9.99% while AB 15% can save the use of natural sand of 14.99% of the total planned sand without using stone ash (AB). This plan value shows that the higher the percentage of stone ash (AB) with a percentage of 0.6% bestittle used in the concrete mixture, the lower the need for natural sand aggregate. The results of testing the weight of fresh concrete mixed with AB concrete with 0.6% bestmittel with an air correction factor value of 0.45 obtained the average value of the volume weight of cylindrical test objects as in Table 9 and Fig. 1.

Figure 2 shows the weight of fresh concrete AB + 0.6% bestmittel which has the effect of decreasing concrete weight sequentially, namely AB 5%, 10% and 15%, the greater the percentage of stone ash used, the lighter the weight of the concrete volume itself. This practice will allow achieving certain properties of fresh and hardened concrete [21]. As also emphasized by [22] the use of appropriate mix proportions of materials for on-site concrete production will allow achieving appropriate mix proportions for a given strength characteristic rather than the usual procedure of using non-approved mix ratios for the design target strength.

The results of the analysis of concrete compressive strength test values using stone ash (AB) with 0.6% bestmittel have an influence on the concrete compressive strength values. The higher the percentage of AB given to

Table 6. The results of concrete mix design abu batu (AB) 0% with bestmittel 0.6%

Concrete material	Weight (kg/m^3)	Ratio to the amount of the cement (kg)	Weight for one sample (kg)	Weight for nine sample (kg)
Water	232.543	0.742	1.479	13.314
Cement	311.111	1.000	1.979	17.812
Sand	484.516	1.557	3.082	27.741
Coarse	1121.82	3.605	7.136	64.230
Amount	2150.00		13.678	123.099

Table 7. The results of concrete mix design abu batu (AB) 5% with bestmittel 0.6%

Concrete material	Weight (kg/m^3)	Ratio to the amount of the cement (kg)	Weight for one sample (kg)	Weight for nine sample (kg)
Water	232.543	0.742	1.479	13.314
Cement	311.111	1.000	1.979	17.812
Sand	460.291	1.479	2.928	26.354
Coarse	1121.82	3.605	7.136	64.230
AB+bestm ittel	24.225	0.077	0.1541	1.386
Amount	2150.00		13.678	123.099

Table 8. The results of concrete mix design abu batu (AB) 10% with bestmittel 0.6%

Concrete material	Weight (kg/m^3)	Ratio to the amount of the cement (kg)	Weight for one sample (kg)	Weight for nine sample (kg)
Water	232.543	0.742	1.479	13.314
Cement	311.111	1.000	1.979	17.812
Sand	436.065	1.401	2.774	24.967
Coarse	1121.82	3.605	7.136	64.230
AB+bestm ittel	48.451	0.155	0.308	2.773
Amount	2150.00		13.678	123.099

Table 9. The results of concrete mix design abu batu (AB) 15% with bestmittel 0.6%

Concrete material	Weight (kg/m^3)	Ratio to the amount of the cement (kg)	Weight for one sample (kg)	Weight for nine sample (kg)
Water	232.543	0.742	1.479	13.314
Cement	311.111	1.000	1.979	17.812
Sand	411.839	1.323	2.620	23.580
Coarse	1121.82	3.605	7.136	64.230
AB+bestm ittel	72.677	1.232	0.462	4.160
Amount	2150.00		13.678	123.099

Table 10. The weight volume of freshly concrete

No	Sampel Concrete	Volume of Freshly Concrete (kg/m^3)
1	AB + Bestmittel 5%	1927.06
2	AB + Bestmittel 10%	1922.35
3	AB + Bestmittel 15%	1911.34

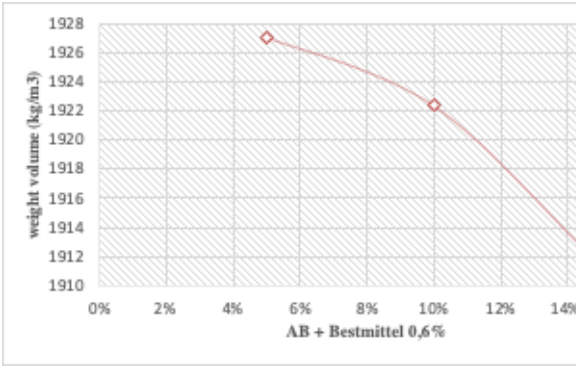

Figure 1. Graphic of weight volume

Table 11. The value of compressive strength Characteristics of concrete

No	Sample Concrete	Value f'c (kg/cm^2)
1	AB + Bestmittel 5%	102.88
2	AB + Bestmittel 10%	105.52
3	AB + Bestmittel 15%	111.04

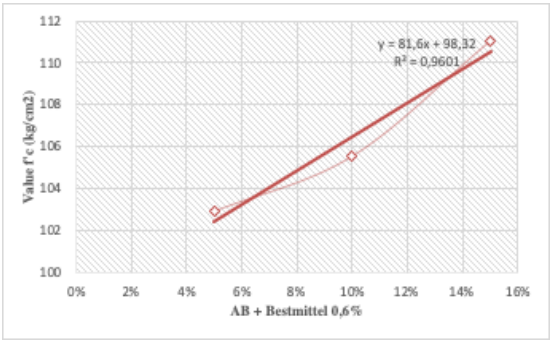

Figure 2. The f`c value

the concrete mixture, the higher the compressive strength value. The characteristic compressive strength values of concrete at 28 days are as in Table 10 and Fig. 2.

Figure 2 shows the compressive strength value of concrete using stone ash (AB) added with 0.6% bestmittel as a partial replacement for natural sand to improve the quality of the concrete. The higher the percentage, the more compressive strength value increases. The compressive strength values of rock ash concrete in the composition of AB 5%, 10% and AB 15% were obtained at 102.88 kg/cm^2, 105.52 kg/cm^2 and 111.04 kg/cm^2, increasing at 28 days. These results prove that stone ash can function as a fine aggregate to replace sand for lightweight concrete mixture formulas, while bestmittel has the role of accelerating concrete hardening and increasing concrete strength.

According to [14] lightweight concrete is concrete that has a compressive strength value of around 6.9-17.3 Mpa. Based on the range of compressive strength values, it shows that the research results of concrete without AB are included in the lightweight concrete category, namely 9.83 Mpa, as well as concrete using 5%, 10% and 15% AB at 28 days has values of 10.08 Mpa, 10.35 Mpa and 10.88 respectively. Mpa so it was concluded that the use of stone ash (AB) with the additive Bestmittel 0.6% increased the compressive strength value of the concrete.

Lightweight concrete according to [21] lightweight concrete has a density between 1000-2000 kg/m^3 with types of lightweight concrete consisting of structural, lightweight and very light structural concrete. Lightweight concrete from rock ash (AB) with 0.6% bestmittel has an average weight of 1920.25 kg/m^3 and a maximum compressive strength value of 10.88 MPa so that the concrete is included in the lightweight structure category.

Classification of lightweight concrete based on the weight of concrete If referring to [16], then most of the weight of light concrete in this study is classified as light structure as an insulator, [14] includes concrete with low density, the classification of [15] includes heat-resistant lightweight concrete and [17] includes lightweight aggregate concrete .

5. Conclusions

The use of nutmeg skin as a coarse aggregate material in the concrete mixture affects the volume weight of the concrete. The weight of the concrete gets lighter along with the higher the percentage used. The average volume weight obtained was 1810,06 kg/m^3. Based on the weight of the concrete sample, it is classified as light structure, includes concrete with low density and includes lightweight aggregate concrete. The compressive strength values for the characteristics of concrete at a composition of 10%, 20% and 30% were obtained at 28.42 kg/cm^2, 31.65 kg/cm^2 and 32.68 kg/cm^2 which increased while the use of nutmeg shells at 40% and 50% compositions was obtained. values of 29.09 kg/cm^2 and 27.38 kg/cm^2 decreased at the age of 28 days. The increase in the value of the compressive strength of concrete (fck') occurred starting at the composition of 20% and 30% at 10.20% and 13.03% and begin to decrease at the composition of 50% by 3.65%.

Research suggestions as further research is needed in determining the appropriate composition for both lightweight concrete and normal concrete. Further research is needed using a smaller percentage interval and It is recommended to use nutmeg shell as coarse aggregate in light concrete with a low density scale and intended for light structures, besides saving costs, it can also reduce waste that has an impact on the environment.

References

[1] R. A. A. Soemitro and H. Suprayitno, "Pemikiran Awal tentang Konsep Dasar Manajemen Aset Fasilitas," *J. Manaj. Aset Infrastruktur Fasilitas*, vol. 2, pp. 1–14, 2018.

[2] L. J. Murdock and K. M. Brooks, *Bahan dan Praktek Beton*, 4th ed. Jakarta: Erlangga, 1999.

[3] "SNI- 03-2847-2002: Tata Cara Perhitungan Struktur Beton untuk Bangunan Gedung," Bandung, 2002.

[4] K. Tjokrodimuljo, *Teknologi Beton*, 3rd ed. Yogyakarta: Yogyakarta Biro penerbit KMTS FT 2012, 2012.

[5] M. L. Zakaria, *Materials and Development, Language and Library Board*. 1978.

[6] M. R. Sarmidi, "First Report Research Project on Light Weight Concrete," Universiti Teknologi Malaysia, 1987.

[7] T. Y. Lo, W. P. Tang, and H. Cui, "The Effects of Aggregate Properties on Lightweight Concrete," *Build. Environ.*, vol. 42, no. 8, pp. 3025–3029, 2007.

[8] Budiman, Imran, and W. T. P. James, "The Use of Nutmeg Shell as a Lightweight Concrete Material," *INTEK J. Penelit.*, vol. 7, no. 2, pp. 116–122, 2022.

[9] S. Hani and Rini, "Pengaruh Campuran Serat Pisang Terhadap Beton," *Educ. Build. J. Pendidik. Tek. Bangunan dan Sipil*, vol. 4, pp. 40–45, 2018.

[10] D. E. Putra and R. Karolina, "Pengaruh Subtitusi Tempurung Kelapa (Endocarp) pada Campuran Beton sebagai Material Serat Peredam Suara," *J. Tek. Sipil USU*, vol. 2, 2013.

[11] R. B. Anugraha and S. Mustaza, "Beton Ringan dari Campuran Styrofoam dan Serbuk Gergaji dengan Semen Portland 250, 300 dan 350 kg/m^3," *J. Apl.*, vol. 8, pp. 57–66, 2010.

[12] E. Rommel, "Pembuatan Beton Ringan dari Aggregat Buatan Berbahan Plastik," *J. GAMMA*, vol. 9, pp. 137–147, 2013.

[13] E. Febriani, "Pengaruh Pemanfaatan Pecahan Beton sebagai Alternatif Pengganti Agregat Kasar sebagai Campuran Beton K 250 KG/CM^2," *KURVAS J. Keilmuan dan Apl. Tek. Sipil*, vol. 1, 2013.

[14] N. K. Raju, *Design of Concrete Mixes*. New Delhi: CBS, 1985.

[15] J. A. Dobrowolski, *Concrete Construction Handbook*. New York: McGraw-Hill, 1998.

[16] A. M. Neville, *Concrete Technology*. Jhon Wiley & Sons, 1987.

[17] "SNI 03-3449-2002: Tata Cara Perancangan Campuran Beton Ringan dengan Agregat Ringan," Jakarta, 2002.

[18] "SNI 03-1974-1990: Metode Pengujian Kuat Tekan Beton," Jakarta, 2011.

[19] Z. Li, *Advanced Concrete Technology*. New York: John Wiley & Sons, 2011.

[20] O. H. Zinkaah, "Influence of Steel Fibers on the Behavior of Light Weight Concrete Made from Crushed Clay Bricks," *Am. J. Civ. Eng.*, vol. 2, pp. 109–116, 2014.

[21] K. O. Olusola, A. J. Babafemi, A. A. Umoh, and B. J. Olawuyi, "Effect of Batching Methods on the Fresh and Hardened Properties of Concrete," *Int. J. Res. Rev. Appl. Sci.*, vol. 13, no. 3, pp. 773–779, 2012.

[22] A. T. Goldbeck and J. E. Gray, *A Method of Proportioning Concrete For Strength Workability and Durability*. National Crushed Stone Association, 1965.

EPI International Journal of Engineering
Volume 6, Number 2, August 2023, pp. 83-91
DOI: 10.25042/epi-ije.082023.05

*p*ISSN 2615-5109
*e*ISSN 2621-0541

Free Vibration of Annular Plates Constrained byTranslational and/or Rotational Springs on Outer and Inner Edges

Yoshihiro Narita*
Faculty of Engineering, Hokkaido University (Professor Emeritus). Email: ynarita1951@gmail.com

Abstract

This paper presents comprehensive lists of natural frequencies for vibration of thin isotropic annular plates with outer and inner edges elastically constrained by translational and rotational springs. A method is extended from a previously presented Ritz approach to include effects of the springs. In numerical examples, sixteen models are considered to cover all general cases of locating translational and/or rotational springs on outer and/or inner edges in addition to classical boundary conditions of free and simple supported edges. After convergence study and comparison test in specific cases are made to validate solution accuracy, frequency parameters of the sixteen models are summarized and frequency variations with increasing spring stiffness are illustrated.

Keywords: Annular plate, vibration, natural frequency, elastic springs, Ritz method

1. Introduction

An annular plate is defined as a flat plate consisting of an outer circular boundary and inner concentric circular boundary, and is often found as structural component or as a model of whole structure in the fields of architectural, mechanical and ocean engineering. The applications in the areas are usually exposed to dynamic environment, and there is a long research history in studying the natural frequencies and mode shapes [1].

For thin annular plates, it was known that the free vibration problem has an exact solution in terms of the Bessel functions J_n and Y_n of the first and second kinds, respectively, and the modified Bessel functions I_n and K_n of the first and second kinds, respectively. The first complete numerical sets of natural frequencies were obtained in 1965 with using these Bessel functions by Vogel and Skinner [2] for nine possible combinations of classical boundary conditions (i.e., free (F), simply supported (S) or clamped (C) edges) along outer and inner edges. Their results are presented in the three significant figures, and are not so with good accuracy due to the subroutines for the special functions in those days. Later in the 1970's and 1980's, there found a number of technical papers [3-8] on the topic, most of them consider polar-orthotropy.

In the 2010's, new analysis techniques are introduced, for example, by Hamiltonian approach [9] and convolution and differential quadrature methods [10]. Other techniques are also used in references [11,12]. More recently, the author presented numerical results in five significant figures for the nine combinations [13].

For practical model of annular plates elastically constrained at two edges, there exist more combinations in edge conditions. Avalos and Laura [14,15] presented analysis in using two-term approximation, and Raju and Rao [16,17] used the finite element method only to give the lowest frequency. Kim and Dickinson [18] covered broader parameters, but still five sets of boundary conditions. The objective of the present paper is therefore to cover all the frequency results for sixteen combinations of translational spring constraint (TS) and rotational spring constraint (RS) in addition to the classical three edge constraints (F, S and C).

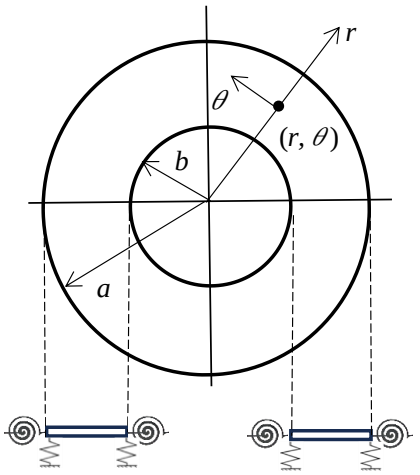

Figure 1. Annular plate with translational and rotational springs and co-ordinate

*Corresponding author.
N-13, W-8, Kitaku
Sapporo, Japan, 060-8628

2. Method of Analysis

Free vibration of a thin annular plate is considered in polar coordinates, as shown in Fig.1. Outer and inner radii are given by *a* and *b*, respectively, and the uniform thickness is by *h*. The plate can be constrained by translational and/or rotational springs along outer and inner edges.

The maximum strain energy of the plate under bending is expressed by

$$U_p = \frac{1}{2}\int_b^a \int_0^{2\pi} \left\{ D_r \left(\frac{\partial^2 w}{\partial r^2} \right)^2 + 2\nu_\theta D_r \left(\frac{\partial^2 w}{\partial r^2} \right) \left(\frac{1}{r}\frac{\partial w}{\partial r} + \frac{1}{r^2}\frac{\partial^2 w}{\partial \theta^2} \right) + D_\theta \left(\frac{1}{r}\frac{\partial w}{\partial r} + \frac{1}{r^2}\frac{\partial^2 w}{\partial \theta^2} \right)^2 \right\} + 4D_k \left[\frac{\partial}{\partial r}\left(\frac{1}{r}\frac{\partial w}{\partial \theta} \right) \right]^2 \Bigg\} r d\theta dr \tag{1}$$

where $w(r,\theta)$ is an amplitude (maximum deflected shape) of plate vibrating in radian frequency ω. A set of the bending stiffness is defined by

$$D_r = \frac{E_r h^3}{12\left(1-\nu_r \nu_\theta\right)},\ D_\theta = \frac{E_\theta h^3}{12\left(1-\nu_r \nu_\theta\right)},\ D_k = \frac{Gh^3}{12} \tag{2}$$

for polar-orthotropic material, where E_r and E_θ are Young's moduli in *r* and θ direction, respectively, *G* is a shear modulus, ν_r and ν_θ are major and minor Poisson's ratios ($\nu_\theta D_r = \nu_r D_\theta$). For isotropic material, they reduce to

$$D_r = D_\theta = D = \frac{Eh^3}{12\left(1-\nu^2\right)},\ H = D_r\nu_\theta + 2D_k = D \tag{3}$$

The expressions of strain energy in the edge springs are

$$U_{ts} = \frac{1}{2}\int_0^{2\pi} k_{ta}\left\{w(a,\theta)\right\}^2 a d\theta + \frac{1}{2}\int_0^{2\pi} k_{tb}\left\{w(b,\theta)\right\}^2 b d\theta \tag{4}$$

for translational springs at $r=a$ and $r=b$, respectively, with translational spring stiffness k_{ta} and k_{tb}, and

$$U_{rs} = \frac{1}{2}\int_0^{2\pi} k_{ra}\left\{\frac{\partial w(a,\theta)}{\partial r}\right\}^2 a d\theta + \frac{1}{2}\int_0^{2\pi} k_{rb}\left\{\frac{\partial w(b,\theta)}{\partial r}\right\}^2 b d\theta \tag{5}$$

for rotational springs with rotational spring stiffness k_{ra} and k_{rb}. The maximum kinetic energy is given by

$$T = \frac{1}{2}\rho h\omega^2 \int_b^a \int_0^{2\pi} w^2 r d\theta dr \tag{6}$$

where ρ is the mass per unit volume.

Next, the amplitude is approximated by a finite series

$$w(r,\theta) \doteq w_{mn}(\eta,\theta) = \sum_{m=0}^{M-1} A_m Y_m(\eta)\cos n\theta,\ \left(\eta = \frac{r}{a}\right) \tag{7}$$

where A_m are undetermined coefficients, $Y_m(\eta)$ is a function in the radial direction to satisfy the kinematical boundary condition at both inner and outer edges, and *n* is an integer to indicate the number of nodal diameters.

This equation is substituted into

$$\frac{\partial}{\partial A_{\bar{m}}}\left[U_p(w_{mn}) + U_{ts}(w_{mn}) + U_{rs}(w_{mn}) - T(w_{mn})\right] = 0 \quad (\bar{m} = 0,1,..,M-1) \tag{8}$$

The resulting frequency equation is given by

$$\begin{aligned} &\sum_{m=0}^{M-1}\Bigg\{ f_1^{(22)} + \nu_\theta\left[f_0^{(21)} + f_0^{(12)} - n^2\left(f_{-1}^{(20)} + f_{-1}^{(02)} \right)\right] \\ &+\left(\frac{D_\theta}{D_r}\right)\left[f_{-1}^{(11)} + n^4 f_{-3}^{(00)} - n^2\left(f_{-2}^{(10)} + f_{-2}^{(01)} \right)\right] \\ &+2n^2\left[\frac{H}{D_r} - \nu_\theta\right]\left(f_{-3}^{(00)} + f_{-1}^{(11)} - f_{-2}^{(01)} - f_{-2}^{(10)} \right) \\ &+k_{ta}^* Y_m(1) Y_{\bar{m}}(1) + k_{tb}^* Y_m(\alpha) Y_{\bar{m}}(\alpha) \\ &+k_{ra}^* \frac{dY_m(1)}{d\eta}\frac{dY_{\bar{m}}(1)}{d\eta} + k_{rb}^* \frac{dY_m(\alpha)}{d\eta}\frac{dY_{\bar{m}}(\alpha)}{d\eta} \\ &\qquad - \Omega^2 f_1^{(00)} \Bigg\}_{m\bar{m}} A_m = 0 \end{aligned} \tag{9}$$

for $\bar{m} = 0,1,..,(M-1)$ and a specific integer *n*. The frequency parameter is defined by

$$\Omega = \omega a^2 \left(\frac{\rho h}{D}\right)^{1/2} \tag{10}$$

and an aspect ratio is $\alpha = b/a$. Function *f* in equation (9) is defined by

$$f_{t,m\bar{m}}^{(pq)} = \int_\alpha^1 \eta^t \left(\frac{d^{(p)}Y_m(\eta)}{d\eta^{(p)}}\right)\left(\frac{d^{(q)}Y_{\bar{m}}(\eta)}{d\eta^{(q)}}\right) d\eta \tag{11}$$

A set of the non-dimensional spring stiffness is given by

$$k_{ta}^* = \frac{k_{ta}a^3}{D} \text{ and } k_{tb}^* = \frac{k_{tb}a^3}{D} \tag{12}$$

for translational springs at outer ($r=a$) and inner ($r=b$) edge, respectively, and similarly by

$$k_{ra}^* = \frac{k_{ra}a}{D} \text{ and } k_{rb}^* = \frac{k_{rb}a}{D} \tag{13}$$

for rotational spring at outer and inner edge, respectively.

In the present Ritz method, an idea of using the boundary index [19,20] is introduced to deal with any combination of classical boundary conditions, i.e., free, simply supported and clamped edges. For this purpose, a function $Y_m(\eta)$ is introduced in the form

$$Y_m(\eta) = \eta^m (\eta-\alpha)^{Bi}(\eta-1)^{Bo} \tag{14}$$

where *Bi* (abbreviation of Boundary index at inner edge) takes 0, 1 and 2 to satisfy kinematical condition for F, S and C, respectively, along inner circular boundary ($r=b$) and similarly, *Bo* (Boundary index at outer edge) does 0, 1 and 2 to satisfy the condition for F, S and C, respectively, along outer circular boundary ($r=a$). Therefore, one can choose any of the nine possible sets of classical boundary conditions, and include the effects of translational and rotational springs additionally.

Table 1. Numerical examples of annular plates with translational and/or rotational springs.

examples		Limiting case		Cross-section of plate
	BC	$k^*=0$	$k^*=\infty$	
Ex.1	F-TS	F-F	F-S	
Ex.2	F-RS	F-S	F-C	
Ex.3	S-TS	S-F	S-S	
Ex.4	S-RS	S-S	S-C	
Ex.5	C-TS	C-F	C-S	
Ex.6	C-RS	C-S	C-C	
Ex.7	TS-F	F-F	S-F	
Ex.8	RS-F	S-F	C-F	
Ex.9	TS-S	F-S	S-S	
Ex.10	RS-S	S-S	C-S	
Ex.11	TS-C	F-C	S-C	
Ex.12	RS-C	S-C	C-C	
Ex.13	TS-TS	F-F	S-S	
Ex.14	TS-RS	F-S	S-C	
Ex.15	RS-TS	S-F	C-S	
Ex.16	RS-RS	S-S	C-C	

3. Numerical results

Numerical examples are listed in Table 1. When one considers three classical boundary conditions (i.e., free (F), simply supported (S), clamped (C)) at each edge, there are nine different combinations (three by three) and their results are already summarized by using Ritz method [13].

In this study, an intermediate condition between free edge and simply supported edge is considered for plates constrained only by translational spring (denoted by TS (Translational Spring)), and this condition can become the free edge in the limit of $k_{ta}=k_{tb}=0$ and simply supported edge in $k_{ta}=k_{tb}=\infty$. Similarly, between simply supported edge and clamped edge, intermediate edge condition is obtained by using rotational spring (denoted by RS (Rotational Spring)) on simply supported edge. In the limit of $k_{ra}=k_{rb}=\infty$, the edge becomes fully clamped. Such limiting cases are listed for each of the sixteen examples in the table.

Table 2 Convergence of frequency parameters Ω (b/a=0.3, ν=0.3).

	M	(n,s)				
		(0,0)	(1,0)	(2,0)	(3,0)	(4,0)
Ex.2	6	4.656	4.490	6.542	12.73	21.90
(k^*=3.333)	7	4.656	4.490	6.542	12.73	21.90
	8	4.656	4.490	6.452	12.73	21.90
	9	4.656	4.490	6.542	12.73	21.90
Ref.[18]		4.656	4.490	6.542	12.73	21.90
Ex.2	6	6.607	6.492	7.903	13.25	22.06
(k^*=333.3)	7	6.606	6.492	7.901	13.25	22.06
	8	6.606	6.492	7.900	13.25	22.06
	9	6.606	6.492	7.900	13.25	22.06
Ref.[18]		6.606	6.492	7.900	13.25	22.06
Ex.8	6	6.108	13.84	25.11	39.77	38.37*
(k^*=1)	7	6.108	13.84	25.11	39.77	38.37*
	8	6.108	13.84	25.11	39.77	38.37*
	9	6.108	13.84	25.11	39.77	38.37*
Ref.[18]		6.108	13.84	25.11	39.77	38.37*

*: (0,1) mode.

Totally, this table summarizes the sixteen examples among twenty five combinations of "five cases (F,TS,S,RS and C) at outer edge" times "five cases (F,TS,S,RS and C) at inner edge". Since the nine cases of "(F,S,C) at outer edge times (F,S,C) at inner edge" was already published [13], the twenty five combinations deducted by nine end up with the sixteen examples as illustrated in Table.1.

For values of spring stiffness used in numerical examples, the same values are used for translational and rotational springs, when these different types of springs appear in one example, as

$$k^* = k_{ta}^* = k_{tb}^* = k_{ra}^* = k_{rb}^* \quad (\text{e.g., } k^* = 1, 10, 10^2, 10^4) \quad (15)$$

for simplicity. But of course, one can calculate frequencies of plates with independent stiffness values of each spring.

Table 2 presents convergence study of Ex.2 and Ex.8 with respect to the number of series terms M in equation (7), and the number of terms is increased from M=6 to 9. It is clearly seen that the fast convergence is seen in the four significant figures. For clarity, the identical values are underlined and are obtained already for M=7. In numerical tables hereafter, M=8 is employed.

The frequency parameters are given basically in increasing order with (n,s) (n: number of nodal diameters, s: number of nodal circles)). Depending on aspect ratio b/a and boundary conditions, the order may change, typically the (0,0) and (1,0) modes, as seen in Ex.2 and Ex.8 in the table. These examples are chosen in the convergence study, because these natural frequencies are available for comparison in [18], and the excellent agreement is found between the present converged values and those cited in the table.

Table 3 Frequency parameters Ω for **(Ex.1)** Annular plate with F outer edge and TS inner edge (ν =0.3).

b/a	k*	(n,s)				
		(0,0)	(1,0)	(2,0)	(3,0)	(4,0)
0.1	0(F-F)	RBM	RBM	5.304	12.44	21.84
	1	0.446	0.063	5.304	12.44	21.84
	10	1.326	0.199	5.304	12.44	21.84
	100	2.783	0.612	5.305	12.44	21.84
	10000	3.443	2.278	5.365	12.44	21.84
	∞(F-S)	3.450	2.439	5.429	12.44	21.84
0.3	0(F-F)	RBM	RBM	4.906	12.27	21.78
	1	0.793	0.328	4.909	12.27	21.78
	10	2.095	0.998	4.934	12.27	21.78
	100	3.188	2.367	5.136	12.29	21.79
	10000	3.420	3.357	6.034	12.57	21.85
	∞(F-S)	3.422	3.374	6.080	12.61	21.88
0.5	0(F-F)	RBM	RBM	4.271	11.43	21.07
	1	1.119	0.723	4.307	11.43	21.07
	10	2.804	2.098	4.595	11.51	21.09
	100	3.920	4.081	6.058	12.05	21.29
	10000	4.119	4.852	7.946	13.96	22.68
	∞(F-S)	4.120	4.860	7.985	14.04	22.79

Table 4 Frequency parameters Ω for **(Ex.2)** Annular plate with F outer edge and RS inner edge (ν=0.3).

b/a	k*	(n,s)				
		(0,0)	(1,0)	(2,0)	(3,0)	(4,0)
0.1	0(F-S)	3.450	2.439	5.429	12.44	21.84
	1	3.527	2.521	5.435	12.44	21.84
	10	3.858	2.913	5.480	12.44	21.84
	100	4.171	3.369	5.583	12.45	21.84
	10000	4.236	3.479	5.624	12.45	21.84
	∞(F-C)	4.238	3.479	5.624	12.45	21.84
0.3	0(F-S)	3.422	3.374	6.080	12.61	21.88
	1	3.937	3.827	6.248	12.65	21.88
	10	5.505	5.322	7.007	12.87	21.94
	100	6.487	6.359	7.781	13.18	22.04
	10000	6.658	6.550	7.956	13.27	22.07
	∞(F-C)	6.660	6.552	7.957	13.28	22.07
0.5	0(F-S)	4.120	4.860	7.985	14.04	22.79
	1	5.652	6.166	8.753	14.41	22.97
	10	9.841	10.09	11.71	16.18	23.94
	100	12.53	12.78	14.19	18.11	25.24
	10000	13.02	13.28	14.70	18.56	25.59
	∞(F-C)	13.02	13.29	14.70	18.56	25.60

Table 5 Frequency parameters Ω for **(Ex.3)** Annular plate with S outer edge and TS inner edge (ν=0.3).

b/a	k*	(n,s)				
		(0,0)	(1,0)	(2,0)	(3,0)	(4,0)
0.1	0(S-F)	4.854	13.87	25.40	39.94	56.84
	1	4.933	13.87	25.40	39.94	56.84
	10	5.574	13.89	25.40	39.94	56.84
	100	8.979	14.03	25.40	39.94	56.84
	10000	14.36	16.36	25.66	39.94	56.84
	∞(S-S)	14.49	16.78	25.94	39.98	56.84
0.3	0(S-F)	4.664	12.82	24.12	38.78	56.25
	1	4.939	12.87	24.13	38.78	56.25
	10	6.867	13.37	24.23	38.80	56.25
	100	14.06	16.61	25.09	38.99	56.29
	10000	20.97	23.15	29.98	41.55	57.26
	∞(S-S)	21.08	23.32	30.27	41.91	57.55
0.5	0(S-F)	5.077	11.61	22.36	35.64	52.03
	1	5.540	11.80	22.44	35.67	52.05
	10	8.606	13.38	23.14	36.01	52.22
	100	20.68	22.55	28.47	38.91	53.76
	10000	39.63	41.33	46.46	55.08	67.23
	∞(S-S)	40.04	41.80	47.09	55.96	68.38

Table 6 Frequency parameters Ω for **(Ex.4)** Annular plate with S outer edge and RS inner edge (ν=0.3).

b/a	k*	(n,s)				
		(0,0)	(1,0)	(2,0)	(3,0)	(4,0)
0.1	0(S-S)	14.49	16.78	25.94	39.98	56.84
	1	14.73	16.93	25.96	39.98	56.84
	10	15.97	17.79	26.14	39.99	56.84
	100	17.43	19.04	26.55	40.04	56.85
	10000	17.79	19.40	26.72	40.06	56.85
	∞(S-C)	17.79	19.40	26.72	40.06	56.85
0.3	0(S-S)	21.08	23.32	30.27	41.91	57.55
	1	21.89	24.00	30.69	42.10	57.62
	10	25.53	27.19	32.83	43.21	58.08
	100	29.17	30.61	35.54	44.94	58.96
	10000	29.97	31.39	36.24	45.45	59.27
	∞(S-C)	29.98	31.40	36.24	45.46	59.27
0.5	0(S-S)	40.04	41.80	47.09	55.96	68.38
	1	41.53	43.20	48.28	56.89	69.06
	10	48.88	50.24	54.49	61.96	72.94
	100	57.64	58.83	62.53	69.12	78.99
	10000	59.80	60.96	64.61	71.08	80.78
	∞(S-C)	59.82	60.99	64.63	71.11	80.80

Table 7 Frequency parameters Ω for **(Ex.5)** Annular plate with C outer edge and TS inner edge (ν=0.3).

b/a	k*	(n,s)				
		(0,0)	(1,0)	(2,0)	(3,0)	(4,0)
0.1	0(C-F)	10.16	21.20	34.54	50.99	69.66
	1	10.22	21.20	34.54	50.99	69.66
	10	10.74	21.22	34.54	50.99	69.66
	100	14.26	21.41	34.54	50.99	69.66
	10000	22.48	24.66	34.96	51.01	69.66
	∞(C-S)	22.70	25.28	35.41	51.07	69.67
0.3	0(C-F)	11.42	19.54	32.59	49.07	68.58
	1	11.60	19.61	32.61	49.07	68.58
	10	13.01	20.19	32.76	49.11	68.59
	100	20.99	24.41	34.07	49.45	68.67
	10000	33.53	35.58	42.21	53.97	70.52
	∞(C-S)	33.77	35.91	42.73	54.61	71.06
0.5	0(C-F)	17.72	22.02	32.12	45.81	63.02
	1	17.91	22.16	32.20	45.86	63.04
	10	19.56	23.44	32.96	46.29	63.28
	100	30.63	32.77	39.20	50.06	65.48
	10000	63.05	64.47	68.87	76.54	87.79
	∞(C-S)	63.97	65.49	70.14	78.18	89.86

Table 8 Frequency parameters Ω for **(Ex.6)** Annular plate with C outer edge and RS inner edge (ν=0.3).

b/a	k*	(n,s)				
		(0,0)	(1,0)	(2,0)	(3,0)	(4,0)
0.1	0(C-S)	22.70	25.28	35.41	51.07	69.67
	1	23.02	25.49	35.45	51.07	69.67
	10	24.66	26.64	35.72	51.09	69.67
	100	26.75	28.40	36.35	51.17	69.67
	10000	27.28	28.91	36.62	51.22	69.68
	∞(C-C)	27.28	28.92	36.62	51.22	69.68
0.3	0(C-S)	33.77	35.91	42.73	54.61	71.06
	1	34.69	36.72	43.28	54.90	71.19
	10	39.16	40.75	46.19	56.56	71.95
	100	44.17	45.49	50.09	59.22	73.42
	10000	45.33	46.63	51.13	60.02	73.94
	∞(C-C)	45.35	46.64	51.14	60.03	73.95
0.5	0(C-S)	63.97	65.49	70.14	78.18	89.86
	1	65.61	67.06	71.54	79.35	90.76
	10	74.33	75.52	79.25	85.95	96.09
	100	86.10	87.10	90.25	95.99	104.8
	10000	89.21	90.19	93.29	98.89	107.5
	∞(C-C)	89.25	90.23	93.32	98.93	107.6

Table 9 Frequency parameters Ω for **(Ex.7)** Annular plate with TS outer edge and F inner edge (ν=0.3).

b/a	k*	(n,s)				
		(0,0)	(1,0)	(2,0)	(3,0)	(4,0)
0.1	0(F-F)	RBM	RBM	5.304	12.44	21.84
	1	1.379	1.988	5.783	12.69	22.00
	10	3.438	5.953	8.893	14.75	23.44
	100	4.661	12.07	18.97	25.68	33.41
	10000	4.852	13.85	25.32	39.74	56.40
	∞(S-F)	4.854	13.87	25.40	39.94	56.84
0.3	0(F-F)	RBM	RBM	4.906	12.27	21.78
	1	1.432	1.995	5.410	12.52	21.95
	10	3.453	5.928	8.589	14.58	23.39
	100	4.508	11.44	18.38	25.37	33.32
	10000	4.663	12.80	24.05	38.59	55.83
	∞(S-F)	4.664	12.82	24.12	38.78	56.25
0.5	0(F-F)	RBM	RBM	4.271	11.43	21.07
	1	1.575	2.047	4.842	11.69	21.23
	10	3.775	5.963	8.220	13.79	22.66
	100	4.908	10.60	17.59	24.25	32.30
	10000	5.075	11.60	22.31	35.49	51.70
	∞(S-F)	5.077	11.61	22.36	35.64	52.03

Table 10 Frequency parameters Ω for **(Ex.8)** Annular plate with RS outer edge and F inner edge (ν=0.3).

b/a	k*	(n,s)				
		(0,0)	(1,0)	(2,0)	(3,0)	(4,0)
0.1	0(S-F)	4.854	13.87	25.40	39.94	56.84
	1	5.998	14.94	26.44	40.98	57.88
	10	8.700	18.50	30.57	45.61	62.89
	100	9.964	20.80	33.90	50.05	68.40
	10000	10.16	21.19	34.53	50.98	69.65
	∞(C-F)	10.16	21.20	34.54	50.99	69.66
0.3	0(S-F)	4.664	12.82	24.12	38.78	56.25
	1	6.108	13.84	25.11	39.76	57.26
	10	9.504	17.14	28.99	44.13	62.11
	100	11.16	19.19	32.02	48.22	67.38
	10000	11.42	19.54	32.59	49.06	68.57
	∞(C-F)	11.42	19.54	32.59	49.07	68.58
0.5	0(S-F)	5.077	11.61	22.36	35.64	52.03
	1	7.590	13.11	23.47	36.61	52.95
	10	13.66	18.06	27.86	40.91	57.30
	100	17.12	21.41	31.42	44.96	61.96
	10000	17.71	22.01	32.11	45.80	63.01
	∞(C-F)	17.72	22.02	32.12	45.81	63.02

Table 11 Frequency parameters Ω for **(Ex.9)** Annular plate with TS outer edge and S inner edge (ν=0.3).

b/a	*k**	(n,s)				
		(0,0)	(1,0)	(2,0)	(3,0)	(4,0)
0.1	0(F-S)	3.450	2.439	5.429	12.44	21.84
	1	4.006	3.216	5.902	12.70	22.00
	10	7.000	6.810	8.998	14.76	23.44
	100	12.76	14.11	19.21	25.69	33.41
	10000	14.47	16.75	25.86	39.78	56.40
	∞(S-S)	14.49	16.78	25.94	39.98	56.84
0.3	0(F-S)	3.422	3.374	6.080	12.61	21.88
	1	4.067	4.057	6.533	12.87	22.04
	10	7.563	7.721	9.602	14.94	23.49
	100	16.47	17.55	20.80	26.09	33.49
	10000	21.03	23.25	30.15	41.67	57.08
	∞(S-S)	21.08	23.32	30.27	41.91	57.55
0.5	0(F-S)	4.120	4.860	7.985	14.04	22.79
	1	4.846	5.501	8.409	14.30	22.96
	10	8.979	9.405	11.48	16.43	24.45
	100	22.94	23.45	25.24	28.89	35.08
	10000	39.76	41.48	46.68	55.38	67.52
	∞(S-S)	40.04	41.80	47.09	55.96	68.38

Table 12 Frequency parameters Ω for **(Ex.10)** Annular plate with RS outer edge and S inner edge (ν=0.3).

b/a	*k**	(n,s)				
		(0,0)	(1,0)	(2,0)	(3,0)	(4,0)
0.1	0(S-S)	14.49	16.78	25.94	39.98	56.84
	1	15.67	17.92	27.00	41.02	57.88
	10	19.65	21.97	31.27	45.67	62.89
	100	22.25	24.78	34.74	50.12	68.40
	10000	22.70	25.28	35.40	51.06	69.65
	∞(C-S)	22.70	25.28	35.41	51.07	69.67
0.3	0(S-S)	21.08	23.32	30.27	41.91	57.55
	1	22.58	24.75	31.55	43.05	58.62
	10	28.34	30.39	36.93	48.27	63.86
	100	32.89	35.00	41.75	53.48	69.71
	10000	33.76	35.90	42.72	54.60	71.05
	∞(C-S)	33.77	35.91	42.73	54.61	71.06
0.5	0(S-S)	40.04	41.80	47.09	55.96	68.38
	1	42.11	43.81	48.95	57.62	69.87
	10	51.65	53.18	57.87	65.94	77.59
	100	61.69	63.19	67.80	75.79	87.37
	10000	63.95	65.46	70.11	78.16	89.83
	∞(C-S)	63.97	65.49	70.14	78.18	89.86

Table 13 Frequency parameters Ω for **(Ex.11)** Annular plate with TS outer edge and C inner edge (ν=0.3).

b/a	*k**	(n,s)				
		(0,0)	(1,0)	(2,0)	(3,0)	(4,0)
0.1	0(F-C)	4.238	3.479	5.624	12.45	21.84
	1	4.754	4.107	6.089	12.71	22.00
	10	7.798	7.524	9.161	14.77	23.44
	100	15.03	15.79	19.55	25.71	33.41
	10000	17.76	19.36	26.64	39.86	56.41
	∞(S-C)	17.79	19.40	26.72	40.06	56.85
0.3	0(F-C)	6.660	6.552	7.957	13.28	22.07
	1	7.095	6.998	8.343	13.53	22.24
	10	10.10	10.07	11.16	15.59	23.69
	100	21.15	21.53	23.17	27.08	33.80
	10000	29.87	31.28	36.06	45.16	58.76
	∞(S-C)	29.98	31.40	36.24	45.46	59.27
0.5	0(F-C)	13.02	13.29	14.70	18.56	25.60
	1	13.34	13.60	14.99	18.79	25.77
	10	15.87	16.09	17.30	20.71	27.24
	100	29.92	30.11	30.98	33.36	38.20
	10000	59.19	60.32	63.85	70.11	79.49
	∞(S-C)	59.82	60.99	64.63	71.11	80.80

Table 14 Frequency parameters Ω for **(Ex.12)** Annular plate with RS outer edge and C inner edge (ν=0.3).

b/a	*k**	(n,s)				
		(0,0)	(1,0)	(2,0)	(3,0)	(4,0)
0.1	0(S-C)	17.79	19.40	26.72	40.06	56.85
	1	19.05	20.61	27.82	41.11	57.88
	10	23.55	25.06	32.25	45.79	62.90
	100	26.71	28.32	35.91	50.27	68.41
	10000	27.27	28.91	36.62	51.21	69.67
	∞(C-C)	27.28	28.92	36.62	51.22	69.68
0.3	0(S-C)	29.98	31.40	36.24	45.46	59.27
	1	31.57	32.95	37.66	46.72	60.41
	10	38.24	39.50	43.90	52.58	66.03
	100	44.14	45.42	49.87	58.68	72.43
	10000	45.33	46.63	51.12	60.02	73.93
	∞(C-C)	45.35	46.64	51.14	60.03	73.95
0.5	0(S-C)	59.82	60.99	64.63	71.11	80.80
	1	62.01	63.14	66.69	73.01	82.53
	10	72.97	73.98	77.16	82.93	91.78
	100	86.05	87.02	90.09	95.66	104.3
	10000	89.22	90.19	93.29	98.89	107.5
	∞(C-C)	89.25	90.23	93.32	98.93	107.6

Table 15 Frequency parameters Ω for **(Ex.13)** Annular plate with TS outer and inner edges (ν =0.3).

b/a	k*	(n,s)				
		(0,0)	(1,0)	(2,0)	(3,0)	(4,0)
0.1	0(F-F)	RBM	RBM	5.304	12.44	21.84
	1	1.460	1.989	5.783	12.69	22.00
	10	3.993	5.959	8.893	14.75	23.44
	100	8.508	12.19	18.98	25.68	33.41
	10000	14.35	16.34	25.59	39.75	56.40
	∞(S-S)	14.49	16.78	25.94	39.98	56.84
0.3	0(F-F)	RBM	RBM	4.906	12.27	21.78
	1	1.674	2.024	5.413	12.52	21.95
	10	4.989	6.106	8.612	14.58	23.39
	100	12.70	14.16	18.83	25.43	34.32
	10000	20.91	23.08	29.86	41.32	56.80
	∞(S-S)	21.08	23.32	30.27	41.91	57.55
0.5	0(F-F)	RBM	RBM	4.271	11.43	21.07
	1	1.993	2.183	4.874	11.70	21.24
	10	6.171	6.714	8.464	13.87	22.69
	100	17.76	18.44	20.75	25.36	32.68
	10000	39.36	41.03	46.07	54.53	66.42
	∞(S-S)	40.04	41.80	47.09	55.96	68.38

Table 16 Frequency parameters Ω for **(Ex.14)** Annular plate with TS outer edge and RS inner edge (ν=0.3).

b/a	k*	(n,s)				
		(0,0)	(1,0)	(2,0)	(3,0)	(4,0)
0.1	0(F-S)	3.450	2.439	5.429	12.44	21.84
	1	4.077	3.282	5.908	12.70	22.00
	10	7.403	7.113	9.041	14.76	23.44
	100	14.81	15.58	19.78	25.70	33.41
	10000	17.76	19.36	26.65	39.87	56.41
	∞(S-C)	17.79	19.40	26.72	40.06	56.85
0.3	0(F-S)	3.442	3.374	6.080	12.61	21.88
	1	4.524	4.452	6.693	12.91	22.05
	10	9.093	9.057	10.35	15.19	23.55
	100	20.82	21.22	22.93	26.94	33.75
	10000	29.86	31.27	36.05	45.16	58.76
	∞(S-C)	29.98	31.40	36.24	45.46	59.27
0.5	0(F-S)	4.120	4.860	7.985	14.04	22.79
	1	6.216	6.691	9.148	14.67	23.14
	10	13.04	13.25	14.57	18.43	25.59
	100	29.39	29.58	30.47	32.89	37.80
	10000	59.17	60.30	63.82	70.09	79.47
	∞(S-C)	59.82	60.99	64.63	71.11	80.80

Table 17 Frequency parameters Ω for **(Ex.15)** Annular plate with RS outer and TS inner edges (ν =0.3).

b/a	k*	(n,s)				
		(0,0)	(1,0)	(2,0)	(3,0)	(4,0)
0.1	0(S-F)	4.854	13.87	25.40	39.94	56.84
	1	6.067	14.94	26.44	40.98	57.88
	10	9.282	18.52	30.57	45.61	62.89
	100	14.03	21.00	33.90	50.05	68.40
	10000	22.47	24.66	34.95	51.00	69.65
	∞(C-S)	22.70	25.28	35.41	51.07	69.67
0.3	0(S-F)	4.664	12.82	24.12	38.78	56.25
	1	6.335	13.90	25.12	39.77	57.26
	10	11.13	17.74	29.13	44.16	62.12
	100	20.64	23.97	33.45	48.58	67.46
	10000	33.52	35.58	42.20	53.96	70.51
	∞(C-S)	33.77	35.91	42.73	54.61	71.06
0.5	0(S-F)	5.077	11.61	22.36	35.64	52.03
	1	7.921	13.29	23.55	36.65	52.97
	10	15.69	19.53	28.66	41.33	57.52
	100	30.00	32.09	38.40	49.11	64.34
	10000	63.02	64.45	68.85	76.52	87.77
	∞(C-S)	63.97	65.49	70.14	78.18	89.86

Table 18 Frequency parameters Ω for **(Ex.16)** Annular plate with RS outer and inner edge (ν=0.3).

b/a	k*	(n,s)				
		(0,0)	(1,0)	(2,0)	(3,0)	(4,0)
0.1	0(S-S)	14.49	16.78	25.94	39.98	56.84
	1	15.92	18.08	27.03	41.02	57.88
	10	21.35	23.14	31.52	45.69	62.89
	100	26.19	27.82	35.65	50.23	68.41
	10000	27.27	28.91	36.62	51.21	69.67
	∞(C-C)	27.28	28.92	36.62	51.22	69.68
0.3	0(S-S)	21.08	23.32	30.27	41.91	57.55
	1	23.39	25.43	31.97	43.25	58.69
	10	33.11	34.62	39.86	49.84	64.53
	100	43.01	44.31	48.87	57.89	71.93
	10000	45.32	46.62	51.11	60.01	73.92
	∞(C-C)	45.35	46.64	51.14	60.03	73.95
0.5	0(S-S)	40.04	41.80	47.09	55.96	68.38
	1	43.58	45.20	50.14	58.56	70.56
	10	60.81	62.00	65.77	72.53	82.73
	100	83.05	84.04	87.17	92.88	101.7
	10000	89.18	90.16	93.25	98.86	107.5
	∞(C-C)	89.25	90.23	93.32	98.93	107.6

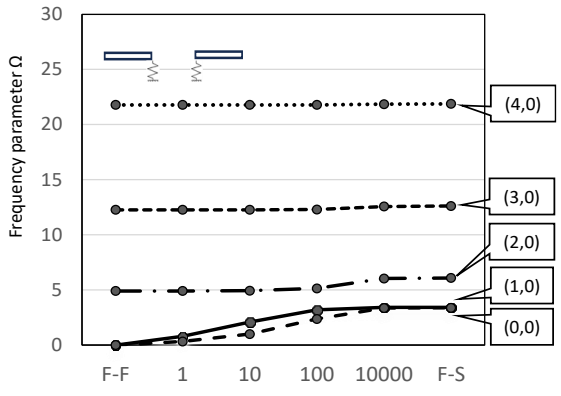

Ex.1 F-TS

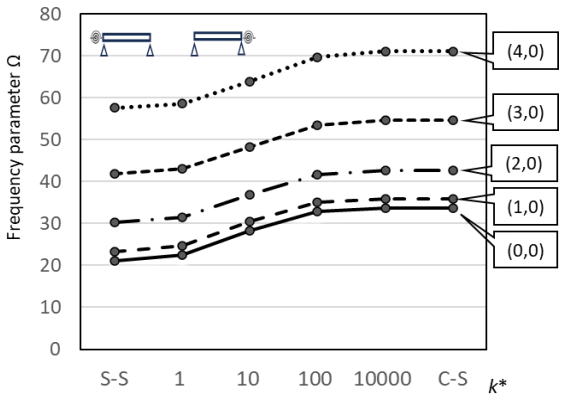

Ex.10 RS-S

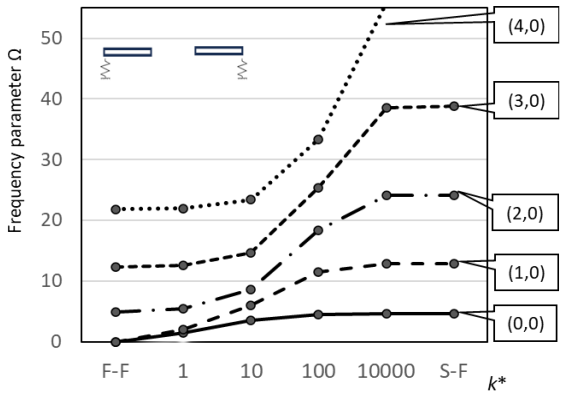

Ex.7 TS-F

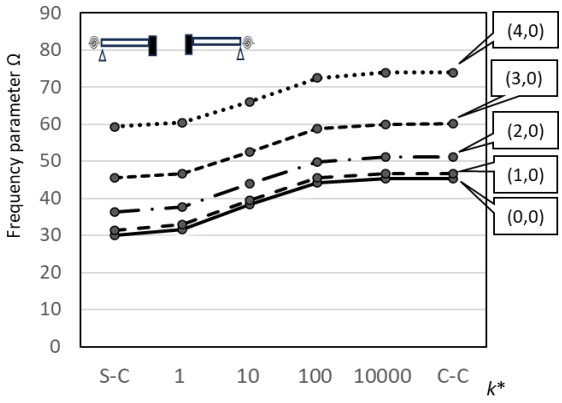

Ex.12 RS-C

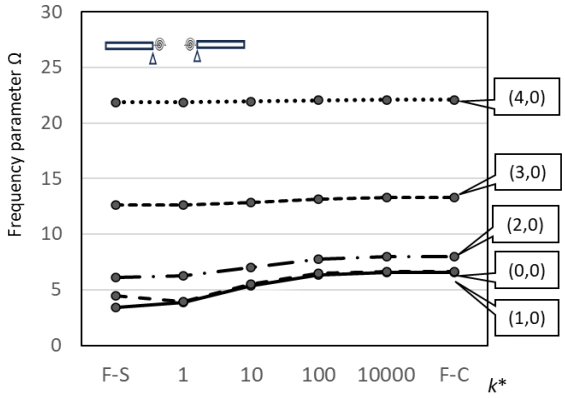

Ex.2 F-RS

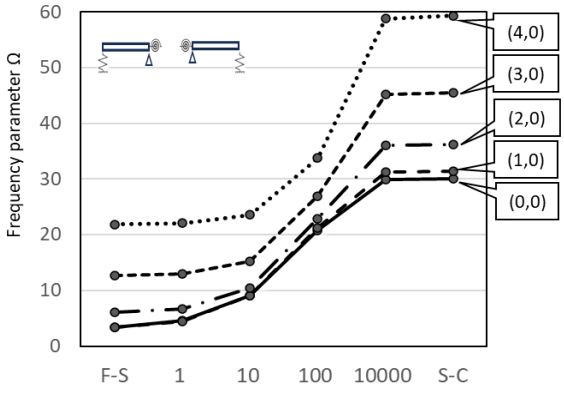

Ex.14 TS-RS

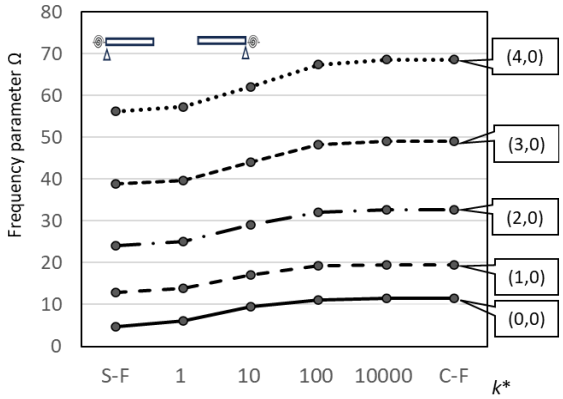

Ex.8 RS-F

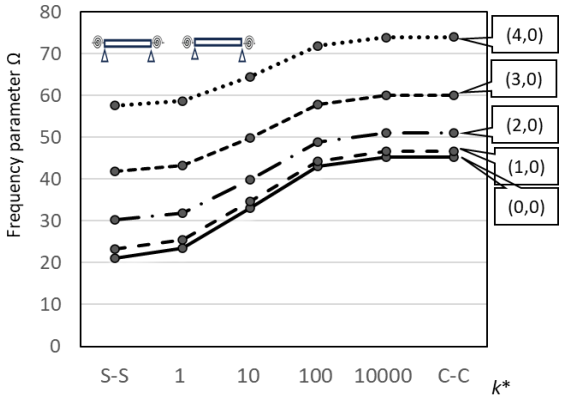

Ex.16 RS-RS

Figure 2. Variations of frequency parameter Ω with stiffness k^* for annular plates (b/a =0.3, ν=0.3).

Tables 3-18 summarize lists of frequency parameter Ω for modes (0,0), (1,0), (2,0), (3,0) and (4,0) of Ex.1-16, respectively. In each table, results are given in the four significant figures for three aspect ratios b/a=0.1, 0.3 and 0.5 and the representative spring stiffness k^*= 0, 1, 10, 100, 10000 and infinity. Basically the lowest five frequencies are shown, but as mentioned above, the sequence of mode changes depending on the aspect ratio and spring stiffness. Therefore, (n,s) is given (n: number of nodal diameters, s: number of nodal circles) in stead of using mode sequence number (e.g., 1st mode, second mode, etc.). For the limiting cases of k^*=0 and infinity, a pair of the (non-elastic) boundary condition (F, S or C) is written in the parenthesis.

In all the tables, as the stiffness increases, the frequencies are monotonically increase, and for k^*=10000 the frequencies almost coincide with those of the non-elastic boundary condition. In other words, such large stiffness can be used to model the limiting case.

Some results in the tables are plotted for b/a=0.3 in Fig.2 to see the monotonical increase of frequencies as the plate edges are more stiffened. Eight cases out of 16 examples are chosen for b/a=0.3. When one compares the first two sets of Ex.1 (F-TS) and Ex.7 (TS-F), the translational stiffening effect along the outer edge is significantly larger than along the inner edge, because the length of outer edge periphery is larger than the inner periphery by $(2\pi a)/(2\pi b)=1/(b/a)$ =1/0.3=3.333. In another comparison between Ex.2 (F-RS) and Ex.8 (RS-F), however, the stiffening effect on the outer edge by rotational spring is not so strong as translational springs. In right column, four cases of Ex.10, Ex.12, Ex.14 and Ex.16 are given. Particularly, two springs are located both on the outer and inner edges, and considerable increase with the stiffness is observed in Ex.14 and Ex.16.

4. Conclusions

Comprehensive freqeuncy data is summarized for the free vibration of thin isotropic annular plates on outer and/or inner edges elastically constrained by translational and rotational springs. General cases of sixteen different combinations are studied, and thorough results may serve for design purpose in structural engineering.

References

[1] Leissa AW, Vibration of Plates, NASA SP-160, 1969.

[2] Vogel SM, Skinner DW, Natural frequencies of transversely vibrating uniform annular plates. J. Applied Mech., 32 (1965), pp.926-931.

[3] Vijayakumar K, Ramaiah GK, On the use of a coordinate transformation for analysis of axisymmetric vibration of polar orthotropic annular plates, J. Sound Vibr. 24 (1972), pp.165-175.

[4] Ramaiah GK, Vijayakumar K, Natural frequencies of polar orthotropic annular plates, J. Sound Vibr. 26 (1973), pp.517-531.

[5] Ramaiah GK, Vijayakumar K, Estimation of higher natural frequencies of polar orthotropic annular plates, J. Sound Vibr. 32 (1974), pp.265-278.

[6] Gorman DG, Natural frequencies of polar orthotropic uniform annular plates, 80 (1982), pp.145-154.

[7] Narita Y, Natural frequencies of completely free annular and circular plates having polar orthotropy. J. Sound Vibr., 92 (1984), pp.33-38.

[8] Narita Y, Free vibration of continuous polar orthotropic annular and circular plates. J. Sound Vibr., 93 (1984), pp.503-511.

[9] Z.H. Zhou, K.W. Wong, X.S. Xu, A.Y.T. Leung, Natural vibration of circular and annular thin plates by Hamiltonian approach, J. Sound Vibr., 330 (2011), pp.1005-1017.

[10] Mercan K, Ersoy H, Civalek O, Free vibration of annular plates by discrete singular convolution and differential quadrature methods, J. Applied Compt. Mech. 2 (2016), pp.128-133.

[11] Rao LB, Rao CK, An exact frequency analysis of annular plated with small core having elastically restrained outer edges and sliding inner edge, Appl. Acous. 109 (2016) pp.69-81.

[12] Janiman Y, Singh B, Free vibration of circular annular plate with different boundary conditions, Vibroengineering PROCEDIA, 29 (2019), pp.82-86.

[13] Narita Y, Accurate results by the Ritz method for free vibration of uniform annular plates, Construction Technologies and Architecture, vol.7, (2023), pp.11-20.

[14] Avalos DR, Laura PAA, A note on transverse vibrations of annular plates elastically restrained against rotation along the edges, J. Sound Vibr., 66 (1979), pp.63-67.

[15] Avalos, DR, Laura PAA, Transverse vibrations of polar orthotropic, annular plates elastically restrained against rotation along the edges, Fibre Sci. Tech., 14 (1981), pp.59-67.

[16] Raju KK, Rao GV, Free vibrations of annular plates with one edge elastically restrained against rotation and other edges free, J. Sound Vibr., 106 (1986), pp.529-532.

[17] Raju KK, Rao GV, Vibrations of isotropic annular plates with edges elastically restrained against rotation, J. Sound Vibr., 109 (1986), pp.353-358.

[18] Kim CS, Dickinson SM, The flexural vibration of thin isotropic and polar orthotropic annular and circular plates with elastically restrained peripheries, J. Sound Vibr. 143 (1990), pp.171-179.

[19] Narita Y, Combinations for the free-vibration behaviors of anisotropic rectangular plates under general edge conditions, Trans. ASME J. Appl.Mech., 67, (2000), pp.568-573.

[20] Narita D, Narita Y., Accurate results for free vibration of doubly curved shallow shells of rectangular planform (Part 1), EPI Int. J. Eng., 4 (2021), pp.29-36.

EPI International Journal of Engineering
Volume 6, Number 2, August 2023, pp. 92-100
DOI: 10.25042/epi-ije.082023.06

*p*ISSN 2615-5109
*e*ISSN 2621-0541

Post-Occupancy Evaluation of Hasanuddin University Urban Park

Etiwu[a,*], Abdul Mufti Radja[b], Afifah Harisah[c]

[a]The Laboratory of Architectural Theory and History, Department of Architecture, Faculty of Engineering, Hasanuddin University. Email: etiwunadji@gmail.com
[b]Department of Architecture, Faculty of Engineering, Hasanuddin University. Email: muftiradja@unhas.ac.id
[c]Department of Architecture, Faculty of Engineering, Hasanuddin University. Email: harisahhussein@gmail.com

Abstract

Urban Park is one of the public open spaces that play a role in preserving the environment. Hasanuddin University Urban Park is known as the lungs of Makassar City. The key of a public open space is influenced by a few ideal criterias based on the ideal criteria for public open space according to Kathleen Madden and the Project for Public Space used in this study, such as sociability (social interaction that occurs); uses and activities; access and linkages, and comfort and image (a comfortable and interesting place to visit). This study aims to identify the condition of the Hasanuddin University Urban Park based on the ideal criterias for public open space according to Kathleen Madden and Project for Public Space and to describe the influence of visitor behavior refer to the condition of Hasanuddin University Urban Park. This study uses a descriptive analysis methods and place centered mapping analysis methods, the data collection techniques is using data triangulation (observations, interviews, and secondary data). The result and discussion shows that the condition of the Hasanuddin University Urban Park refer to the ideal criteria for public open space according to Kathleen Madden and Project for Public Space, is some aspects of intangibles and aspects of measurements have not met the criteria. Visitor behavior that occurs in urban parks is influenced by the condition of existing park facilities and attributes such as visitor parking behavior, visitor environmental hygiene behavior and visitor alert behavior.

Keywords: Post-occupancy evaluation; ideal criteria for public open space; urban parks; visitor behavior

1. Introduction

In urban areas, the environment does not only consist of buildings but also consists of spaces without buildings or open spaces. Open space exists to be an ecological environment and open space can harmonize between built and unbuilt areas. The definition of space is a container that includes land space, sea space, and air space, including space within the earth as a unified territory, where humans and other creatures live, carry out activities and maintain their survival [1]. Open spaces are spaces within a city or a wider area, either in the form of an area/region or the form of an elongated area/lane wherein its use is more open and basically without buildings [2]. According to Hakim (2014), open space is a space that can be accessed by the public, either directly for a limited period or indirectly for an indefinite period. The open space itself can be in the form of roads, sidewalks, and green open spaces such as city parks, forests, and so on [3]. So, a green open space is an open space that functions as a place to accommodate joint activities in the open air that allows for social interaction between communities. The existence of green open space is one of the important elements in forming a comfortable, beautiful, and healthy city environment.

Hasanuddin University is one of the major state universities in Eastern Indonesia, located in Makassar City, South Sulawesi. Hasanuddin University, which was then abbreviated as Unhas, was established on September 10, 1956, in Baraya, then in the 1980s, Unhas was moved to Tamalanrea until now. Unhas campus which occupies an area of 220 hectares in Tamalanrea has various facilities. In addition to functioning as an educational space, it is also an area of green open space which became known as the Unhas Urban Park. Previously, Unhas Urban Park was a deer breeding area that was moved to the back opposite the postgraduate building. Then in 2017, Unhas Urban Park in the welcome area comes with a design that is unique and attracts the attention of the public to become a destination for relaxing and doing outdoor activities. Unhas Urban Park is public and can be accessed by all levels of society.

In an excerpt from a written statement of the Public Communication Bureau of the Ministry of PUPR on Sunday, November 5, 2017, PUPR Minister Hadimuljono said the green open space of the Unhas campus which has an area of about 2.4 hectares is one of the urban forest areas and is known as the lungs of Makassar City [4]. In Carmona, et al, 2003, a good public open space is

*Corresponding author. Telp.: +6285-343-690-899
Jalan Palm Raja
Makassar, Indonesia, 90222

characterized by the public interest in using it and also indicated by the ease of visiting it [5]. So green open space can also be used as a public open space that can improve the quality of life of the community in line with human needs in carrying out joint activities (Siahaan, 2010) [6]. Therefore, as a public green open space, Unhas Urban Park is expected to be a place to carry out various activities.

Preliminary observations indicate that the use of space and activities that occur in the space has not been utilized optimally. There are overlapping activities that occur simultaneously. Public open space is said to be successful if it has ideal criteria, including (1) sociability, which can create a friendly atmosphere in social interaction between individuals; (2) uses and activities, which can accommodate activities in the open air such as exercising, relaxing, sightseeing, leisurely walks, and so on; (3) access and linkages, namely having good access and traffic, adequate facilities such as pedestrian paths, garden paths, seats, parking availability; (4) comfort and image, which is comfortable, cool, clean, healthy and has good visuals (in Kathleen Madden and Project for Public Spaces) [7]. In addition to the four criteria above, the success of public open spaces can also be influenced by the behavior of visitors as users of the space.

Unhas Urban Park as a public green open space has an essential function for urban communities. So that the urban park can be enjoyed in the long term and used by the community, periodic evaluation is needed to identify problems that occur. This study aims to identify the condition of the Hasanuddin University Urban Park based on the ideal criteria for public open space according to Madden and Project for Public Space and explain the influence of visitor behavior on the condition of the Hasanuddin University Urban Park (Fig. 1).

2. Literature Review

2.1. Ideal criteria for public open space

A great neighborhood is a friendly neighborhood is a quote from a book entitled "The Great Neighborhood Book: A Do it Yourself Guide to Placemaking", (Walljasper, Jay, and Project for Public Spaces, 2007) [8]. In the book, it is explained that the environment is the basis of human civilization and is interdependent and how the environment can be shaped by humans themselves. The environment that exists in cities, suburbs, villages, or

Figure 1. The front view of Hasanuddin University urban park

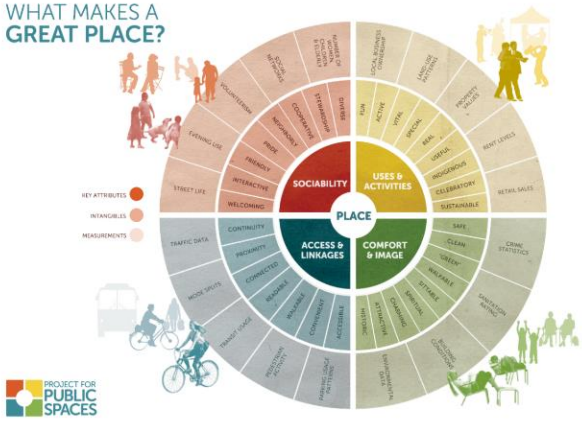

Figure 2. Diagram of the ideal criteria of public open space according to Madden and Project for Public Space (2000)

small towns is the level of social organization in which people interact naturally. Humans can create and determine what kind of environment they will live in.

Madden and Project for Public Spaces (2000) illustrate in a pie chart the ideal criteria for public open space (Fig. 2). Public space can be said to be ideal if it meets the following criteria [7]:

- Sociability, a good public space has social value where every individual can meet, greet each other, and interact with strangers with a comfortable and safe feeling because the environment is comfortable and safe as well. An ideal public space can create and grow social activities.
- Uses and Activities, good public space can foster visitor activity. The activities created can provide reasons why individuals need to come to the place and can visit again.
- Access and Linkages, a good public space is a public space that is easily accessible, traversed, and has good visibility from both a distance and a short distance. Accessibility of a place is seen from its connectivity with the environment, both visual and physical. Accessibility of public spaces also takes into account the distance to the parking lot and the distance of temporary stops for public transport.
- Comfort and Image, a good public space is able to provide comfort, security, and visuals for the space itself. Convenience and security are visitor perceptions of the cleanliness, safety, accessibility, and coolness of the place. Visual public space also gives an impression to visitors.

2.2. Visitor behavior

Community behavior is closely related to the space that accommodates it because human behavior can form patterns of activity that can also affect the shape of the space. In the aspect of environmental behavior, there are several important concepts in the study of environmental architecture and behavior, (Haryadi and B. Setiawan, 1996) as follows [9]:

- Behavior Setting, is an interaction between an activity and a specific place where a group of people carries out an activity, either the activity or behavior of the group of people, the place where the activity is carried

out, and the time the activity is carried out. Each group or group of people can form a different set of behavior, depending on the values, opportunities, and decisions formed by the group.

- Environment Learning, this concept relates to how to understand and give meaning to the environment or explain the relationship between humans and their environment. The process of understanding this environment includes a thorough and continuous understanding of an environment by individuals, where a person's environmental perception is subjective and dynamic.
- Personal Space and Crowding, Personal space is defined as an invisible boundary around a person that no one else is allowed to enter. Personal space can also be dynamic and adaptive, depending on one's environmental and psychological situation. A crowded is a situation of someone is unable to maintain his personal space. Congestion can be influenced by environmental factors, situational factors, and intrapersonal factors.

3. Research Method

The research location is in the Hasanuddin University campus area, precisely at the front of the entrance lane as a welcome area (Fig. 3).

This research is qualitative research that uses a rationalism paradigm with a descriptive analysis approach and behavioral analysis method, namely place-centered mapping. Data collection techniques use data triangulation, namely observations, interviews, and document analysis. Observations were made in November and December 2021 by sampling independently (randomly) and incidental techniques. Observations were made by taking into account the weather conditions, namely in the absence of rain (cloudy, overcast, and sunny).

The condition of visitors does not experience density every day. This study looks for the density of visiting times so that it can provide tangible results from Monday to Sunday. Observations were made randomly and between observations from Monday to Sunday, observations were taken with dense visitors, namely on weekdays, namely Monday and Thursday, and on holidays, namely Saturday and Sunday. Visitors are divided into individual visitors and group visitors. Of the total visitors per day (Monday, Thursday, Saturday, and Sunday) 3 individual visitors and 10 group visitors were taken with the number of individuals in different groups. The sample of individual visitors is determined by a maximum of 3 visitors according to the field situation because individual visitors per day in the morning, afternoon, and evening are usually no more than 3 people. For group visitors, a maximum sample of 10 group visitors is taken.

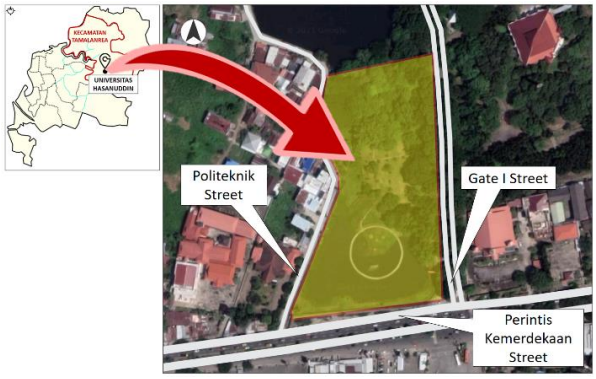

Figure 3. Hasanuddin University urban park map

4. Results and Discussion

4.1. Physical condition

Unhas Urban Park can be reached through the main entrance to the Unhas campus, which is Jalan Pintu I. Unhas Urban Park consists of several zoning areas including an entrance, pedestrian hall, infinite bridge, courtyard, amphitheater, and wetland. As for the parking area across from the park, (Fig. 4).

- Softscape Elements

The vegetation contained in the park is tree vegetation that serves as a shade, namely rain trees (*Samanea saman*) and spanish cherry trees (*Mimusops elengi*) (Fig. 5).

Figure 4. The physical condition of Hasanuddin University urban park: 1 Parking area; 2. Entrance; 3. Pedestrian Hall; 4. Wetland; 5. Infinite bridge; 6. Courtyard and amphitheatre

Figure 5. Tree Vegetation as Shade: 1. Pedestrian Hall; 2. Wetland; 3. Courtyard; 4. Amphitheatre

- Hardscape Elements

The pedestrian path for the pedestrian hall area uses concrete pavement material with a road width of 10.25 meters. The pedestrian path in the courtyard and amphitheater area uses concrete pavement with a road width of 1.6 meters. The front of the amphitheater uses grass block material, while the courtyard is a green page overgrown with young spanish cherry trees. The infinite bridge uses concrete pavement material with a pier diameter of 50 meters and a road width of 2 meters. There is a wooden bridge that connects the courtyard area to the infinite bridge pier. In the wetland area, the pedestrian path has a floor height with the ground, using iron and conwood frame materials as floor coverings, the width of the road is 1.8 meters (Fig. 6).

- Other Attributes

Other attributes found in the park are one large billboard, one security post, and bicycle parking at the entrance area. In the pedestrian hall area, there is one small billboard, two information boards, garden lights, and four park benches spread over several points at a certain distance. In the wetland area, there are garden lights, box panels, and a trash can (Fig. 7).

Figure 6. Condition of the pedestrian path in the area: 1. Pedestrian hall; 2,5,6. Courtyard; 3. The bridge to the infinite bridge pier; 4. In front of the amphitheater; 7,8. Wetland

Figure 7. Attributes of the Park: 1. Big billboard; 2. Security post; 3. Bicycle parking; 4. Small billboards; 5. Information boards; 6. Park bench; 7. Box panels; 8. Trash can; 9,10,11. Garden lamp

4.2. Behavioral observation with place-centered mapping technique

Activities that occur to individual visitors in the form of sitting, walking, reading/studying, and playing cellphone. Meanwhile, group visitors held meeting activities such as organizational meetings, meetings with colleagues, taking graduation photos, and pre-wedding with photographers.

On Monday morning 2 individual visitors were observed sitting, studying, and playing with their cellphones in the wetland and pedestrian hall areas. There are 2 groups of visitors who are sitting and chatting in the wetland area (Fig. 8).

On Thursday afternoon, 1 individual visitor was observed who was sitting and playing on mobile phones in the wetland area. 3 group visitors were sitting and chatting having a study meeting and taking their graduation photos in the wetland and pedestrian hall areas (Fig. 9).

On Saturday afternoon there was 1 individual visitor who was observed sitting using a laptop in the wetland area. There were 5 groups of visitors scattered in the wetland, courtyard, and pedestrian hall areas who were walking, sitting, chatting, playing with mobile phones, and playing with children (Fig. 10).

Figure 8. Visitor activities on Monday

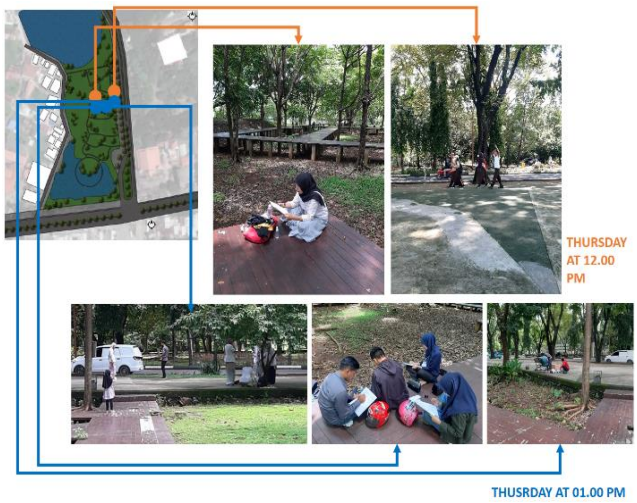

Figure 9. Visitor activities on Thursday

Figure 10. Visitor activities on Saturday

Figure 11. Visitor activities on Sunday

On Sunday afternoon there were 5 group visitors who were observed in the wetland area and pedestrian hall. Group visitors observed were visitors who with their families sat, chatted, took pictures, played on cellphones, and played with children (Fig. 11).

In Zhang and Lawson (2009), Gehl divides outdoor activities into three categories, including (a) important activities, routine activities that must be carried out in all conditions that everyone has, such as work, school, shopping, and also activities in the movement system such as walking to work, to bus stops, and so on; (b) optional activities, in the form of activities that have a priority level under important activities. We can choose to take a leisurely walk in the afternoon or postpone it when it's not sunny; (c) social activities, emphasizing the occurrence of social processes, namely the form of physical contact and passive contact [10].

The following is a graph of the average number of visitors to the Hasanuddin University Urban Park from Monday to Sunday.

Based on Fig. 12, it can be observed that the most visitors on weekdays in the morning for age restrictions <14 years old M/F are on Tuesday, Thursday, and Friday totaling 3 people, visitors aged 15-29 years M/F are on Monday totaling 13 people, and visitors with an age limit of >30 years M/F on Mondays and Thursdays amounting to 5 people. While the most visitors on holidays in the morning for age restrictions <14 years old M/F are on Saturday totaling 6 people, visitors aged 15-29 years M/F are on Sunday totaling 21 people, and visitors aged limiting >30 years M/F are on Saturday and Sunday totaling 5 people.

Based on Fig. 13, it can be observed that the most visitors on weekdays at noon for age restrictions <14 years old M/F are on Thursday totaling 9 people, visitors aged 15-29 years M/F are on Monday totaling 24 people, and visitors with an age limit of >30 years M/F are 9 people on Monday, Tuesday, Thursday. While the most visitors on holidays during the day for age restrictions <14 years old M/F are on Saturday totaling 8 people, visitors age limiting 15-29 years old M/F are on Saturday totaling 34 people, and aged limiting visitors >30 years M/F are on Sunday totaling 9 people.

Based on Fig. 14, it can be observed that the most visitors on weekdays in the afternoon for age restrictions <14 years old M/F are on Monday totaling 10 people, visitors aged 15-29 years M/F are on Thursday totaling 38

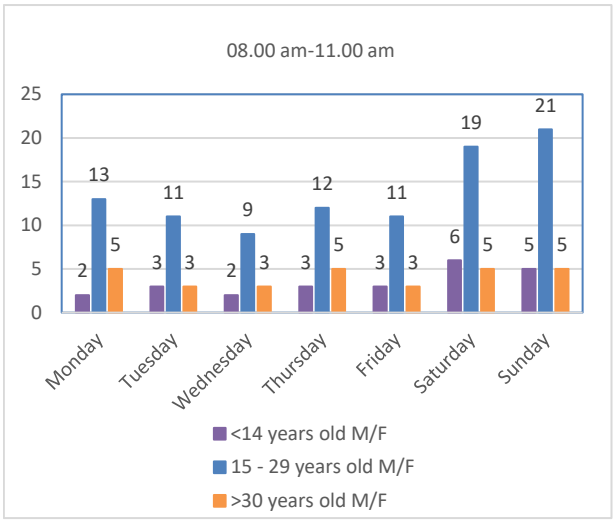

Figure 12. Average number of visitors in the morning

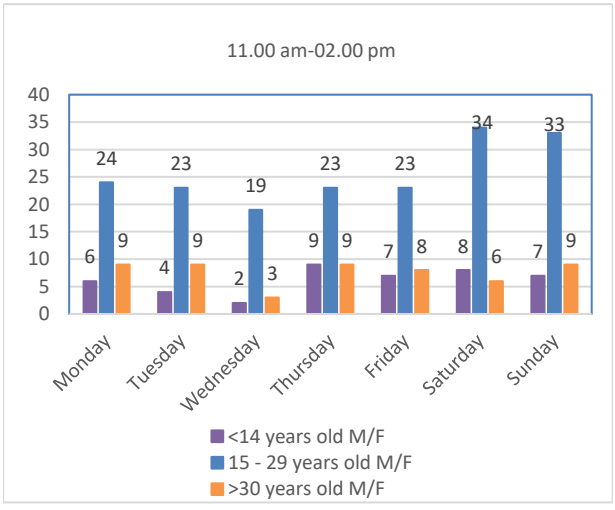

Figure 13. Average number of visitors in the afternoon

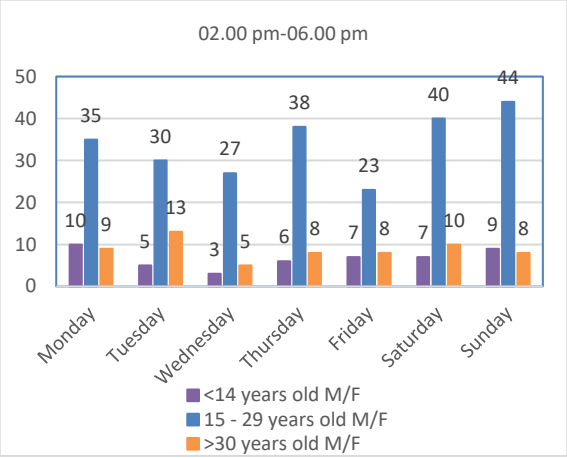

Figure 14. Average number of visitors in the afternoon

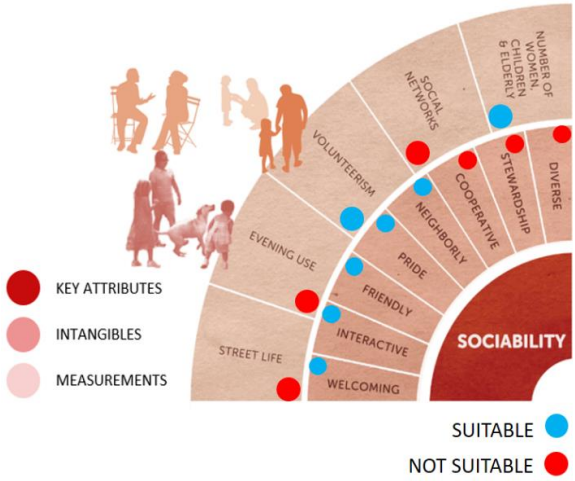

Figure 15. The compatibility of the ideal sociability criteria with the conditions of the Hasanuddin University urban park

people, and visitors with an age limit of >30 years. M/F is on Tuesday totaling 13 people. While the most visitors on holidays in the afternoon for age restrictions <14 years old M/F are on Sunday totaling 9 people, visitors aged 15-29 years M/F are on Sunday totaling 44 people, and visitors aged limiting >30 years M/F are on Saturday totaling 10 people.

4.3. The condition of the Hasanuddin University urban park based on the ideal criteria for public open space according to Kathleen Madden and project for public space

- Sociability Ideal Criteria

According to the diagram of the ideal criteria for public open space on the sociability criteria, Unhas Urban Park is based on observations: (a) it can be visited freely and voluntarily by various groups, not limited to age, gender, and certain groups. Can be visited anytime according to campus opening hours or until 06.00 pm so there is no activity at night and there is no entrance fee to visit the park; (b) activities that occur in the form of individual activities, such as sitting, walking leisurely, selfies, studying, and group activities, that is planned activities such as recreation, group study meetings, organizational meetings, meetings with colleagues; (c) social networks can occur when interactions between individuals with other individuals, interactions between one group and another can occur by chance, unplanned with people who have never been met before. Interaction between urban park visitors that occurs is interaction only with people who come together or in their group, not interacting with other people or strangers. So, the criteria for the intangibles and measurements aspects, there are criteria that are not suitable and there are criteria that are by the conditions of the park, (Fig. 15).

Based on information through an interview with one of the visitors, a young mother in the morning, Unhas Urban Park has a good place to carry out her children's school activities outside the room, however, information about permission to use the park has not been obtained. Campus apart from being a place for education can also function as a place to fulfill psychological needs (such as recreation) and biological functions (green open space) that can be utilized by the academic community and the general public [11].

Based on the description above, it can be concluded that Unhas Urban Park when viewed based on sociability criteria, it appears that the activities that occur overlap each other due to the lack of space visibility in the form of public events in the park so that it affects social interaction. The social interactions that occur are interactions with each visiting group.

- Uses and Activities Ideal Criteria

Following the ideal criteria diagram for public open space in the uses and activities criteria, Unhas Urban Park is based on observations: (a) On the pattern of spatial planning, Unhas Urban Park consists of interconnected spaces that have different spatial concepts. Pedestrian hall is pedestrian traffic access both to the park and to campus which has a road width of 10.25 meters, an infinite bridge with the concept of a park area close to the lakeshore, the courtyard has a lawn concept that functions for relaxing activities, the amphitheater serves for outdoor activities with a small-scale audience, and a wetland area with wet deck area concept, has a small path that can be used for leisurely walking and sitting; (b) The activities that occur are overlapped each other, namely, the same activities are carried out by several people or groups so that they produce same or double activity, such as sitting, walking, taking pictures, and discussing with their groups. There is no commercial activity or sales activity.

Public open space must be responsive, democratic, and meaningful. Responsive means that space can be used to carry out various activities and broad interests that have environmental functions. Democratic means that space can be used by various groups of people with social, economic, and cultural backgrounds. Meaningful means that there is a relationship between space and humans as users [12].

Based on information through an interview with one of the individual visitors, she is an office worker who was taking a lunch break, that Unhas Urban Park has a cool place to take a break from the stress of work, especially in

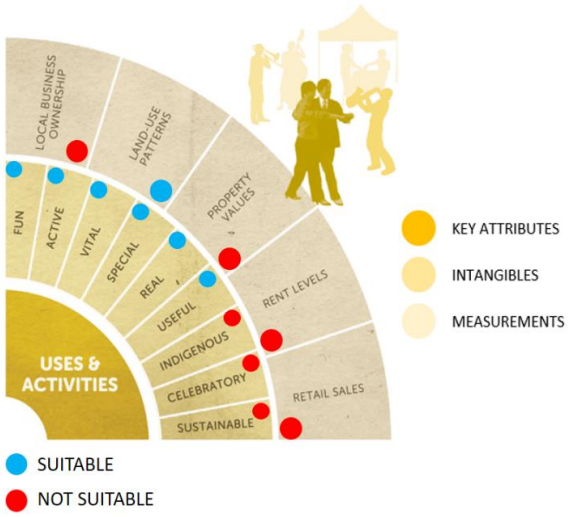

Figure 16. The compatibility of the ideal uses and activities criteria with the conditions of the Hasanuddin University urban park

the wetland area, but to visit this park, that woman needed to bring her lunch or snacks to eat in the park. This is due to the unavailability of food and drinks stalls around the park, and it is forbidden to sell in the park area. So that visitors usually bring snacks or lunch, some even order through the gofood application.

Based on the description above, it can be concluded that Unhas Urban Park is based on the uses and activities criteria, the activities that occur are activities to relax so that there are no commercial activities in the park area. Thus, the criteria for the intangible aspect have criteria that are not suitable and some criteria are by the conditions of the park, while for the measurements aspect there are no criteria that match the conditions of the park except for the criteria of spatial planning patterns (Fig. 16).

- Access and Linkages Ideal Criteria

Based on information through interviews with one of the visitor groups consisting of a mother, father, and two children. The visitor who was interviewed was the mother, in the afternoon that Unhas Urban Park, has a garden atmosphere with a large area and is not crowded for their children who like to run around. Usually, on weekend afternoons, the mother brings her children to visit the Unhas urban park. The activities that are usually carried out are walking around from the pedestrian hall to the courtyard, and amphitheater, then to the wetland area. The mother thought that some of the path lanes in the wetland began to have holes and the height of the roads was high enough for her children which made her feel worried. However, Unhas Urban Park is an alternative to visiting the park, which according to her is very cool and shady to take her children for a walk other than a playground at the mall.

Unhas Urban Park from the aspect of intangibles is in accordance with the condition of the park, namely continuity, proximity, connected, readable, walkable, convenient, and accessible, (Fig. 17). This can be seen from the finding that Unhas Urban Park has a state of interconnected space with pedestrian paths so that it is easy to access. Unhas Urban Park is seen from the aspect

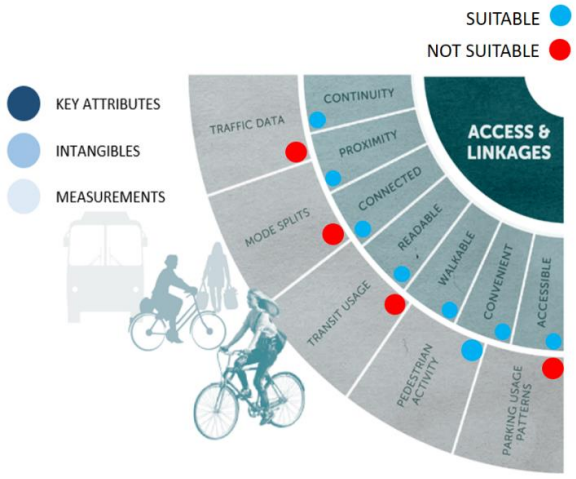

Figure 17. The compatibility of the ideal access and linkages criteria with the conditions of the Hasanuddin University urban park

of appropriate measurements, namely pedestrian activity, while those that are not appropriate are traffic data, mode splits, transit usage, and parking usage patterns, (Fig. 17). This can be seen from the observations that Unhas Urban Park is for easily accessible pedestrian traffic, and spatial planning patterns, each of which has a barrier between spaces but are still interconnected, the park is not a resting place for transit from long trips. As for the condition of the pedestrian path at several points damaged/hollow, the location and access to parking are across the park. Gehl (2011), a person in carrying out walking activities in open spaces is influenced by the distance or length of the road path and the quality of the road path both in terms of road comfort and safety [13].

- Comfort and Image Ideal Criteria

According to the ideal criteria diagram for public open spaces on comfort and image criteria, Unhas Urban Park based on observations has a beautiful and cool atmosphere that makes visitors feel comfortable to just sit back, read, play on mobile phones, and chat with friends for a long time. This is because the park is overgrown with large shady trees that serve as shade.

Based on information through interviews with several visitors, in the morning, some officers reprimanded and forbade bringing food and drinks into the wetland area because officers always get garbage wrapping food and drinks scattered around the wetlands. So that some of the visitors feel uncomfortable due to the reprimand because these visitors feel they did not do it. This shows that the lack of environmental hygiene behavior of visitors is influenced by the lack of availability of trash bins around the park, this can trigger a habit of visitors to leave their food and drink packaging waste because they do not see the surrounding trash cans. According to Shirvani (in Djainuddin., et al, 2019), public open spaces are designed according to the needs and criteria of their users so that they can provide comfort and convenience in carrying out their activities [14].

Unhas Urban Park from the intangible aspect, according to the ideal criteria such as comfort, coolness, beauty, and shadiness, (Fig. 18). Unhas Urban Park from

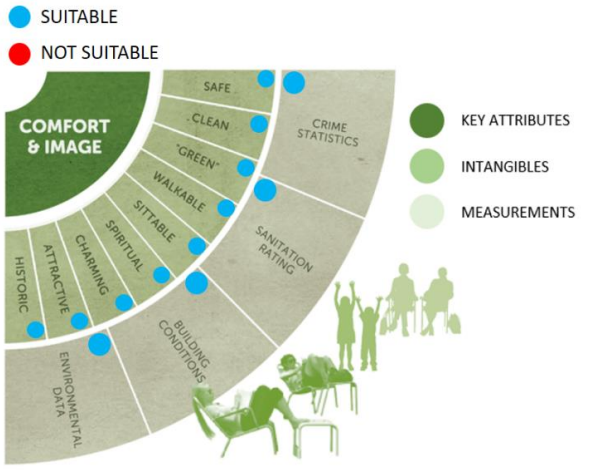

Figure 18. The compatibility of the ideal comfort and image criteria with the conditions of the Hasanuddin University urban park

the aspect of measurements, for crime statistics based on the results of an interview with one of the security guards at the security post, crimes are rare in the area, this is due to the location of the park which is close to the security post and there is no activity at night. As for the sanitation rating, in parks with sanitation conditions, flooding occurs when heavy rains occur for 2-3 days in a row, causing lake water to overflow up to the Perintis highway and gate I, as in early December 2021. For building conditions, it can be seen from the condition of the post office security and the condition of park facilities such as pedestrian paths. As for environmental data, you can use applications to measure temperature and humidity in the park area.

4.4. The effect of visitor's behavior on the condition of the Hasanuddin University urban park

Human behavior is closely related to the space that accommodates them because human behavior can form patterns of activity which can also affect the shape of the space. In addition to meeting the physical aspects of the ideal criteria of public open space, the behavior of visitors, as well as users of open space, has an important role in realizing a successful public open space.

The physical environment can evoke an emotional response of both relaxed and alert awareness at the same time. In helping a person to understand his environment can be done by improving the perceived qualities that are influenced by the quality of his physical environment [15].

Based on the findings, we summarize the visitor behaviors that influence each other with the condition of the existing facilities in the park, including:

- Visitor's parking behavior with the condition of the parking space

Parking behavior is one of the concerns because it has an impact on traffic jams. Parking behavior in a city environment can be influenced by internal factors and external factors. Internal factors come from within a person such as the same desire to park in a place with many parked vehicles without having to pay attention to the situation which later becomes a habit. External factors can be in the form of lack of parking space, lack of parking

(a) (b)

Figure 19. Visitor's parking behavior in front of the pedestrian hall: (a) Cars parked on the side of the road in front of the pedestrian hall; (b) Motorcycles parked on the side of the road in front of the pedestrian hall

(a) (b)

Figure 20. (a) Littering Behavior; (b) Garbage strewn across the Wetland area

information boards, and the distance of the parking area from the location of the visit.

Based on observations, at busy times which occur in the afternoon, most visitors park on the side of the road in front of the pedestrian hall. This can be caused by internal factors as well as external factors, given the absence of information confirming that parking is prohibited along this road and information on the existence of parking spaces (Fig. 19).

- The behavior of visitors to the cleanliness of the park environment

The cleanliness of the urban environment is influenced by human actions in managing and tackling the waste they produce. Environmental hygiene behavior can be realized by being built, formed, and organized continuously through the actions of its inhabitants. Hygiene behavior can be realized with the presence of resources, consisting of (a) residents (people), residents need to have high motivation to create and maintain a clean environment, regularly invite, remind, and encourage each other to maintain environmental cleanliness, supervise and reprimand if there are deviations; (b) equipment, in the form of trash bins; (c) information exposure, in the form of information indirectly through information boards at several points in the park, (d) reserve resources, in the form of cleaning workers.

Based on observations, there is still a lot of garbage that is not disposed of in its place and there is only one trash can whose size is inversely proportional to the amount of waste produced by visitors, (Fig. 20).

Figure 21. Cautiousness behavior of visitors about park facilities: 1. Visitors cross to the park from the parking location; 2. Condition of a damaged pedestrian in the wetland area; 3. Broken bench; 4. The condition of the wooden bridge towards the infinite bridge pier; 5,6,7. Adult visitors and children in the wetland area

- Cautiousness behavior and visitor alertness

Alertness affects the sense of security when in a place, it can be in the form of the condition of the facilities available in the park, statistics on crimes that can occur in an environment, and weather conditions. Based on observations, the condition of the park pedestrians, especially in the wetland area, was damaged at several points, the condition of the roads became slippery after the rain, the condition of the park benches was damaged, and there were no pedestrian paths for people with disabilities, as well as some areas were not child-friendly, such as the pedestrian path that has different floor heights. This can increase the awareness of visitors, especially visitors who bring children (Fig. 21).

5. Conclusions and Recommendations

5.1. Conclusions

Based on the findings and discussion, it can be concluded that the condition of the Hasanuddin University Urban Park is based on the ideal criteria of public open space according to Madden and the Project for Public Space, in some aspects of intangibles and aspects of measurements on each of the existing criteria, some are appropriate, some are not. Parks seen from the criteria of sociability and social networks do not meet these criteria because the social interactions that occur are joint only in their respective groups when visiting. The park is seen from the uses and activities criteria, it is not appropriate because it has not shown commercial activities. The park is seen from the access and linkages criteria does not meet the criteria due to the arrangement of parking patterns. The park is seen from the criteria of comfort and images, the atmosphere of the park is suitable for the criteria.

The behavior of visitors at the Hasanuddin University Urban Park is influenced by the facilities in the park which affect the parking behavior of visitors, environmental hygiene behavior, and visitor alertness behavior due to the condition of the existing facilities in the park.

5.2. Recommendations

Based on the result of findings from the post-occupancy evaluation of the Hasanuddin University Urban Park by observing behavior (behavior mapping), the authors provide suggestions and recommendations by:

- Maintaining the existing design afterward developing and increasing the visibility of space from both the physical and non-physical aspects of the park. Space visibility is meant to create a space that increases the interest of visitors to visit and do various activities.
- Recommendations for other researchers are to conduct more in-depth research related to problems that occur in the field in detail. For this reason, it is recommended for future researchers who are interested in conducting further studies or research so that they can carry out better.

References

[1] "Undang-undang (UU) Nomor 26 Tahun 2007 tentang Penataan Ruang," Jakarta, 2007.

[2] "Peraturan Menteri Pekerjaan Umum dan Perumahan Rakyat Nomor 05/PRT/M/2008 Tahun 2008 tentang Pedoman Penyediaan dan Pemanfaatan Ruang Terbuka Hijau di Kawasan Perkotaan," Jakarta, 2008.

[3] R. Hakim, *Komponen Perancangan Arsitektur Lansekap: Prinsip-Unsur dan Aplikasi Desain*, 2nd ed. Jakarta: Bumi Aksara, 2014.

[4] I. Falah, "Kementerian PUPR Bangun 2,4 hektar Ruang Terbuka Hijau Baru di Kota Makassar," *InfoPublik*, 2017. https://infopublik.id/read/232051/kementerian-pupr-bangun-24-hektar-ruang-terbuka-hijau-baru-di-kota-makassar-.html (accessed Jan. 19, 2024).

[5] M. Carmona, *Public Places-Urban Spaces: The Dimensions of Urban Design*. London: Architectural Press, 2003.

[6] J. Siahaan, "Ruang Publik: Antara Harapan dan Kenyataan," *Bulletin Tata Ruang*, 2010. http://bulletin.penataanruang.net/index.asp?mod=_fullart&idart=265 (accessed Jan. 19, 2024).

[7] Project for Public Spaces, *How to Turn a Place Around: A Handbook for Creating Successful Public Spaces*. Project for Public Spaces, 2000.

[8] J. Walljasper, B. Fried, and Project for Public Spaces, *The Great Neighborhood: Book A Do-it-Yourself Guide to Placemaking.* New Society Publishers, 2007.

[9] Haryadi and B. Setiawan, *Arsitektur Lingkungan dan Perilaku : Pengantar ke Teori Metodologi dan Aplikasi*. Departemen Pendidikan dan Kebudayaan, 1995.

[10] W. Zhang and G. Lawson, "Meeting and Greeting: Activities in Public Outdoor Spaces Outside High-Density Urban Residential Communities," *Urban Des. Int.*, vol. 14, pp. 207–214, 2009.

[11] A. M. Radja, R. Wikantari, and A. Harisah, "Characteristic of Student Informal Gathering Space (SIGS) Faculty of Engineering Hasanuddin University at Gowa Campus," in *The 3rd EPI International Conference on Science and Engineering*, 2019, pp. 1–8.

[12] Miftahuljannah, T. Martosenjoyo, and R. Mulyadi, "The influence of Transit Area in Public Open Space of Losari Beach Makassar Pavilion on the Activities of Group Visitors," *EPI Int. J. Eng.*, vol. 4, pp. 93–100, 2021.

[13] J. Gehl, *Life Between Buildings: Using Public Space*. Washington DC: Island Press, 2011.

[14] A. M. I. Djainuddin, A. Harisah, and A. M. Radja, "The Visitors' Perception toward the Comfort of Social Interaction in Public Space (A Case study in Karebosi Field Makassar)," *EPI Int. J. Eng.*, vol. 2, pp. 149–156, 2019.

[15] E. H. Zube and I. Altman, *Public Places and Spaces*. Springer US, 2012.

EPI International Journal of Engineering
Volume 6, Number 2, August 2023, pp. 101-106
DOI: 10.25042/epi-ije.082023.07

*p*ISSN 2615-5109
*e*ISSN 2621-0541

Identification of Thermal Comfort of Open Space in Soppeng Regency

Nurhasanah[a,*], Rosady Mulyadi[b], Asniawaty Kusno[c]

[a]Laboratory of Building Science and Technology, Faculty of Engineering, Universitas Hasanuddin. Email: an.nurhasanah.996@gmail.com
[b]Department of Architecture, Faculty of Engineering, Universitas Hasanuddin. Email: rosady@unhas.ac.id
[c] Department of Architecture, Faculty of Engineering, Universitas Hasanuddin. Email: asniawaty@unhas.ac.id

Abstract

Thermal comfort is always associated with the climatic situation. Thermal comfort, known as a sense of comfort in the thermal situation in the surrounding environment, is also a necessity for space users. Open space is a place for space users who must be able to create a comfortable situation, one of which is thermal comfort. Temperature, humidity, wind velocity, and radiation intensity are elements of the thermal environment, as well as human metabolism and clothing insulation as human physical and physiological factors, are the six parameters of outdoor thermal comfort level according to ASHRAE Standard. This research is a type of descriptive research that aims to explain the thermal conditions felt by the perpetrators of activities in one of the open spaces in the Soppeng Regency, the Ompo Lake Tourism Area. The results obtained were from 349 respondents and as many as 216 respondents felt comfortable in the most comfortable temperature conditions in the range of 27.1 - 31˚C, with humidity>70%, wind velocity 0.2 – 0.5 m/s, and radiation intensity <150 W/m^2. Activity with a relaxed sitting (1 met) and moderate tropical clothes (0.3 – 0.5 clo).

Keywords: Thermal comfort, open space, thermal environment elements

1. Introduction

Thermal comfort is the condition of the individual feeling comfortable with the thermal situation in the environment around the body. Thermal comfort is one of the needs of space users. Activities can be done anywhere, one of which is in an open space. Open space is something that can accommodate human activities either individually or in groups [1].

Some people are reluctant to do outdoor activities because feeling hot, sweaty and uncomfortable can interfere with outdoor activities. With high air temperature coupled with the amount of solar radiation accompanied by high air humidity, it can cause a feeling of heat and sweating which makes it uncomfortable [2].

With a comfortable outdoor environment, the users of the activity will be more comfortable in their activities. Figure 1 shows that Soppeng Regency is located on the island of South Sulawesi and one of 24 regencies in South Sulawesi. In Soppeng Regency, there are several open spaces for the community that can be used for various purposes, ranging from sports, relaxing, playing, gathering with relatives, or simply being a means of releasing human stress. One of them in the Soppeng Regency is the Ompo Tourism Area. Precisely located in Lalabata District.

*Corresponding author. Tel.: +62-811-4050-955
Aroeppala Street
Makassar, Indonesia, 902221

Figure 1. Research sites

2. Literature Review

Thermal comfort is a condition where a person feels comfortable moving in an environment/room with a certain temperature [2]. Thermal comfort is defined as the human perception of the thermal conditions of the environment. Thermal comfort is always associated with climatic situations [3]. Lippsmeier (1994) that three climate components are the parameters for determining thermal comfort [4]:

a. Air Temperature
   Based on research by Mom and Wiesebrom in 1940, the criteria for comfort based on air temperature for native Indonesians are divided into three, namely; cool and comfortable, with a

temperature of 20.5°C - 22.8°C (TE); optimal comfort with a temperature of 22.8°C - 25.8°C (TE); and warm comfort with a temperature of 25.8°C - 27.1°C (TE) [5].

b. Humidity
Humidity is the amount of water content in the air expressed in percent. The humidity of the air that is comfortable for the body ranges from 40%-70%. In places like the seaside, it ranges from 80% - to 98%. If the humidity of the air is saturated, then our bodies cannot evaporate sweat anymore [6].

c. Wind Velocity
The wind speed for indoor comfort is within speed limits between 0.1 m/sec to 0.5 m/sec., if it exceeds that limit (above/below) then the sensation is said to be uncomfortable (neutral).

In the ASHRAE standard that temperature (˚C), humidity (RH%), wind speed (m/s), radiation intensity (W/m^2), body metabolism (met), and clothing insulation (clo) are the six parameters that determine thermal comfort [7]. Fanger (1970) said that the combination of two factors that affect thermal comfort, in addition to thermal environmental factors, namely air temperature, humidity, wind speed, and radiation, there are also personal factors including metabolic rate based on activity and climate. value-based on clothing [8].

In the human body, there is always a biological process that produces heat. This process is called thermal metabolism. Measurement of activity is expressed in units of "met" (metabolism). The higher or stronger the human activity, the greater the production of heat from the body. This situation causes changes in other variables in the thermal equilibrium process if a stable equilibrium is desired to achieve thermal comfort. To achieve thermal equilibrium of the body which is about 5 - 20 minutes [9]. As clothing forms an intermediate environment between humans and their environment. Each type of clothing has a characteristic number that is associated with the percentage of covering or coating on the skin of the human body to the outside air environment. The standard of tropical human clothing is 0.15 – 0.30 clo (light), 0.30 – 0.50 (moderate), > 0.50 (heavy) with the lowest value being 0 where humans are not dressed at all [3].

Various studies have been conducted by researchers regarding the factors that influence thermal comfort. With the movement of the wind, the effect of wind speed is quite significant on the comfort of humans who are active in outdoor spaces [7]. While radiation has a stronger effect on the thermal environment in the humid tropics than wind [10]. The amount of solar radiation hitting a flat surface in a tropical climate can reach more than 1000 W/m2, which is close to the solar constant of 1368 W/m^2 [3].

In open space, there are physical components that make up the space, one of which is vegetation. Vegetation is a variety of plants or plants that occupy an ecosystem. In the humid tropics, shading through vegetation and outdoor morphology is an effective effort to create thermal comfort in outdoor spaces by preventing direct radiation [5]. The presence of vegetation in several zones is sufficient to help provide shade for active users [11]. Meanwhile, surface materials with a high albedo, such as asphalt and concrete, are capable of storing material heat which will increase the air temperature when the heat is released [12], [13].

Figure 2. Ompo lake tourist area
(Source: instagram.com/ayokesoppeng_/?hl=id, 2018)

3. Methods

This type of research is descriptive research. In this study, a survey will be conducted by measuring the climate component at predetermined measuring points and asking respondents beliefs, opinions, and characteristics of objects through written questions and the same questions (questionnaires). For respondent data collection was carried out on Saturdays and Sundays where at that time more visitors were active than on usual days so the process of collecting respondent data was easier to do. Data collection was carried out only on sunny days for 12 days.

This research was conducted in Soppeng Regency, the research site is in the Ompo Lake Tourist Area (Fig. 2) which is an area within the Lalabata District, Ompo Village. The area chosen as the measuring point is based on the area that contains activities in it, so with this consideration, the number of measuring points is determined to be 10 points. Can be seen in Fig. 3 is the location of the measuring points.

The sampling technique used in this research is quota sampling and purposive sampling. Namely determining the sample that has certain characteristics until the specified amount (quota) has been met. In this study, the number of samples determined was approximately 60 samples in a day of research carried out in 2 time periods, morning and afternoon. Therefore, it will be obtained approximately 30 samples in the morning and approximately 30 samples in the afternoon.

In measuring climate, instruments are used in the form of a Thermohygro Meter to measure temperature (˚C) and humidity (%), an anemometer to measure wind velocity (m/s), and a Solar Power Meter to measure radiation intensity (W/m2). This study also use a questionnaire in

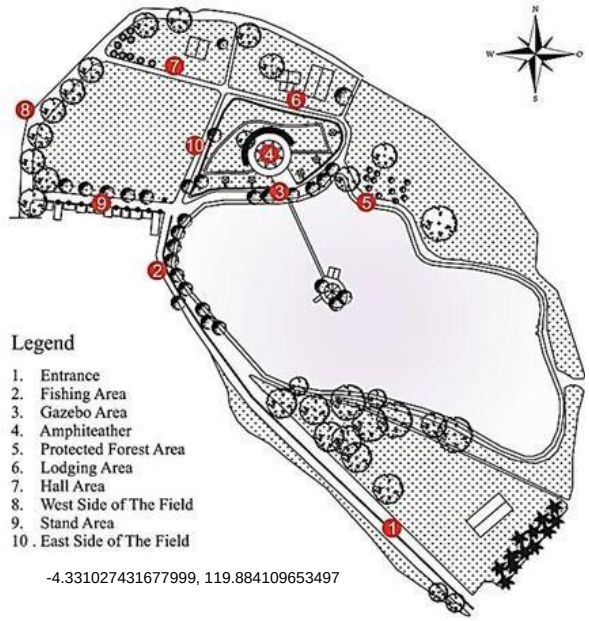

Figure 3. Measuring points

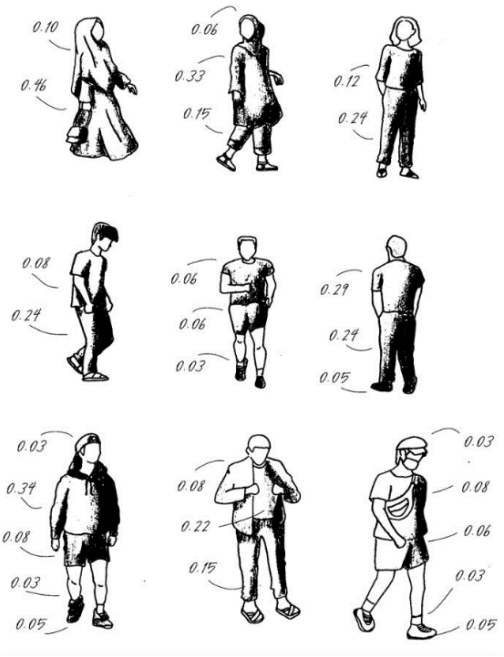

Figure 4. Illustration of the type of clothing used by the respondent

collecting data. Questionnaires are data collection techniques that are carried out by giving a set of questions or written statements to respondents to answer [14]. The questionnaire method is the right way to collect subjective thermospatial perception information from respondents as space users. Thermospatial perception is influenced by the duration of experience of the thermospatial condition [15].

Respondents will be asked to state the type of activity and how long they have been in the open space for each category of thermal quality of the place. This type of activity is to show the kinetic condition of the respondent while in an open space. Achieve thermal equilibrium of the body which is about 5-20 minutes. In the process of this research, respondents were selected based on the activities and the type of clothing used. The respondent's activities in the open space include sitting relaxed, sitting fishing, or sitting down to eat in tropical clothes (clothes that are generally for outdoor activities).

Respondents were selected based on predetermined criteria, namely selecting respondents with sitting and relaxing activities (relaxed sitting, sitting while eating, sitting while fishing), choosing respondents who had been doing activities for 20 minutes or more with the intention that the respondent had achieved thermal equilibrium. As well as the selection of respondents with light tropical to moderate tropical clothing (0.1 – 0.5 clo). The illustration of the respondent's clothes and the value of the insulation can be seen in Fig. 4.

The number population is unknown, then in determining the number of samples refers to the table determining the number of samples by isaac and michael, so the number of samples determined is 349 sample.

4. Results and Discussions

With a total of 349 respondents the questionnaire was asked about the thermal perception of each individual where this perception is influenced by situational factors and personal factors. Thermal perception is divided into two questions, namely sensation and comfort level related to temperature, wind velocity, and radiation. The sensation is an individual's first response to external stimuli, while comfort level is an individual's comprehensive assessment of his environment. The respondent's characteristic variable consisted of 6 question items ranging from age, gender, domicile, type of shade, duration of activity, activities carried out, and type of clothing used.

Table 1 shows the result of the correlation test between the respondent's characteristics in the form of age, type of shade, activity and the type of clothing having a sig value <0.05 or it can be concluded that there is a correlation or there is a relationship with the sensation felt by the respondent with the value of the strength of the relationship (coefficient).

Based on the results of the correlation test, it is known that there is a relationship between age and sensation or it can be said that the lower age is followed by a decrease in sensation. And there is a strong relationship between the type of shade and sensation or it can be said that the better the type of shade, the better the sensation will be. There is also a moderate relationship between activity and sensation, where the higher the activity, the lower the sensation. There is a moderate relationship between the type of clothing and sensation, namely the lower the insulation value of the clothing, the better the sensation felt.

Table 1. The results of the correlation test of respondents' characteristics with sensation

No	Characteristics of Respondents	Level Comfort		Description
		Sig	Coeff	
1	Age	0.000	-0.288	Corelate
2	Domicile	0.649	0.024	Uncorrelated
3	Shade Type	0.000	0.719	Corelate
4	Activity Duration	0.860	0.092	Uncorrelated
5	Activity	0.000	-0.420	Corelate
6	Visit Frequency	0.768	0.016	Uncorrelated
7	Clothing Type	0.017	0.560	Corelate

Table 2. The results of the correlation test of the respondent's characteristics with the level of comfort

No	Characteristics of Respondents	Level Comfort		Description
		Sig	Koef	
1	Age	0.974	-0.002	Uncorrelated
2	Domicile	0.860	0.009	Uncorrelated
3	Shade Type	0.525	-0.034	Uncorrelated
4	Activity Duration	0.409	0.044	Uncorrelated
5	Activity	0.770	0.016	Uncorrelated
6	Visit Frequency	0.724	0.019	Uncorrelated
7	Clothing Type	0.369	-0.048	Uncorrelated

While the characteristics in the form of domicile, duration of the activity, and frequency of visits have a sig value > 0.05 or it can be concluded that there is no correlation or there is no relationship with the sensation of the respondent. Based on assumptions, there is no relationship between domicile and sensation because the sensation is the individual's first response to external stimuli. As well as the duration of activity with the frequency of visits.

Table 2 shows the result of the correlation test between the characteristics of the respondents and the comfort levels of the respondents. Overall, with the sig value > 0.05 or it can be concluded that there is no correlation or there is no relationship between the characteristics of the respondents and the level of comfort.

Based on the assumption, there is no relationship between the characteristics and the level of comfort because the level of comfort is an individual assessment of the environment, in this case, it is related to adjustments to environmental conditions. So even though the respondent feels a hot sensation, with this condition the respondent feels comfortable because it has adapted to its environment and because of other influencing factors such as the wind.

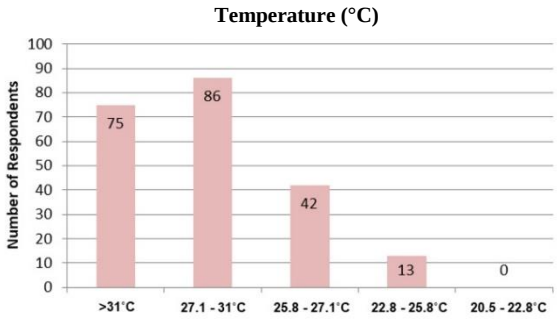

(a) Temperature

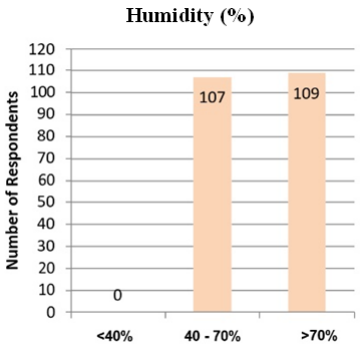

(b) Humidity

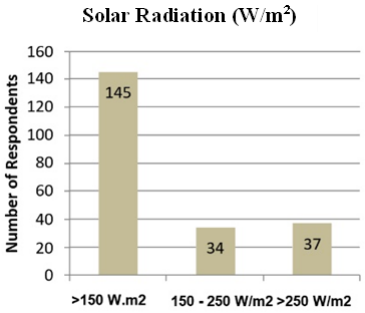

(c) Solar radiation

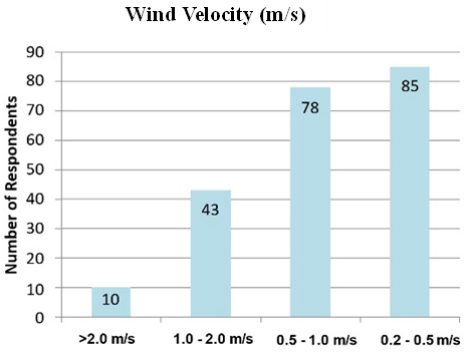

(d) Wind velocity

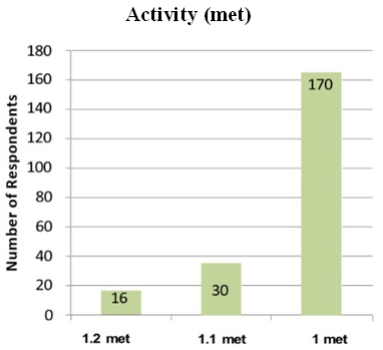

(e) Activity

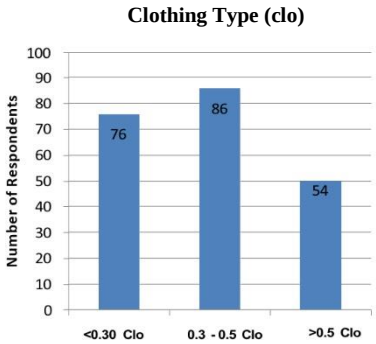

Figure 5. Respondents with comfortable conditions based on six elements that determine thermal comfort

Figure 5 is the number of respondents with comfortable conditions based on the six elements that determine thermal comfort according to ASHRAE, namely air temperature, humidity, wind velocity, radiation intensity, type of activity, and type of clothing. The number of respondents who felt slightly comfortable (Scale 5) comfortable (scale 6) was 216 respondents from 349 respondents.

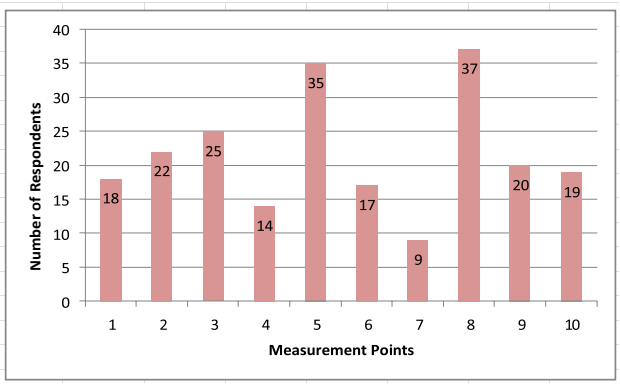

Figure 6. Number of respondents with comfortable conditions based on measuring points

Based on the large number of respondents who answered that they felt comfortable, it can be concluded that comfortable conditions are felt when the air temperature is at a range of 27.1˚C - 31˚C, with humidity > 70%, wind velocity 0.2 m/s – 0.5 m/s, radiation intensity <150 W/m^2, with the type of activity relaxed sitting and wearing moderate tropical clothes (0.3 Clo – 0.5 Clo).

Based on a large number of respondents can be seen in Fig. 6, it can be concluded that comfortable conditions are felt at measuring points 8 and 5. Measuring points 5 and 8 are measuring points that have vegetation other than measuring points 2, 3, and 9. However, measuring points 5 and 8 have a high level of canopy density, wide tree canopy, and the distance between trees that are close to each other. When taking measurements, the two measuring points always have a value that is included in the comfortable category.

Based on age in Fig. 7, out of 216 respondents who felt comfortable were teenager, 116 responded with a percentage of 54.2%. Based on gender who feel comfortable are men. Local people are more comfortable with their thermal conditions. Trees are a more comfortable type of protection than buildings and other types of protection. Respondents felt comfortable after being in the research location for more than one hour.

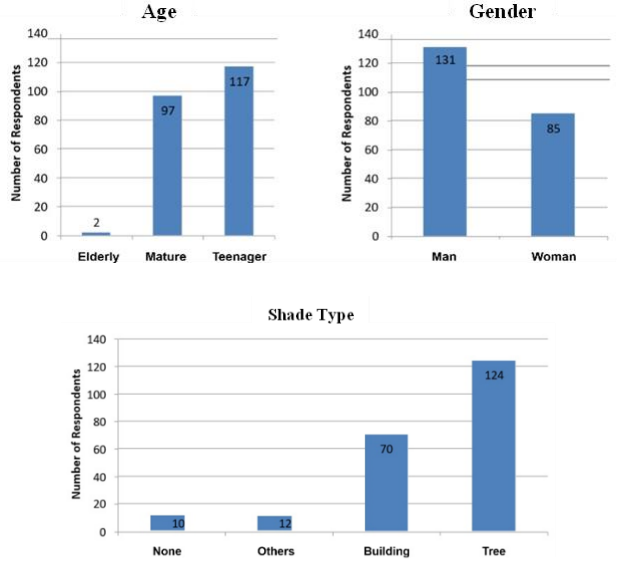

Figure 7. Number of respondents with comfortable conditions based on age, gender, domicile, shades type, and activity duration

5. Conclusions

By the 349 respondents, 216 (61.9%) of respondents felt comfortable. With the most comfortable temperature in the range of 27.1 - 31˚C, with humidity >70%, wind velocity 0.2 – 0.5 m/s and radiation intensity <150 W/m^2. And with a relaxing sitting activity (1 met) with moderate tropical clothes (0.3 – 0.5 clo). The most comfortable measuring points felt by respondents are measuring points 5 and measuring points 8.

There is a relationship between age and sensation or it can be said that the lower age is followed by a decrease in sensation. And there is a strong relationship between the type of shade and sensation or it can be said that the better the type of shade, the better the sensation will be. There is also a moderate relationship between activity and sensation, where the higher the activity, the lower the sensation. And there is a moderate relationship between the type of clothing and sensation, namely the lower the insulation value of the clothing, the better the sensation felt.

References

[1] R. Hakim, *Komponen Perancangan Arsitektur Lansekap: Prinsip Unsur dan Aplikasi Desain*. Jakarta: Bumi Aksara, 2011.

[2] T. H. Karyono, “Kenyamanan Termal dalam Arsitektur Tropis,” in *Arsitektur dan Kota Tropis Dunia Ketiga: Suatu Bahasan tentang Indonesia*, RajaGrafindo Persada, 2013.

[3] Sangkertadi, *Kenyamanan Termis di Ruang Luar Beriklim Tropis Lembab*. Alfabeta, 2013.

[4] Santi, S. Belinda, and H. Rianty, “Identifikasi Iklim Mikro dan Kenyama Termal Ruang Terbuka Hijau di Kendari,” *NALARs J. Arsit.*, vol. 18, pp. 23–34, 2019.

[5] E. Johansson, M. W. Yahia, I. Arroyo, and C. Bengs, “Outdoor Thermal Comfort in Public Space in Warm-Humid Guayaquil, Ecuador,” *Int. J. Biometeorol.*, vol. 62, pp. 387–399, 2018.

[6] B. Suyono and E. Prianto, “Kajian Sensasi Kenyamanan Termal dan Konsumsi Energi di Taman Srigunting Kota Lama Semarang,” *MODUL*, vol. 17, pp. 17–25, 2017.

[7] ANSI/ASHRAE Standard 55, “Thermal Environmental Conditions for Human Occupancy,” 2021.

[8] C. Ekici and I. Atilgan, “A Comparison of Suit Dresses and Summer Clothes in the Terms of Thermal Comfort,” *J. Environ. Heal. Sci. Eng.*, vol. 11, p. 32, 2013.

[9] Y. Sangaji, Sangkertadi, and A. Sembel, “Kajian Kenyamanan Termal bagi Pejalan Kaki pada Jalur Pedestrian Universitas Sam Ratulangi,” *Spasial*, vol. 2, pp. 98–106, 2015.

[10] N. Makaremi, E. Salleh, M. Z. Jaafar, and A. Ghaffarianhoseini, “Thermal Comfort Conditions of Shaded Outdoor Spaces in Hot and Humid Climate of Malaysia,” *Build. Environ.*, vol. 48, pp. 7–14, 2012.

[11] I. W. W. Sastrawan and I. G. S. Darmawan, “Perception of Thermal Comfort Level in Outdoor Space on Urban Public Space (Case Study: Lumintang Park in Denpasar),” in *Proceedings of the 3nd Warmadewa Research and Development Seminar, WARDS 2020*, 2021.

[12] M. J. Santamouris, “Cooling the Cities – A Review of Reflective and Green Roof Mitigation Technologies to Fight Heat Island and Improve Comfort in Urban Environments,” *Sol. Energy*, vol. 103, pp. 682–703, 2014.

[13] G. Evola *et al.*, "UHI Effects and Strategies to Improve Outdoor Thermal Comfort in Dense and Old Neighbourhoods," *Energy Procedia*, vol. 134, pp. 692–701, 2017.

[14] Sugiyono, *Metode Penelitian Kualitatif, Kuantitatif dan R&D*, 2nd ed. Alfabeta, 2020.

[15] S. Lenzholzer, W. Klemm, and C. Vasilikou, "Qualitative Methods to Explore Thermo-Spatial Perception in Outdoor Urban Spaces," *Urban Clim.*, vol. 23, pp. 231–249, 2018.